

Proposed Gyrotrons and FELs frequency distributed multiplication

A.A.Andronov and M.A.Novikov

Institute for Physics of Microstructures RAS, Nizhny Novgorod, Russia, andron@ipmras.ru

THz Gyrotrons and FELs have intrinsic frequency band limit. Natural way to broad the bands and to have possibility for reach frequency deeper in THz band is frequency multiplication. Power of the sources permits to use distributed (bulk) multiplication systems. Both second and third harmonics generation is possible.

In this report we are discussing two approaches for the frequency multiplication: 1. Multiplication in nonlinear crystal (GaP, GaAs and others with high nonlinear coefficient in THz band for the second harmonic and Si for the third) which has almost ideal harmonic wave synchronism in THz band and can have low enough absorption; large enough dimension of the crystals are available. This approach is well known in nonlinear optic but to the best of our knowledge have not been used for THz Gyrotrons and FELs. 2. Multiple (superlattice) GaAs-AlAs varactor system. In the latter the synchronism is fulfilled “automatically.” Varactors are commonly uses for frequency multiplication in microwave bands. In the report details of this multiplication scheme will be presented. The maximal powers of existing in Russia sub THz and THz gyrotrons and FELs are quite high [1, 2] to provide enough power for harmonic generation.

Gyrotrons from IAP RAS: 670 GHz, 50 kW, 30 picoseconds

Novosibirsk THz FEL, 0.5- 2 THz, 1 MW in 100ps micro pulses, about 6 MHz repetition rate and average power about 1 kW.

In the crystal based approach for second harmonic generation one needs high quality crystals without center of symmetry with also weak absorption in THz band and high quadratic nonlinear coefficient. Suitable are inorganic GaAs, GaP and GaSe crystals. In particular GaSe has the lowest absorption coefficient in the terahertz and millimeter wave regions among all the inorganic nonlinear crystals. Further more, a GaSe crystal has a large second-order nonlinear coefficient. The present authors have GaP crystal 10 by 10 by 10 mm³. It has low absorption coefficient and almost no dispersion (providing almost ideal wave synchronism condition) and also quite high quadratic nonlinearity in THz. We consider such crystal as the first candidate for the gyrotron and FEL harmonic generation. Estimate based on available data on GaP parameter provide second harmonic power for IAP RAS gyrotron in the above GaP crystal at the level of several Watts. Organic crystals (DAST and others) could be also suitable and promising for second harmonic generation. But we will not discuss this here.

Another approach for harmonic generation we are discussing is system (superlattice) of multiple varactors. Contrary to crystals this is an artificial medium which can be design to fulfill requirement for harmonic generation. Each varactor in the superlattice is low doped GaAs well surrounded by high AlAs barriers (Fig 1A). Under applied AC field electron distribution sweeps there and back of the well (Fig 1B) providing oscillation dipole with saturation (Fig 2) herewith establishing in the dipole harmonics of the AC field. Fig 1 and Fig 2 represent symmetric doping of the superlattice well; this gives only odd harmonic. For non symmetric doping also even harmonic appear.

Consider now harmonics emission in the case shown in Fig 3; this case looks the most promising for harmonics generation. Here pump performs total internal reflection from boundary air-superlattice. Nonlinear dipole moment in superlattice emits harmonics also only to superlattice and substrate because phase velocity of the harmonics along air – structure boundary is equal to the one of the pump. Now (supposing that thickness of the superlattice is smaller than wavelength of harmonic) one have situation similar to traveling wave antenna. Indeed the whole nonlinear dipole moment of the superlattice may be written as: $P_0 = M e d N_s \{ \alpha_2 (E/E_d)^2 + \alpha_3 (E/E_d)^3 \} = L e N_s \{ \alpha_2 (E/E_d)^2 + \alpha_3 (E/E_d)^3 \}$. Here $p = ed N_s$ is saturated dipole moment of a well, N_s is well delta doping per cm², $E_d = (4\pi/\epsilon_0)e N_s$ is characteristic field, M is well number in the superlattice, L its whole thickness and α_2, α_3 are frequency dependent numerical factors. Now density of nonlinear dipole moment perpendicular to air-structure surface under influence of AC electric field may be written approximately as: $P_y^{nonl} = [\beta E_y^2 + \gamma E_y^3] \delta(y-a) = [\beta E_0^2 \exp(i\Omega_2 t - iK_2 x) + \gamma E_0^3 \exp\{i\Omega_3 t - iK_3 x\}] \delta(y-a)$, where y is axis perpendicular to the surface, $\Omega_{2,3} = 2,3 \omega$, $K_{2,3} = 2,3 k_x$ are harmonic frequencies and wave vectors along the surface while ω and k_x are the ones for pump. We see that harmonic phase velocity (along the surface) is equal to one of the pump. As the result it should be emitted nearby the reflected from the surface pump as shown in Fig 3. It is quite simple to calculate emission of this dipole moment P_y^{nonl} . To have high emission we should optimized parameters (d and N_s) of superlattice. We will not discuss these things her: they are too lengthy. Let us present some estimated of harmonics power which could be achieved with presented above gyrotron and FEL sources.

Taking available date on nonlinearity of GaAs and GaP we have gotten for sub THz IAP RAS gyrotron (50 kW pulses) about several watts for crystal of 1 cm. With micro pulses from Novosibirsk FEL one should expect harmonic power up to 1 kW. However

high average power of the FEL needs some off and on switch to have micro pulses trains in microsecond range for the crystals not to be burn out. For the superlattice varactor with period d about 400 angstroms, number of periods $M = 50$ (L about 2 micrometers), N_s about 10^{18} to 10^{19} cm^{-3} one should expect both second and third harmonics power from IAP RAS gyrotron about one Watt.

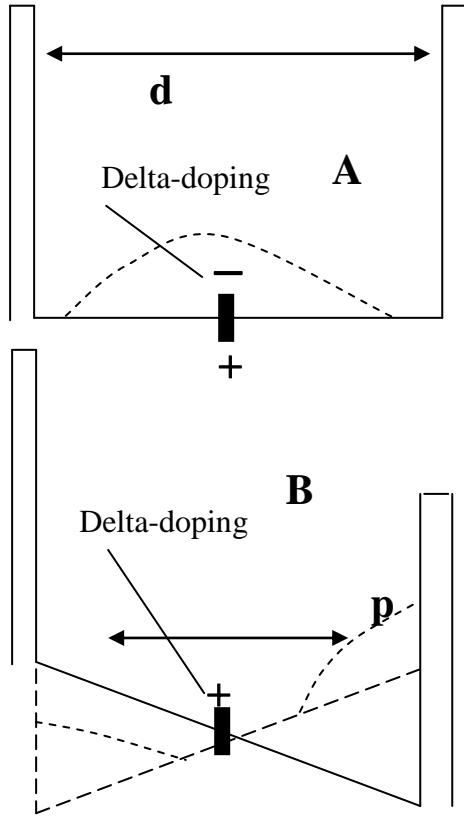


Fig 1 Scheme of one period of varactor superlattice for symmetric doping. A – without applied field ; B. with ac field ; sweeping of electron density under ac field which produced third harmonic dipole moment of the varactor in this symmetric case.

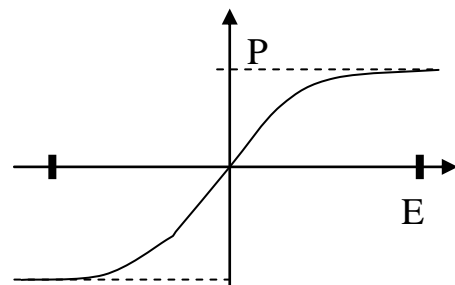


Fig 2 Scheme of dipole moment P dependence on electric field E (static or moderately HF) applied across varactor layer for symmetric varactor in Fig 1

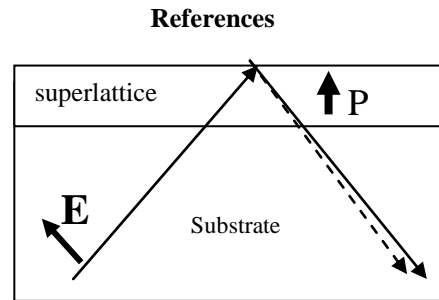


Fig 3. First harmonic pump of varactor SL under total internal reflection inside whole system: SL at substrate. Full line – pump; dotted - harmonic

1. Glyavin M Yu, Luchinin A G, Golubiatnikov G Yu Phys. Rev. Lett. 100 015101 (2008)
2. B.F. Knyazev, G.N.Kulipanov and N.A. Vinokurov, Novosibirsk THz FEL: instrumentation development and experimental achievements, Measurement Science and Technology., 21, (2010) 054017 (13 pp)

Novel schemes for Compact FELs in the THz region: ENEA Experience and Perspectives

A. Doria, G. P. Gallerano

ENEA- Fusion Physics Division – Radiation Sources, Antennas and Diagnostics Laboratory
Via E. Fermi 45, 00044 Frascati – Italy, andrea.doria@enea.it

The rapid advance of Terahertz technologies, in terms of radiation generators, systems and scientific or industrial applications, have put a particular focus on compact sources with challenging performances in terms of generated power (peak and/or average), radiation time structure and frequency tunability.

Free Electrons based sources are probably the best candidates to express such a versatility; there are a number of schemes that have been investigated over the years to generate coherent radiation from free electrons in the mm-wave and Terahertz regions of the spectrum, covering a wide frequency range from approximately 100 GHz to 10 THz. At such long wavelengths, good performance in terms of output power and gain can be achieved with a short length of the interaction region (< 50 cm) and with different mechanisms of energy transfer from the electron beam to the radiation field. These include the magnetic undulator, dielectric loaded waveguides for Cerenkov emission, and metal grating devices, based on the Smith-Purcell effect. This study will propose novel schemes for exploring the limits in performance of radio-frequency driven free electron devices in terms of ultra-short pulse duration, wide bandwidth operation and energy recovery for near CW operation.

Auston Switch and Optical rectification

Conventional THz emitters have gained popularity due to their characteristics and peculiarities. The so called Auston Switch, named after its inventor, and the Optical Rectifiers are the most widely used devices [1]. The Switch is made up with a coplanar strip antenna deposited on a non absorbing substrate. Along the strips there is a point where the gap is very small, of the order of $10\ \mu\text{m}$. If a powerful short laser pulse is focalised on this gap, the photons generate free carriers that drift under the action of the electric field generated by this bias voltage. This transient current gives rise to a time dependent dipole moment that acts as a source of a time dependent electric field according to expression. The result is the generation of an electric pulse which duration, and thus spectrum are related to the duration of the laser pulse. A picosecond or a sub-picosecond laser pulse generate a radiation burst in the THz range that is propagated and irradiated by the antenna.

The above illustrated approach suffers of some drawbacks. The most important is the limited bandwidth of the conventional micro-strip antennas that introduce distortion and frequency dispersion on the THz pulse ending with a rapid lengthening of the pulse.

To overcome these limitations electro-optic devices, realised with a non-absorbing material, are used. The interaction mechanism is now a second order process: the rapidly oscillating electric field of the laser pulse excite in the medium a polarisation vector which is proportional to the modulus of the electric field itself. This polarisation vector is the source for an Hertzian vector potential that generates a radiation field. This is a rectification process because the rapid oscillation of the electric field of the laser pulse are compensated in the frequency domain and only the envelope of this pulse remains. The important feature of this device is that, being the medium non absorbing, the polarisation is very fast in following the laser envelope; this means that there is no physical limit in the bandwidth of the THz pulse that can be generated with this device. The only drawback is that being this a second order process, the intensities of the THz radiation are smaller respect to the previous cases, but it is now well compensated by the more powerful short-pulse laser source now available also commercially.

A Free Electron Device as THz Radiator

“Flexibility” is the most relevant feature a Free Electron Device (FED) because any component of such a source can, in principle, be designed in order to emphasise a specific characteristics of the generated radiation [2]. Broadband emission is, in fact, ensured by a short interaction region and by avoiding optical resonators, that usually filter frequency components; these precautions, together with the use of a low energy electron beam, allow an easy and compact design of the source. The most significant peculiarity of a FED is the coherence of an electron beam generated by a Radio-Frequency (RF) accelerator. The coherent emission dominates when the electron bunch length is comparable to wavelength of the radiation to be emitted. As a result coherent emission dominates in the THz range or at longer wavelengths. Another characteristics of RF based FED is the coherence among the bunches. An RF accelerator generates a train of bunches, and if the correlation among bunches is good, the radiation will be emitted at discrete frequencies which are harmonics of the RF. This is exactly what we have measured experimentally in our compact FED in ENEA [3-4]. A further degree of coherence can be exploited when a proper energy-phase correlation is introduced in the electron beam, before entering the interaction region, in order to minimise the negative interferences among the single electrons’ emissions. Several techniques can be ap-

plied to get such a correlation, but the final result is a single-pass emission of a broad-band short pulse emission as reported in Fig. 1 (result obtained for an electron beam with $\gamma=15$, $I_{AV}=20$ mA and an undulator of $\lambda_u=2.5$ cm period and $K=1.45$ as magnetic parameter).

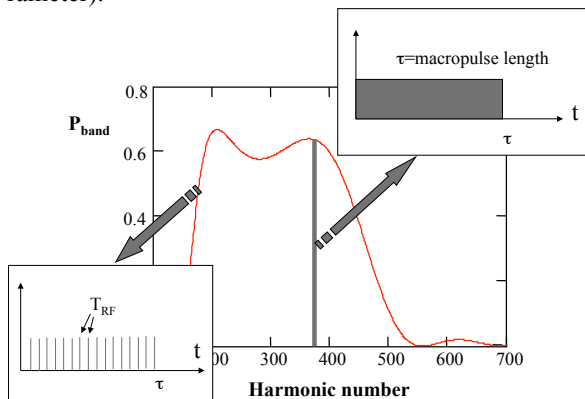


Fig. 1. Power spectrum in a Free Electron Device in the Energy-Phase Correlation regime

Analysing Fig. 1 it is evident that in the Energy-Phase correlation regime it is possible to isolate the single harmonic, with an interferometer, still having an average power for the single frequency around 0.5 W. This is not possible with the conventional THz sources. Moreover another interesting result is that the single frequency, being an harmonic of the RF has a temporal structure equal to that of the RF macropulse. If we look at the whole bandwidth, the temporal structure is the well known train of microbunches separated by the RF period. In conclusion FED can be considered a convenient flexible and powerful source for the generation of coherent radiation in the THz spectral region.

A way to get a correlated bunching in the THz region is the use of a two frequency RF device. Such cavities, in fact, offer appealing possibilities to control the bunch length of an electron beam generated by a RF accelerator. The use of a double frequency cavity requires that the second frequency be an harmonic of the fundamental one. The electrons passing through the cavity will see a field that is the result of the sum of the two fields of the fundamental and its harmonic according to:

$$V(\phi) = V_0 [\sin(\phi + \phi_s) + k \sin(n\phi + \phi_n)] \quad (1)$$

There are some design parameters that can be set like the harmonic number n , the relative amplitude ratio k that contribute to the bunch length, but the most relevant is the relative phase $(\phi_s - \phi_n)$ between the fundamental and the harmonic. These parameters establish the slope of the total field in the cavity. Two different regimes can be in principle realised: one in which one can realise a bunch-lengthening, which spread can help in damping coherent instabilities that often cut down the bunch lifetime in re-circulated accelerators; and a second in which the particles bunch reduces with respect to the reference electron. In Fig. 2 we report the behaviour of the electron bunch intensity profile as a function of the phase ϕ ,

for different harmonics n in the RF cavity ($k=-0.6$, $\phi_n=\pi$, $\phi_s=0$).

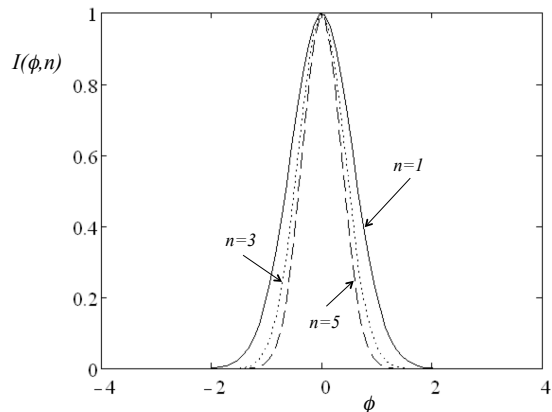


Fig. 2. Bunch shortening in a double frequency RF cavity for different harmonics.

One of the problems suffered by RF accelerator based FED, both normal-conducting and superconducting, is the relatively low efficiency. Considering the basic generation mechanism the power extraction from the electron beam in favour of the radiation never exceed few per cent, both in high gain and low gain regimes. In addition to the use of auto-resonant mechanisms (CARM), a possibility to increase the efficiency of an FED is to design a scheme for recovering the electron beam kinetic energy remained after the interaction. The energy recovered can be used to accelerate a new bunch of electrons thus lowering the accelerator radio-frequency power requirements. The possibility to manage a lower RF power and, at the same time, an exhausted electron beam of low energy, is very useful when designing the device. Generally speaking there are two possibilities for the energy recovering: one is to recycle the electron beam after the interaction region. The second possibility is to recover only the kinetic energy of the electrons before the beam dumps.

Energy recovery devices are particularly useful when designing a radiation source based on superconducting RF accelerators, or on normal conducting cavities working at very low temperatures. These accelerators, in fact, can guarantee a long bunch operation or a quasi-CW operation.

References

1. Sakai, K. Terahertz Optoelectronics // Berlin: Springer-Verlag. 2005.
2. Dattoli, G., Doria, A., Sabia, E., Artioli, M, Charged Beam Dynamics, Particle Accelerators and Free Electron Lasers // Bristol: IOP Publishing. 2017.
3. Biedron, S., Gallerano, G. P., et al. Compact, High Power Electron Beam based Terahertz Sources // Proc. Of the IEEE 2007. V. 95, No. 8, P. 1666-1678.
4. Doria, A. Relativistic Electron based THz Sources: Principles of Operation and the ENEA Experience // Physics and application of Terahertz Radiation, edited by M. Perenzoni and D. J. Paul. Dordrecht: Springer. 2014. P. 123-148.

Possible gyrotron operation in the ‘no start current’ zone

Olgierd Dumbrajs¹, Gregory S. Nusinovich²

¹Institute of Solid State Physics, University of Latvia, Kengaraga Street 8, LV-1063, Riga, Latvia, olgerts.dumbrajs@lu.lv

²Institute for Research in Electronics and Applied Physics, University of Maryland, College Park, MD 20742-3511, USA

It is known that gyrotrons can operate either in the regime of soft or hard self-excitation. In the regime of soft self-excitation the beam current exceeds its starting value, thus, the oscillations can start to grow from the noise produced by electrons. In the regime of hard self-excitation the beam current is less than its starting value. Therefore for exciting the oscillations a certain start-up scenario is required, which may include the variation of the mod-anode and/or beam voltage or guiding magnetic field. It was found recently [1] that some gyrotrons can also operate in the region of magnetic fields where there is no start current at all. In the present paper it is shown that this sort of operation can be attributed to the presence of the axial dependence of the phase of the resonator field.

The linear theory of gyrotrons summarized in [2] shows that in the process of electron interaction with the waves under the cyclotron resonance condition electrons exhibit two sorts of electron bunching. The first one is the linear bunching which evolves with time t linearly and the second is the quadratic bunching, which grows with the interaction time as t^2 . Below, we will denote the terms related to the linear and quadratic bunchings by subscripts (1) and (2), respectively.

In the simple models, the linear bunching always leads to the wave absorption by an electron beam, while the quadratic bunching, under proper conditions may result in the coherent electromagnetic radiation. This statement can be illustrated by consideration of the active part of the electron conductivity with respect to the wave, as it was done in [2]. This part of the conductivity is equivalent to the imaginary part of the electron susceptibility used elsewhere [3]. In the framework of the linear theory, this imaginary part of the susceptibility is given as

$$\chi_{lin}'' = -\left(s + \frac{\partial}{\partial \Delta}\right) \left| \int_{\zeta_{in}}^{\zeta_{out}} f(\zeta) e^{i\Delta\zeta} d\zeta \right|^2$$

where s is harmonic number, Δ is the cyclotron resonance mismatch, the function $f(\zeta)$ describes the axial profile of the electromagnetic wave amplitude, ζ is the normalized axial coordinate. Here the first term is proportional to the intensity of the spectrum of the high-frequency electromagnetic field acting on electrons and is negative, while the second term proportional to the derivative of this intensity over the cyclotron resonance mismatch can be positive that may result in the wave amplification.

Let us represent this susceptibility as $\chi_{lin}'' = \chi_{lin(1)}'' + \chi_{lin(2)}''$. For the case of the Gaussian axial profile of the wave it is shown in Fig. 1.

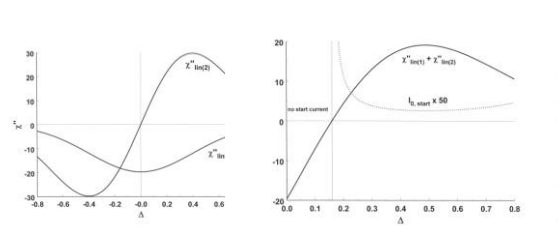


Fig. 1. Imaginary part of the susceptibility in the linear theory for a gyrotron with the Gaussian structure of the resonator field: (left) two terms corresponding to the linear and quadratic bunching; (right) the total susceptibility and the corresponding starting current

On the right from the thin vertical line this total susceptibility is positive and, hence, an electron beam can support EM oscillations there when the beam current is high enough. The balance between the microwave power losses in the gyrotron resonator and the power withdrawn by the electromagnetic field from the beam can be described by the balance equation $I_0 \cdot \chi'' = 1$.

In the case of the linear theory the corresponding value of the normalized beam current parameter I_0 determines the start current: $I_{0,start} = 1/\chi_{lin}''$. For a given value of the electron beam current, the microwave oscillations can be excited in the region where this current exceeds its starting value $I_0 \geq I_{0,start}$. This region is known as the region of soft self-excitation. On the right side from it, the electron beam current is smaller than its starting value $I_0 < I_{0,start}$. To excite oscillations there, one should initially increase the beam current for realizing the condition $I_0 \geq I_{0,start}$. Then, after oscillation amplitude becomes large enough, the current can be reduced to its nominal value. Now, we would like to call attention to the point in Fig. 1 (right) where the absolute value of the imaginary susceptibility caused by the linear bunching is equal to the susceptibility caused by the quadratic bunching, and, hence, $\chi_{lin}'' = \chi_{lin(1)}'' + \chi_{lin(2)}'' = 0$. This happens at $\Delta=0.16$. As follows from the balance equation, the start current at this point is infinite, and there is no start current to the left from this point. Our study is devoted to the analysis of gyrotron possible operation in this ‘no-start-current’ zone. So far, this region was assumed to be free from oscillations. This opinion was based on the numerous studies of the saturation effect causing the deformation of the gain curve (imaginary part of the susceptibility). A typical deformation of this curve with the amplitude of oscil-

lations F is shown in Fig. 2 (left) for the Gaussian profile of the resonator field.

As follows from Fig. 2 (left), the oscillations may exist only in the region on the right from the point where in the framework of the linear theory the imaginary susceptibility equals zero. Recently, however, it was found in [1] that in some resonators (Fig. 3) the gain curve with the growth of the amplitude of oscillations can be shifted to the left from this zero point. The sequence of the gain curves in gyrotrons with such resonators is illustrated by Fig. 2 (right).

The axial structure of the complex amplitude of the field in such a resonator is shown in Fig. 4. So, in such gyrotrons the oscillations can be excited in the zone where there is no start current.

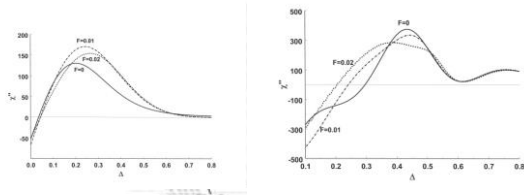


Fig. 2. Dependence of the imaginary part of the electron susceptibility on the cyclotron resonance mismatch at several values of the amplitude F in the gyrotron with the Gaussian axial structure of the resonator field (left) and a realistic axial profile of this field shown in Fig. 3 (right)

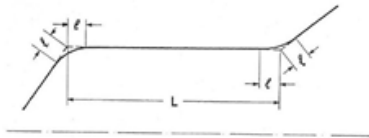


Fig. 3. Gyrotron cavity with smooth transition [4]

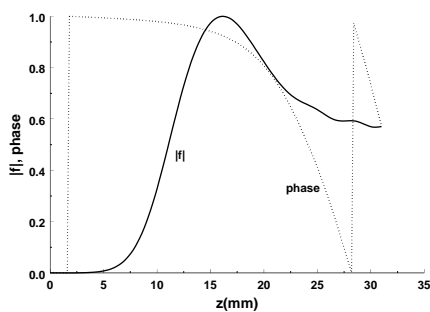


Fig. 4. The absolute value (solid line) and the phase (dotted line, the phase is normalized to π) of the field in the resonator, whose profile is shown in Fig. 3.

Contours of equal values of the orbital efficiency in the plane ‘amplitude F versus the cyclotron resonance mismatch Δ for the latter gyrotron are shown in Fig. 5. As one can see, in accordance with results shown in Fig. 2 (right), in the lower left corner of Fig. 5 the operation expands to the left, in the region of mismatches where the oscillations do not exist at very small amplitudes.

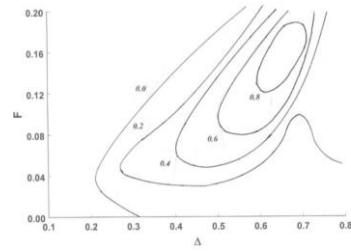


Fig. 5. Contours of equal values of the orbital efficiency

By using the balance equation, one can convert calculated dependences of the efficiency on the amplitude F into the dependence of the orbital efficiency $\eta_{\perp} = |F|^2 \cdot \chi''$ on the beam current. In the regimes with no start current, such dependences illustrated by Fig. 6 resemble the dependence discussed in [5] with regard to the parametric excitation of oscillations at harmonics of the mechanical system with the oscillation frequency dependent on the amplitude of oscillations.

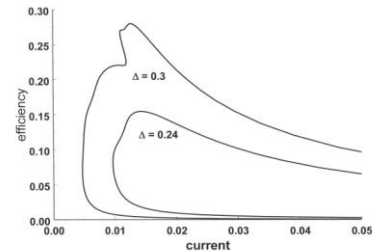


Fig. 6. The orbital efficiency as a function of the beam current parameter in the region of ‘no-start-current’

This anomalous behavior of gyrotron can, apparently, be explained by the difference in the axial structure of the resonator field. There are two important distinctions of this structure from the Gaussian one: first, the absolute value of the field in the second half of the resonator is much larger than the Gaussian profile, and second, in this second half of the resonator the phase strongly depends on the axial coordinate, while in the Gaussian case it is always zero.

References

1. *Dumbrajs, O., Nusinovich, G.S.* Efficiency of gyrotrons with a tapered magnetic field in the regime of soft self-excitation // *Phys. Plasmas* 2018. V. 25, P. 013121-013127.
2. *Gaponov, A.V., Petelin, M.I., Yulpatov, V.K.* The induced radiation of excited classical oscillators and its use in high-frequency electronics // *Radiophys. Quantum Electron.* 1967. V. 10. P. 794-813.
3. *Petelin, M.I., Yulpatov, V.K.* Linear theory of a CRM-monotron // *Radiophys. Quantum Electron.* 1975. V. 18, P. 212-219.
4. *Dumbrajs, O., Thumm, M., Pretterebner, J., Wagner, D.* A cavity with reduced mode conversion for gyrotrons // *Int. J. Infrared and Mill. Waves* 1992, V. 33, P.825-840.
5. *Landau, L.D., Lifshitz, E.M.* *Mechanics*, 3rd Edition, Butterworth-Heinemann, Oxford, 1981, P. 93.

Generation of Sub-Terahertz Surface Waves by Relativistic Electron Beams: Quasioptical Theory, Simulations and Experiments

Naum S. Ginzburg¹, A.M. Malkin¹, I.V. Zheleznov¹, V.Yu. Zaslavsky¹, A.S. Sergeev¹,
I.V. Zotova¹, and M.I. Yalandin²

¹Institute of Applied Physics RAS, Nizhny Novgorod, Russia, ginzburg@appl.sci-nnov.ru

²Institute of Electrophysics RAS, Ekaterinburg, Russia

Advancement of vacuum electronic devices into sub-THz and THz frequency ranges calls for oversized beam-wave interaction space due to the fact that the dimensions of the beam guiding systems can not be reduced lower than the millimeter scale. Thus, in order to provide coherent THz radiation from the spatially extended beams, excitation of surface modes existing in 1D and 2D corrugated systems appears to be attractive [1,2,5,6].

In this paper, we present recent results of theoretical and experimental studies of sub-terahertz generation based on excitation of surface waves by electron beams and extended bunches. Using oversized slow-wave structures allows for a significant increase of total current and, correspondingly, radiation power. Based on superradiance of electron bunches, 150 ps superradiant pulses with a central frequency of 0.14 THz, and an extremely high peak power of 50-70 MW were obtained in the joint effort by the Institute of Electrophysics RAS and IAP RAS. We also report of the first successful experiments on the cylindrical 0.03 THz Cherenkov oscillator with a 2D corrugation conducted at IAP RAS with an output power of 1.5 - 2 MW.

Generation of Sub-THz SR Pulses Based on Excitation of Surface Waves in Oversized Waveguides

Cherenkov SR of electron bunch exciting the surface wave in an oversized 1D corrugated cylindrical waveguide (Fig. 1a) can be considered within quasioptical approach [1]. In this case the radiation field near a shallow corrugation is presented as a sum of two counter-propagating *TM* polarized wave-beams:

$$H_\varphi = \text{Re}(A_+(z, r, t)e^{i\omega t - ikz} + A_-(z, r, t)e^{i\omega t + ikz}), \quad (1)$$

propagation and mutual coupling of which is described by two non-uniform parabolic equations. The synchronous interaction of electrons with a forward partial wave leads to development a self-bunching and formation of powerful SR pulse.

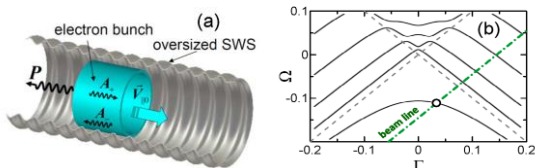


Fig. 1. (a) Scheme of SR pulse generation with excitation of a surface wave in an oversized periodically corrugated waveguide. (b) Dispersion characteristics of a corrugated waveguide and an electron beam.

Simulations show that the most optimal conditions for SR emission correspond to excitation of the backward surface wave near the Bragg frequency (π -regime, Fig.1b). For parameters of an electron bunch formed by an accelerator RADAN (electron energy of 300 keV, a total current of 2 kA, a bunch duration of 500 ps) and a corrugated waveguide with the mean radius of 3.75 mm, corrugation period of 0.825 mm, and corrugation depth of 0.36 mm the operating frequency in the resonant point is of 0.14 THz ($2r_0/\lambda \approx 3.5$). In this case the power of generated SR pulse emitted in $-z$ direction achieves ~ 200 MW for pulse duration of ~ 200 ps (Fig. 2a). As it is seen in Fig. 2b the instant spatial structure of the partial wave corresponds to formation of the evanescent surface wave with the field amplitude exponentially decaying from the corrugation.

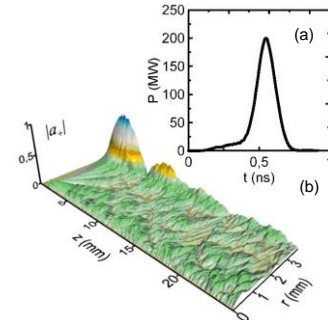


Fig. 2. SR emission with excitation of the backward surface wave: (a) generated SR pulse, (b) the structure of the forward partial wave.

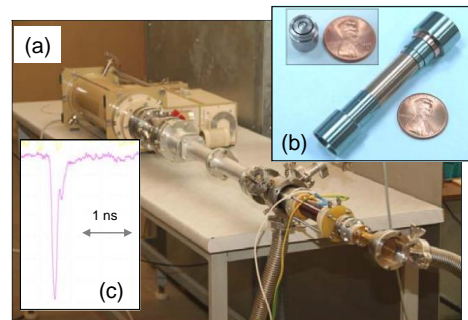


Fig. 3. Photo of the experimental set-up (a), corrugated waveguide and coaxial reflector (b) used for observation of superradiance with excitation of a surface wave. (c) Oscilloscope trace of the 0.14 THz SR pulse with duration of 150 ps and peak power up to 70 MW.

Based on a theoretical analysis, experiments on observation of the sub-terahertz SR pulse generation were carried out in IEP RAS (Ekaterinburg). Photo of the experimental set-up is shown in Fig. 3. A typical

oscilloscope trace of generated SR pulses with a duration of about 150 ps and a rise time of 100 ps reconstructed in the “power-time” coordinates is presented in Fig. 3c. Frequency measurements using a set of cut-off waveguide filters show that the pulse spectrum has a central frequency in the interval 0.13-0.15 THz. The peak power of generated SR pulses was estimated by integrating the detector signal over the directional pattern and achieved of 50-70 MW, that strongly exceeds the value obtained in the previous sub-terahertz experiments [2] with single-mode waveguides.

Ka-band surface-wave oscillator based on 2D periodical corrugated structure

For spatially extended relativistic electron beams, the use of two-dimensional (2D) distributed feedback is beneficial for providing spatial coherence of radiation and can be exploited in order to increase the total radiation power in the microwave generators [3]. Such 2D feedback can be realized in planar or coaxial 2D Bragg structures (resonators) having double-periodic corrugation (Fig.4a)

$$r = \frac{\tilde{r}}{4} \left[\cos(\bar{M}\varphi - \bar{h}_z z) + \cos(\bar{M}\varphi + \bar{h}_z z) \right], \quad (2)$$

which provides coupling and mutual scattering of the four wavebeams (Fig.4b),

$$\vec{H} = \text{Re} \left[\vec{x}_0 (C_z^+ e^{-ihz} + C_z^- e^{ihz}) + \vec{z}_0 (C_x^+ e^{-ihx} + C_x^- e^{ihx}) \right] e^{i\omega t}$$

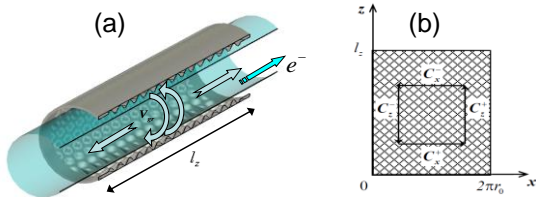


Fig. 4. (a) Scheme of an oversized SWO with 2D corrugated structure. Directions of propagation of the partial wave fluxes and tubular electron beam are shown. (b) Diagram illustrating coupling of partial waves at the 2D corrugation.

Experimental studies of free electron masers (FEMs) based on the novel feedback mechanism have been performed in Ka-band and in W-band in collaboration with the Institute of Applied Physics RAS [4]. As a result, narrow-band generation with an output power of 50 - 100 MW, which is a record for millimeter wavelength FEMs, was obtained.

At present, theoretical and experimental studies of Cherenkov masers with 2D distributed feedback are in progress [5,6]. Among relativistic masers of such type, surface wave oscillators (SWO) appear to be preferable due to the larger values of the electron-wave coupling impedance. Besides, formation of a surface mode ensures the regular field distribution along the coordinate directed perpendicularly to the corrugated surface and, thus, can solve the problem of mode selection over this coordinate. In SWOs, a 2D periodic structure can be exploited both as a slow-wave system and as a highly selective Bragg resonator simultaneously. It provides effective mode control over azimuthal coordinate.

Numerical simulations within the quasi-optical model and using 3D numerical codes show that the resulting mode to be excited in such system depends on the accelerating voltage rise time. In order to excite an azimuthally symmetric mode, this value should be small in the scale of the field excitation increment.

Experimental investigations of the SWO with 2D slow-wave structure based on the 300 keV / 100 A / 4 μs SATURN thermionic accelerator were conducted at IAP RAS [6]. The results are presented in Fig.5. Narrow-spectrum excitation of the 3rd azimuthal mode was observed.

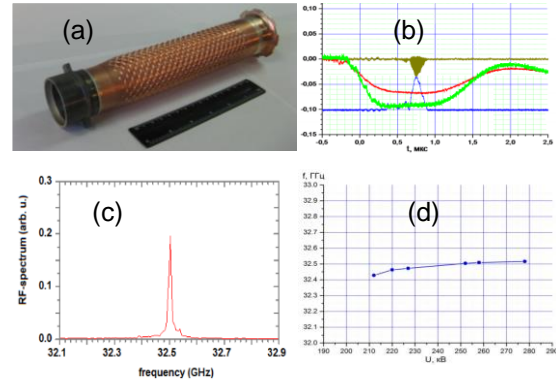


Fig. 5. Results of experimental studies of oversized Ka-band SWO based on the SATURN accelerator: (a) photograph of double periodic slow-wave structure; (b) typical oscilloscope traces of the accelerating voltage (green curve), beam current (red curve), signal from a heterodyne mixer (brown curve) and output RF-pulse (blue curve); (c) spectrum of the output radiation and (d) dependence of the radiation frequency on the accelerating voltage.

This research was performed within the framework of the state task (projects No. 0035-2014-012), and, in part, by RFBR Grant No. 17-08-01072

References

1. *Ginzburg, N.S., Malkin, A.M., Sergeev, A.S. et al.* Generation of Sub-Terahertz Superradiance Pulses Based on Excitation of a Surface Wave by Relativistic Electron Bunches Moving in Oversized Corrugated Waveguides // *Phys. Rev. Lett.* 2016. V.117 P.204801
2. *Yalandin, M.I., Shpak, V.G., Shunailov, S.A., et al* Generation of powerful subnanosecond microwave pulses in the range of 38–150 GHz// *IEEE Trans. on Plasma Sci.* 2000. V.28, Iss.5 P.1615
3. *N.S.Ginzburg, N.Yu.Peskov, A.S.Sergeev,* Dynamics of free-electron lasers with two-dimensional distributed feedback // *Optics Commun.*, **112**, 151 (1994).
4. *A.V.Arzhannikov, N.S.Ginzburg, P.V.Kalinin, et al.,* Using Two-Dimensional Distributed Feedback for Synchronization of Radiation from Two Parallel-Sheet Electron Beams in a Free-Electron Maser // *Phys. Rev. Lett.* V. **117**, 114801 (2016).
5. *N.S.Ginzburg, A.M.Malkin, A.S.Sergeev, and V.Yu.Zaslavsky,* Powerful surface-wave oscillators with two-dimensional periodic structures // *Appl. Phys. Lett.* 100, 143510 (2012)
6. *N.S.Ginzburg, E.V.Ilyakov, I.S.Kulagin, et al.,* Theoretical and experimental studies of relativistic oversized Ka-band surface-wave oscillator based on 2D periodical corrugated structure // *Phys. Rev. AB.* V. **21**, 080701 (2018).

SIMULATION OF COMPONENTS FOR GYRO-DEVICES COUPLED IN A FEEDBACK LOOP TO GENERATE ULTRA-SHORT RF PULSES

A. Marek¹, K. A. Avramidis¹, S. M. Coplestone², N. S. Ginzburg³, S. Illy¹,
J. Jelonnek^{1,4}, J. Jin¹, P. Ortwein² and M. Thumm^{1,4}

¹IHM, ⁴IHE, Karlsruhe Institute of Technology (KIT), Karlsruhe, Germany

²Institute of Aerodynamics and Gas Dynamics, University of Stuttgart, Stuttgart, Germany

³Institute of Applied Physics, Russian Academy of Sciences (IAP- RAS), Nizhny Novgorod, Russia

Abstract - A periodic series of ultra-short pulses of millimeter and sub-millimeter waves can be generated in a microwave oscillator consisting of an amplifier and a saturable absorber. The pulse generation method is analogous to the method of passive mode locking, widely used in laser physics. In this work, simulation results for the different components of such a microwave oscillator are presented.

Introduction

In an ongoing joined RSF-DFG project led by the Institute of Applied Physics (IAP-RAS) supported by the Institute for Pulsed Power and Microwave Technology (IHM-KIT), the generation of a periodic sequence of powerful, ultra-short RF pulses is studied [1]. Such powerful pulses of millimeter and sub-millimeter waves can be useful for a number of fundamental problems and practical applications, including DNP-NMR spectroscopy, diagnostics of plasmas, photochemistry, biophysics and new locating systems.

In [1], it is proposed to generate a periodic sequence of coherent pulses with high power in the millimeter frequency range by a feedback loop consisting of an amplifier and a non-linear saturable absorber. The saturable absorber acts as a non-linear filter which transmits high intensity signals, while signals with low intensity are strongly attenuated. In such a feedback loop, the periodic signal is generated by the mechanism of passive mode locking, well known from laser physics [2]. For millimeter waves, gyro-devices e.g. the gyro-traveling-wave-tube (gyro-TWT) are well suited for the realization of both, the amplifier and the nonlinear absorber.

Quasi-Optical Feedback System

The coupling of the two gyro-devices can be obtained by a quasi-optical mirror system. Both, amplifier and absorber will be realized as devices with a single window for the input and output of the signal. This feature simplifies the quasi-optical feedback system. A quasi-optical feedback system is shown in figure 1. To separate a fraction of the signal oscillating in the feedback loop, a semi-transparent mirror is required. For optimum operation of the microwave oscillator, the decoupling should take place only on the signal trail from the absorber to the amplifier. This requires a separation of the signal paths “amplifier to absorber” and “absorber to

amplifier”. For this purpose the polarization characteristic of helical gyro-TWTs in single window operation can be utilized. The output signal is cross-polarized to the input signal and therefore, a polarization splitter can be used to separate the input and output signals.

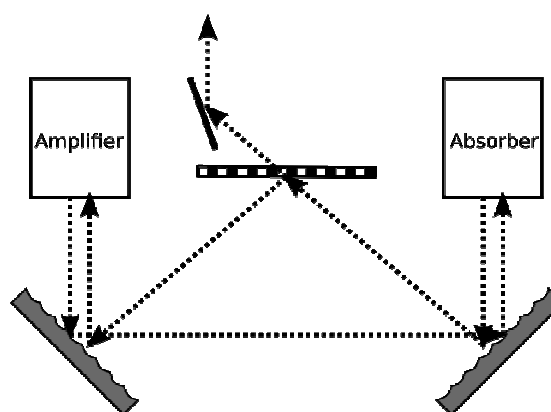


Fig. 1. Amplifier and absorber devices working with single input-output window coupled with a quasi-optical mirror system.

Polarization Splitter

The polarization splitter used for the separation of the input and output signals has to fulfill three major requirements: (1) suited for high power signals, (2) broad bandwidth and (3) simple to manufacture. These requirements can be fulfilled by mirrors with sinusoidal grating [3]. The simulation results show that for an assumed center frequency of 260 GHz and a required power efficiency of more than 97 %, a bandwidth of 20 GHz can be realized. To improve the beam parameters, the sinusoidal grating can be combined with a parabolic shape.

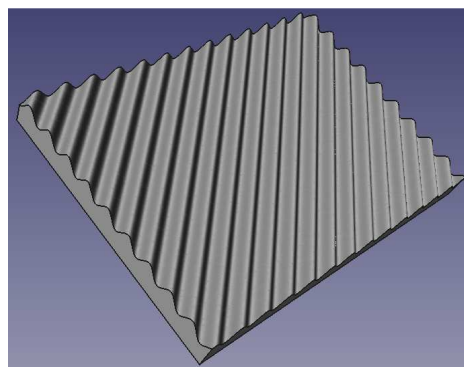


Fig. 2. Polarization splitter with sinusoidal grating.

Semi-Transparent Mirror

A semi-transparent mirror can be realized as a polarizing beam-splitter based on a stack of rectangular metal plates as described in [4]. In an experimental setup, a semi-transparent mirror based on a polarization beam-splitter has the advantage that the reflection coefficient can easily be adjusted by rotating the beam-splitter relative to the beam. In addition, it is possible to apply a slight parabolic shape to the polarization splitter. This allows improving the beam parameters of the reflected signal.

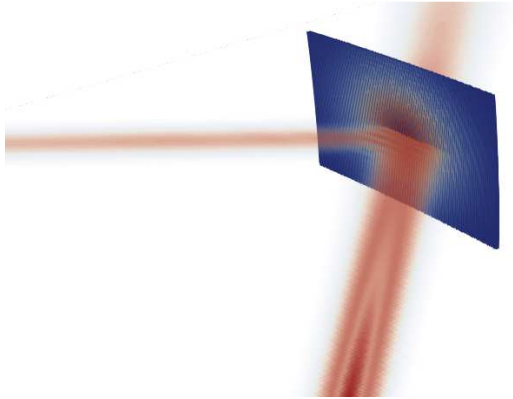


Fig. 3. Polarizing beam-splitter as semi-transparent mirror. A parabolic shape improves the parameters of the reflected beam.

Gyro-TWT as Saturable Absorber

A well suited technology for the high power RF amplifier and the non-linear saturable absorber are gyro-TWTs with helical interaction regions [5]. These devices provide a series of advantages compared to classical gyro-TWTs based on cylindrical interaction circuits with dielectric losses. The helical gyro-TWTs can operate at the 2nd cyclotron harmonic and, therefore, the required magnetic field is reduced by the factor of 2 compared to classical gyro-TWTs operating at the fundamental cyclotron harmonic. Further advantages are the broader bandwidth and the lower sensitivity to velocity spread of the electron beam.

For full-wave PIC simulations of the gyro-devices the advanced simulation program PICLas [6] is used. PICLas is developed by the Institute of Aerodynamics and Gas Dynamics (IAG) at the University of Stuttgart. In the following, simulation results of an absorber as suggested in [7] for a feedback loop at a center frequency of 30 GHz are discussed. The suggested feedback loop is designed to provide pulses with a peak-power up to 400 kW and a pulse-width of only 0.25 ns by a separation of 5-10 ns [7]. The absorber has a mean waveguide radius of 0.4 cm with a corrugation of amplitude 0.1 cm and a periodicity of 1.0 cm. The electron beam has a beam voltage of 54 kV, a current of 2.4 A and a pitch factor of 0.53. In figure 4, the simulated transmission coefficient for short Gaussian pulses with different peak powers is

shown. While weak signals are almost completely absorbed, high power signals are only weakly attenuated. Therefore, the simulations proof the qualification of gyro-TWTs operating in the Kompfner dip regime as saturable absorbers.

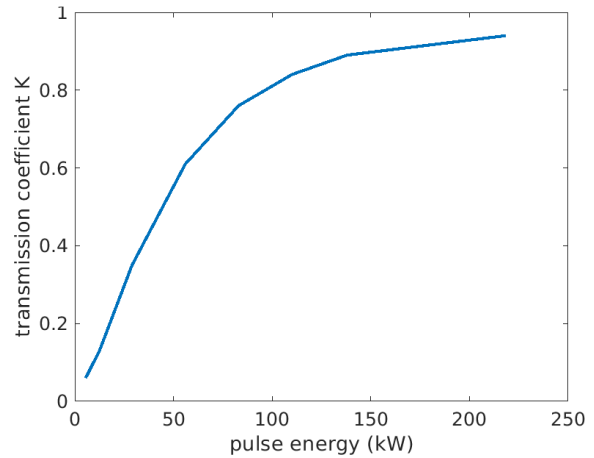


Fig. 4. Transmission coefficient versus power of the incident signal for a helical gyro-TWT operating in the Kompfner dip regime.

Acknowledgements

The authors would like to express their gratitude to the Deutsche Forschungsgemeinschaft (DFG) and the Russian Science Foundation (RSF) for the support of this work which is ongoing within the joint RSF-DFG project (Je 711/1-1, 16-42-01078) "Generation of Ultrashort Pulses in Millimeter and Submillimeter Bands for Spectroscopy and Diagnostic of Various Media Based on Passive Mode-locking in Electronic Devices with Nonlinear Cyclotron Absorber in the Feedback Loop".

References

1. Ginzburg, N. S., et al. "Generation of a periodic sequence of powerful ultrashort pulses in a traveling wave tube with bleachable absorber in the feedback loop." *Technical Physics Letters* 41.9 (2015): 836-839.
2. Hermiann, J., and B. Wilhelmi. "Laser fir Ultrakurze Lichtimpulse." *Akademie-Verlag, Berlin* (1984).
3. Samsonov, S. V., et al. "Quasi-Optical Orthomode Splitters for Input-Output of a Powerful W-Band Gyro-TWT." *IEEE Transactions on Electron Devices* 99 (2018): 1-7.
4. Mendis, Rajind, et al. "Artificial dielectric polarizing-beamsplitter and isolator for the terahertz region." *Scientific Reports* 7.1 (2017): 5909.
5. Denisov, Gregory G., et al. "Microwave system for feeding and extracting power to and from a gyrotron traveling-wave tube through one window." *IEEE Electron Device Letters* 35.7 (2014): 789-791.
6. Munz, Claus-Dieter, et al. "Coupled particle-in-cell and direct simulation Monte Carlo method for simulating reactive plasma flows." *Comptes Rendus Mécanique* 342.10-11 (2014): 662-670.
7. Ginzburg, Naum S., et al. "Ultrawideband Millimeter-Wave Oscillators Based on Two Coupled Gyro-TWTs With Helical Waveguide." *IEEE Transactions on Electron Devices* 65.6 (2018): 2334-2339.

UNKNOWN PECULIARITY OF THE OROTRON TWO ROW PERIODIC STRUCTURE

Myasin E.A., Solov`ev A.N.

Fryazino branch of the Kotel'nikov Institute of Radioengineering and Electronics of RAS

Russian Federation, 141190, Moscow region, Fryazino, Vvedevskogo sq., 1.

eam168@ms.ire.rssi.ru

The calculation results of the electrodynamic characteristics (EDCH) of open resonators (OR), formed by the multifocus spherical and plane mirrors are presented in this work. These calculations were fulfilled early [1] for OR plane mirror without periodic structure (PS), with PS with $\lambda/4$ "b₀" comb and PS with "b₀" $\lambda/2$ comb, where λ is wave length. The PS with comb $\lambda/4 < b_0 < \lambda/2$ ("intermediate") will be investigated in this work. The EDCH calculation results will be represented for last PS. Two last PS are double row periodic structure (DRPS). The multifocus focusing mirror with the focuses number N_f and with constant distance L_c between first and last focuses will be used. Distance between the next focuses is $L_f = L_c/(N_f - 1)$.

The calculations are performed for the TEM_{00q} fundamental modes (q is the number of half wavelengths along the height of the resonator) at the wavelength from $\lambda \approx 1$ mm to 1.8 mm with the use of Program complex CST Microwave Studio [2].

1. The construction of the orotron with DRPS and the long interaction length.

Scheme of the orotron construction with the focusing five-focus mirror is represented on Fig.1. This mirror is created as the crossing spherical surfaces with equal R_0 radius. Distance between symmetric axis of these surfaces is chosen to supply the Gaussian HF field distribution along an electron beam at the beginning of interaction region, in order to obtain the smooth HF field distribution and the Gaussian HF field distribution at the end of interaction region.

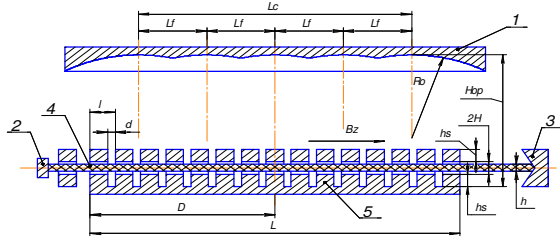


Fig.1. Scheme of the orotron construction with five-focus focusing mirror:

Here 1 - the focusing mirror in the OR, 2 - the electron gun, 3 - collector, 4 - the electron flow, and 5 - a plane mirror.

The DRPS with period I , slot d between the projections, the ratio $d/I = 0.5$, and the distance $2H$ between the rows for the electron transit is located on plane mirror 5 (see Fig. 1). The DRPS occupies the entire surface of the plane mirror. The distance between mirrors is H_{OR} . Focusing magnetic field B_z is aligned with the Z axis.

2. Initial data for calculations

At first wavelength is $\lambda \approx 1$ mm. The curvature radius of the spherical mirror is $R_0 = 65$ mm and the height is $H_{OR} = 2.5$ mm. Hence, at the approximate wavelength value $\lambda = 1$ mm, the caustic radius is $r_c = 1.995$ mm according work [3] for the fundamental oscillation type TEM_{00q} excited in the OR, which is formed by the focusing and plane mirrors. The relatively small height of the OR is used in order to minimize the calculation time. Multifocus mirror is used in which the number of N_f focuses changes from 5 to 11 but distance between the first and last focuses is constant and equal 20 mm ($10r_c$). As it has been noted before, distance between the next focuses is $L_f = L_c/(N_f - 1)$. The wavelength changes from $\lambda \approx 1$ mm to 1.8 mm.

The DRPS with period $I = 0.182$ mm, slot d between the projections is 0.08 mm, the ratio $d/I = 0.5$, and the distance $2H = 0.1$ mm between the rows for the electron transit is located on plane mirror 5 (Fig. 1). The width $2C$ of transit canal is $4r_c$. Height of rows is 0.148 mm. Height of DRPS comb is $b_0 = 0.5$ mm for $b_0 = \lambda/2$ comb and $b_0 = 2h_z + 2H = 2 \times 0.148 + 0.1 = 0.396$ mm < 0.5 mm, if comb is $\lambda/4 < b_0 < \lambda/2$.

3. The calculation of the electrodynamic characteristics

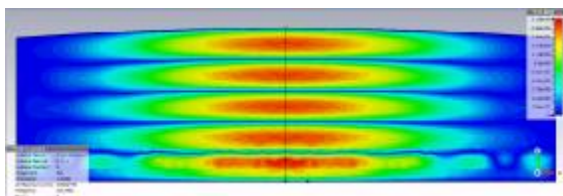
The electrodynamic characteristics (EDCH) of open resonators (OR), formed by the multifocus spherical and plane mirrors for DRPS with $b_0 < \lambda/2$, are calculated. These EDCH are the resonance frequencies f_0 , quality factor Q_0 , the norm N_r of the oscillations, the relative loss power - $P_{\Pi}/W = 2\pi f_0/Q_0$.

Firstly the dependence of OR electrodynamic parameters on the focus number N_f was fulfilled [4]. The results of computing show that when the "intermediate" comb is used in OR its proper quality factor is 1.4 times as much and relative losses power is 1.45 times as many in comparison to OR with "half-wave" comb and proper quality factor is 2.4

times as much and relative losses power is 2.4 times as many in comparison to OR with $\lambda/4$ comb. Then the calculations of dependence the OR electrodynamic parameters on comb height was fulfilled for OR with $N_f = 11$ from $h_z = 0.25$ mm ($\lambda/4$ comb) till $h_z = 0.5$ mm ($\lambda/2$ comb). Firstly for $h_z = 0.25$ mm and $h_z = 0.396$ mm and then for $0.4 \text{ mm} \leq h_z \leq 0.5$ mm with 0.02 mm step near $\lambda = 1$ mm. The optimal electrodynamic OR parameters for $H_{OR} = 2.5$ mm were fixed for $h_z = 0.396$ mm.

Electrodynamics OR parameters dependencies for “intermediate” comb with $h_z = 0.396$ mm on OR height $2.5 \text{ mm} \leq H_{OR} \leq 4$ mm were calculated with step 0.2 mm for 11 focus mirror. For every value of H_{OR} animation images and high frequency distribution on three axis: longitudinal Z along electron beam, transverse X and vertical Y parallel to OR symmetry axis. The most informative examples of Y axe distributions will be demonstrated here. It is interesting to observe the brightness changes along Y axis.

1) $H_{OR} = \lambda/2 = 2.5$ mm, $f_0 = 295,897$ GHz



g.1. Animation image of HF field E_{005} along Y axis

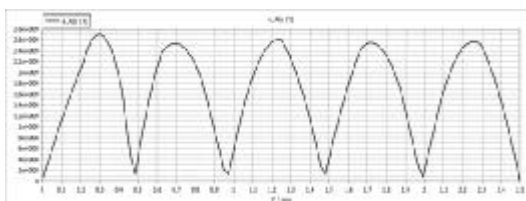


Fig.2. HF field vertical distribution (along y coordinate, $x=0, z=0$).

These types distributions along Y axis are repeated till $H_{OR} = 3$ mm

2) $H_{OR} = 3$ mm, $f_0 = 243,783$ GHz

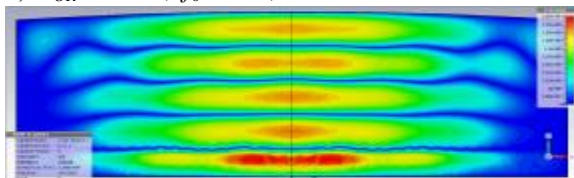


Fig.3. Animation image of HF field E_{005} along Y axis

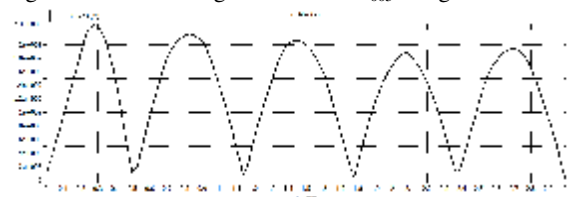


Fig.4. HF field vertical distribution (along y coordinate, $x=0, z=0$).

It is shown on Fig.3 the maximum of the brightness appears in transit canal, but this maximum is practically absent on HF field distribution on this axis (Fig. 4).

3) $H_{OR} = 3.2$ mm, $f_0 = 228,212$ GHz, $\lambda = 1.31$ mm

$b_0/\lambda = 0.396/1.31=0.302$

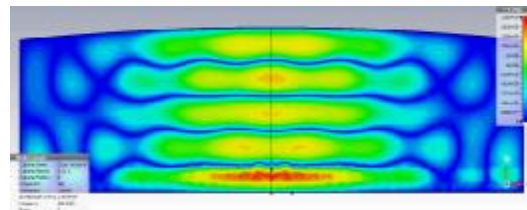


Fig.5. Animation image of HF field E_{005} along Y axis

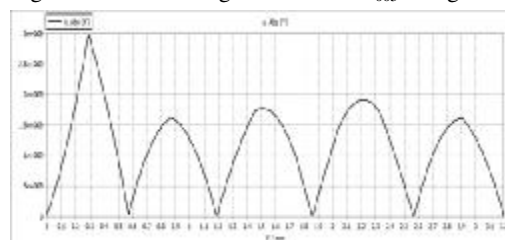


Fig.6. HF field vertical distribution (along y coordinate, $x=0, z=0$).

The same type distribution continues till $H_{OR} = 4$ mm.

Conclusion

As a result of analysis **it was established for the first time** that vertical HF field distribution in “intermediate” comb may be of “half-wave” type DRPS with $b_0 = \lambda/2$ or of “quarter-wave” comb type with $b_0 = \lambda/4$. Hence the $\lambda/4$ resonance takes place to increase the electron-wave interaction efficiency in orotron when b_0/λ is less than 0.3.

References

1. Myasin E.A., Solov'ev A.N. Analysis of electrodynamic characteristics for open resonators with the multifocusing spherical mirrors at wavelength 1 mm. //Radiotekhnika I electronica. 2018. V.63. N7. P.670-677 (in Russian).
2. Kurushin A.A., Plasticov A.N. Design of HF Devices in CST Microwave Studio medium// Moscow. MEI Izdatelstvo. 2010. 160 pp.
3. Vainshtein L. A., Open Resonators and Open Waveguides //Sovetskoe Radio, Moscow, 1966, 475 pp (in Russian).
4. Myasin E.A., Solov'ev A.N. Analysis of electrodynamic characteristics for open resonators with the multifocusing spherical mirrors at wavelength 1 mm. // Proc. 27-th Inter.. Crimian Conf. “HF technics and telecommunication technology”. 2017. V.1. P.170-177. Sevastopol. Crimea. Russia.

SUBTERAHERTZ OROTRON WITH ONE AND TWO ELECTRON BEAMS

¹Myasin E.A., ¹Evdokimov V.V., ¹И'yn A.Yu.

¹Fryazino branch of the Kotel'nikov Institute of Radioengineering and Electronics of Russian academy of sciences, 141190, Russian Federation, Moscow region, Fryazino, Vvedenskogo sq., 1
eam168@ms.ire.rssi.ru

Abstract: Experiments on output increasing in submillimeter orotron with double-row periodic structure (DRPS) and 5-focus spherocylindrical mirror open resonator (OR) were carried out. Additional electron beam was introduced near the upper row of DRPS. The mirror cylinder axes were perpendicular to the beam direction. The positive results depend on optimal OR-load coupling.

Keywords: Orotron, submillimeter wavelength range, open resonators, multifocusing spherocylindrical mirrors, double-row periodic structure.

1. Introduction

At present there is a strong trend to investigate the terahertz frequency range (or submillimeter wavelength range), see for example [1-4]. In these conditions the problem of orotron with DRPS power increase in this range is of great interest.

2. The objects of investigations and experimental method

The objects of investigation were the experimental specimens of orotrons with DRPS operating under continuous pumping. The period of DRPS was 0.182 mm, the thickness of first row elements was $b_1 = 0.154$ mm, in second row $b_2 = 0.147$ mm, the spacing of interaction channel was $2H = 0.1$ mm. So, the total size of PS was $b_0 = 0.401$ mm [5]. The OR plane mirror with first PS row had dimensions 34 x 19 mm. The focusing mirror of OR consisted of 5 spherocylinders with longitudinal axis perpendicular to the beam motion direction. The interfocusing distance was equal to 4.75 mm with cylindrical part 4 mm. The method of experiment was as noted below. Firstly the frequency tuning of a model of orotron with one electron beam passing inside the interaction channel was investigated. Then the new configuration of electron optical system was mounted to produce additional electron beam moving outside the upper row of PS. In this case the collector current registered was equal to the total current of two beams. This variant of electron optical system included special anode with two 0.1 mm slots and 0.15 mm bridge between them and was scrupulously adjusted to guarantee the 100% filling of interrow interaction channel. Cathode height in this case was equal to 4 mm to provide the forming of two electron beams. One can conclude the effect of second beam on output power increase by comparison of two operation regimes.

3. Estimation of second electron beam influence on electron-wave interaction and experimental results

In [6] the hypotheses about the possibility of electron-wave efficiency increase in orotron with DRPS when the second electron beam is introduced outside the upper DRPS row, i.e. on the distance b_0 from plane mirror. This preposition was based on the fact that if one can ignore the height $2H$ of interaction channel in comparison with two rows height, then orotron with DRPS is analogue of F.S.Rusin's orotron with $\lambda/4$ comb and so called "quote-wave resonance". In [7] the formulae for resonance dependence of space harmonic amplitude A_n to OR wave amplitude A_0 ratio on b_0/λ for OP formed by two plane mirrors. Fig.1 presents these dependencies for the 1-th, 3-d and 5-th space harmonics [8].

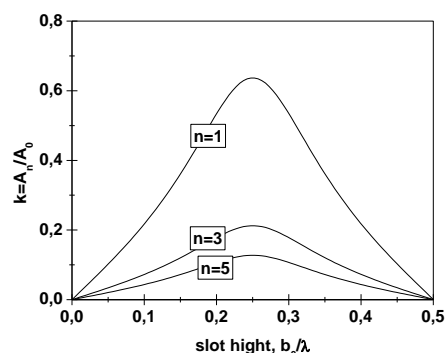


Fig. 1

In this Fig.1 we see, that for $\lambda = 0.88$ mm ($f \approx 340$ GHz) $b_0/\lambda = 0.4/0.88 = 0.45$ and $A_1/A_0 \sim 0.1$. Some increase in field amplitude (\sqrt{Q} fold) will be realized by resonance conditions. Electric component of HF field will be diminished as $\exp(-2\pi x/l)$ where x is the distance from upper row outside, l is the period of DRPS. As simple estimation shows the most effective is only thin (about $\Delta \leq 0.025$ mm) layer of second electron beam adjusting to the surface of upper row. It is important in this case that the height of upper DRPS row would be a little higher than the upper surface of anode "bridge". As experiment had showed this condition was fulfilled in "hot" regimes.

In Fig.2 results of orotron tuning with one and two electron beams are presented. Data $I_{col.1}$, P_1 , correspond to values of collector current and output power in orotron with one electron beam and data

$I_{col1}+I_{col2}$, $P1+P2$ – in orotron with two electron beams.

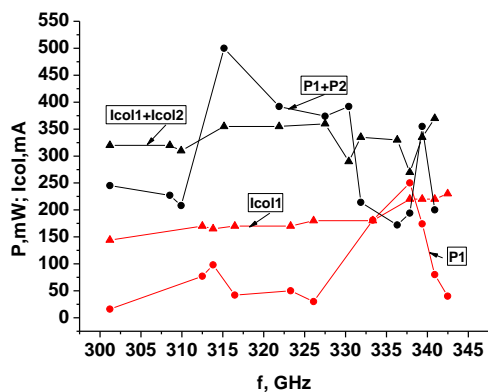


Fig.2

Fig.2 shows experimental results for coupling $D=3$ mm when the value of general current of two electron beams is twice its value in one-beam orotron. In this case the effect of additional electron beam on the increase of output power is more evident in 310 – 330 GHz frequency range when the OR – load coupling in one-beam orotron was not optimal. But in 332 – 337 GHz frequency range where this coupling was optimal one observes the abrupt decay of $P1+P2$ power with its minimum in $P1$ maximum. Then we can see its rise till the maximum near 340 GHz and slow decrease with frequency on the level exceeded that in one-beam orotron.

4. Conclusion

On the basis of experimental results received one can conclude that the introduction of additional electron beam outside the surface of upper DRPC row is sufficiently simple and effective method to increase the output power of the THz frequency range orotron. OR with multifocal spherocylindrical mirrors can be used. The search of optimal value of OR – load coupling coefficient is necessary to realize this effect as the increase of total collector current in two-beam orotron changes this coupling in comparison to one electron beam operation regimes.

Acknowledgements

Authors are grateful to Dyubua B. Tch. and Bat'kova T.A for making cathodes of experimental orotrons and Kazantsev Yu.N. for taking us developed interferometer for frequency measurements. The work was supported partly by Physics Sciences Department of RAS (Program “New sources of millimeter and terahertz radiation and its perspective applications).

References

1. Eremka V.D., Kuraev A.A., Sinitsin A.K. Orbotrons – multibeam generators of millimeter and submillimeter waves//Proc. Of 14-th Intern. Conf. CRIMICO'2004. Sevastopol,2004. P.199-202.
2. Bratman V.L., Ginsburg V.A., Grishin Yu.A., Dumesh V.S.,Rusin F.S.,Fedotov A.E. Pulse wideband millimeter and submillimeter orotrons //Izv.vusov. Radiophysics. 2006. V. 11, № 49. P. 958-963.
3. Glavin N.Yu., Zaval'skiy N.A., Zapevalov V.E., Moiseev M.A., Sedov A.S. Digital modeling of submillimeter gyrotrons on second harmonic of cyclotron frequency//, Izv.vusov. Radiophysics .2009, V.52, №5-6. P.408-417.
4. Zaval'skiy N.A., Zapevalov V.E., Moiseev M.A., Sedov A.S. Investigation of subterahertz gyrotrons for DPY spectroscopy in API of RAS// Izv.vusov.AND. 2012, V. 20, №3. P.70-80.
5. Myasin E.A. Orotron.// Patent RF № 2634304. 10.06. 2016
6. Myasin E.A., Evdokimov V.V., Il'yn A.Yu. Quoter-wave resonance in orotron with double-row periodic structure//. Thez.Dokl.All-Russia seminar on radiophysics of millimeter and submillimeter waves.12-15 Mars 2009. N.Novgorod .P45.
- 7 Rusin F.S. , Bogomolov G.D. Electronica bokshikh moshnostey.//Moscu. “Nauka”.1968, #5.P.38. (in Russian).
8. Myasin E.A. Orotron –high power O-type resonance generator of santimeter and millimeter wavelength range.//Radioterhnica.2004.#2.P.22. (in Russian).

THz generation from high-Q Fano metallic metamaterial

Seontae Kim¹, Gun-Sik Park^{1*}

¹Department of Physics and Astronomy, Seoul National University, Seoul, Korea, gunsik@snu.ac.kr

Ever since Cerenkov and two other scientists were awarded the Nobel prize in 1958 for their discovery of the luminescence of uranyl salt solutions under gamma-ray irradiation,[1] there has been continuing interest in understanding the interaction of moving charged particles with surrounding matter. The so called Cerenkov radiation (CR) is a cathodoluminescent phenomenon that occurs when a charged particle passes faster than the phase velocity of light traveling through a dielectric medium. Since its discovery, CR has been applied in various detection and radiation devices for medical imaging, therapy, novel light sources, and acceleration of particles.[2] Often, the development of such CR-based applications is limited by thermal and dielectric breakdown issues.[3,4] Another limitation is that, due to the velocity threshold, large facilities are required to generate highly energetic particles. These limitations restrict the upper and lower size and performance boundaries in vital applications. Nowadays, metallic metamaterial devices have been proposed, which overcome the limitations of conventional Cerenkov devices to realize reversed CR from the negative-refractive index, [5] the ultralow threshold of kinetic energy in hyperbolic metamaterials, [6] and various metallic metamaterials comprised of subwavelength slits. [7–9] However, the realization of a high quality factor (Q) is still an outstanding roadblock for practical Cerenkov devices. Previous works on Cerenkov lasing (CL) using mirrors were limited by a lower electron beam impedance due to the interaction device and the radio-frequency (RF) coupling mechanism. Here, to achieve a high Q for highly efficient CL, we focus on maximally trapping the electromagnetic Cerenkov radiation wave to extend its interaction with the electron beam and on controlling the radiation damping, as has been described in Rayleigh scattering to maximize the efficiency of CL. In this paper, we demonstrate that the interplay between an extremely low group velocity from the infinite transverse permittivity of the anisotropic metamaterials and the subradiant damping from Fano-type slit modes plays a key role in high- Q metallic metamaterials. The subwavelength metallic slits used to form asymmetric unit cells in the proposed material, in which waveguide modes are used to concentrate strong electromagnetic fields, can be considered as a Fano system that induces a strong asymmetric resonance. The asymmetric spectral signature of Fano resonances is described as the interference between the localized and propagating surface waves. The effective anisotropy of the metallic metamaterial induces a decrease in the group velocity and increases the local density of states to maximize the Q near the band edge. The optimum Q for optimum output RF coupling can be obtained by controlling the

radiation damping or Rayleigh scattering of the trapped electromagnetic wave based on structural asymmetries. The maximum Q was measured to be ≈ 700 , which is the highest value reported thus far in various Fano systems. As the moving electron beam interacts with the waveguide modes of the metallic metamaterial, dipole-like modes are induced at each slit aperture, leading to the formation of a surface wave, the phase velocity of which is adjusted to match that of the electron beam. The proposed high- Q metallic Fano metamaterial that realizes highly efficient CL without mirrors is a strong candidate for several practical applications, especially in very high frequency electronic devices.

We experimentally and theoretically demonstrated high- Q Fano resonances in metallic Fano metamaterials. In these materials, trapped light was slowed down due to the large effective anisotropy, and the subradiant damping resulting from a low structural asymmetry was responsible for the high- Q Fano resonances as they retained a large amount of electromagnetic energy in the narrow slits. As an example of an active device, we also demonstrated that the efficiency of CL was enhanced using this metallic Fano metamaterial. The Q of the Fano resonance is best optimized for maximum efficiency in CL, which is in good agreement with the results of recent theoretical works that employ two ideal mirrors with high reflectivity for describing the confinement and emission of CR. The Fano resonances in metallic metamaterials demonstrated in this study confirm that high- Q cavities can be realized for efficient CL. It is also interesting to note that our results confirming efficient CL with the enhancement of trapped light and a large Q/V , where V is the volume of the trapped light, are quite similar to the Purcell effect of enhanced spontaneous emission in a microcavity. The Q measured in this study was ≈ 700 , which validates our understanding of the operating conditions related to the convection of electrons. This will be experimentally explored further in future works. This high- Q metallic metamaterial with a collimated output scheme can be realized experimentally similarly done in the vacuum electron device such as backward-wave oscillators. Also this high- Q metallic metamaterial can be considered to be scalable to terahertz/IR/optical frequencies. The relatively lower Q -factor is expected for the device with IR/optical frequencies due to the plasmonic Fano resonance than one with terahertz frequency. Q -value of few hundreds is predicted in the device with terahertz frequency. Q of this structure can become much larger on adjusting the geometric parameters for other applications, such as switching, sensing, subdiffraction focusing, and collimated emission. The asymmetries

can also be described as “well-controlled” structural disorder that interplay with the periodicity-induced scattering of light and lead to the strong localization of light in disordered periodic media in Fano systems.

The Fano resonances in this metamaterial is formed by two different paths of scattered light. The first is the ordinary Fabry–Perot (FP) resonance that results from direct and nonresonant scattering. The broad part of the spectral lines in Figure 1 shows the FP scattering background in the transmission spectrum T_{FP} with $\Delta_x = \Delta_y = 0$. The FP resonance is formed by dipole-like scattering of propagating waveguide modes at the apertures of the subwavelength slits. Given the subwavelength condition, the scattering caused by the array of dipoles can be effectively described as a Fresnel coefficient under p-polarized incidence, as shown previous studies of the transmission spectrum and Brewster angle. The second scattered light path is due to the diffractive coupling of the incoming waves to the trapped modes. The trapped modes are formed by nearfield coupling among the waveguide modes. The trapped modes then experience radiative damping caused by the asymmetry and thus emit far-field electromagnetic waves to free space. The dipole scattering of the trapped modes due to the structural asymmetry is responsible for the formation of Fano resonances T_F that interfere with FP scattered waves.

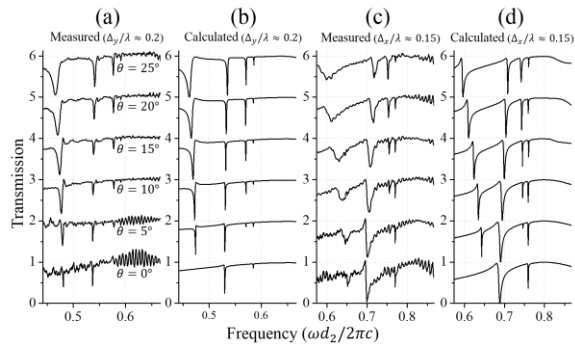


Fig. 1. Dependence of the incidence angle on the Q of the Fano resonances and its relationship with band-gap formation. (a)–(d) Transmission results with different angles of incidence and structural asymmetries. The four sharp dips ($m = -2, -1, +1, +2$) represent the excitation of the Fano resonance by capturing the p-polarized incident wave.

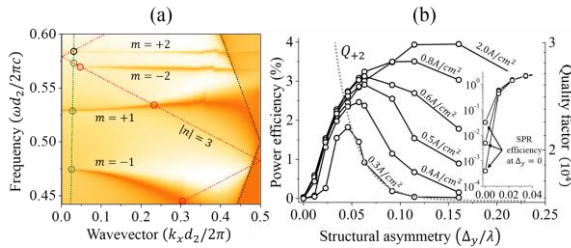


Fig. 2. Description of CL in the metallic Fano metamaterial. (a) Dispersion diagram of the Fano resonances with space-charge evanescent (red) and radiative (green) modes. The light lines are shown as black dotted lines and the red hollow circles represent the spectral positions of the electrons interacting with the trapped modes that result in Cerenkov

radiation in this metallic metamaterial. The green hollow circles represent the spectral positions of the Fano resonances with radiation damping. (b) The power efficiency (radiation power divided by voltage (10.431 keV) and current (6–40 mA based on a 10-mm width of the sheet electron beam) as a function of the asymmetry.

References

1. a) P. A. Cherenkov, Dokl. Akad. Nauk SSSR 1934, 2, 451; b) F. J. Garcia De Abajo, Rev. Mod. Phys. 2010, 82, 209.
2. a) T. M. Shaffer, E. C. Pratt, J. Grimm, Nat. Nanotechnol. 2017, 12, 106; b) M. Silveirinha, Nat. Photonics 2017, 11, 269; c) G. Andonian, D. Stratakis, M. Babzien, S. Barber, M. Fedurin, E. Hemsing, K. Kusche, P. Muggli, B. O’Shea, X. Wei, O. Williams, V. Yakimenko, J. B. Rosenzweig, Phys. Rev. Lett. 2012, 108, 244801.
3. M. C. Thompson, H. Badakov, A. M. Cook, J. B. Rosenzweig, R. Tikhoplav, G. Travish, I. Blumenfeld, M. J. Hogan, R. Ischebeck, N. Kirby, R. Siemann, D. Walz, P. Muggli, A. Scott, R. B. Yoder, Phys. Rev. Lett. 2008, 100, 214801.
4. I. J. Owens, J. H. Brownell, J. Appl. Phys. 2005, 97, 104915.
5. Z. Duan, X. Tang, Z. Wang, Y. Zhang, X. Chen, M. Chen, Y. Gong, Nat. Commun. 2017, 8, 14901.
6. F. Liu, L. Xiao, Y. Ye, M. Wang, K. Cui, X. Feng, W. Zhang, Y. Huang, Nat. Photonics 2017, 11, 289.
7. N. A. Vinokurov, Y. U. Jeong, Phys. Rev. Lett. 2013, 110, 064805.
8. A. Bera, R. K. Barik, M. Sattarov, O. Kwon, S.-H. Min, I.-K. Baek, S. Kim, J.-K. So, G.-S. Park, Opt. Express 2014, 22, 3039.
9. J. K. So, J. H. Won, M. A. Sattarov, S. H. Bak, K. H. Jang, G. S. Park, D. S. Kim, F. J. Garcia-Vidal, Appl. Phys. Lett. 2010, 97, 151107.
10. S. Kim, I.-K. Baek, R. Bhattacharya, D. Hong, M. Sattarov, A. Bera, J.-K. So, D.-S. Kim, G.-S. Park, Adv. Opt. Mat., June (2018)

Towards Fully Automated Systems for the Generation of Very High Order Modes in Oversized Waveguides

T. Ruess¹, K. A. Avramidis¹, M. Fuchs, G. Gantenbein¹, S. Illy¹, F.-C. Lutz¹, A. Marek¹, S. Ruess^{1,2}, T. Rzesnicki¹, M. Thumm^{1,2}, D. Wagner³, J. Weggen¹, and J. Jelonnek^{1,2}

¹IHM, ²IHE, Karlsruhe Institute of Technology (KIT), Kaiserstr. 12, D-76131 Karlsruhe, Germany

³Max Planck Institute for Plasma Physics, Boltzmannstr. 2, D-85748 Garching, Germany

Introduction

Fusion plasma experiments require very powerful heating systems to achieve the needed high plasma temperatures. For Electron Cyclotron Resonance Heating and Current Drive (ECRH&CD), the gyrotron oscillator is the only known source which is capable to produce a megawatt-level RF output power [1] in the range from 30 GHz up to 300 GHz for a possible future DEMO EC heating system. The excitation of the main operating mode in the gyrotron cavity and the separation of this mode from the different possible competing modes is a very challenging task due to the very high order of that modes. A similar problem exists for the excitation of the wanted high-order mode in low-power test systems to validate the quasi-optical output system of that kind of gyrotrons. But, the availability of such a test system is vital during the gyrotron design and validation phases. Particularly, the launcher of the quasi-optical output coupler, which converts the rotating high-order operating cavity mode into a linearly polarized Gaussian output beam, is the critical component here. The existing test set-up at Karlsruhe Institute of Technology (KIT) which basic idea bases on [2], includes a quasi-optical mode generator using fully manually operated mechanical sliding units [3]. Obviously, those manual sliding units suffer from a large hysteresis, hence, require a very time-consuming adjustment. Here the first steps towards a fully automated test system are presented.

First steps towards a fully automated mode generator setup

Moving towards a fully automated test system at KIT required three major steps: the introduction of a fully automated mechanical adjustment of the mode generator, the replacement of the frequency multiplier and harmonic mixer [4] by a new vector network analyzer which is even capable to cover the complete frequency range from 140 GHz to 330 GHz using different frequency extension modules and an intelligent algorithm which finds autonomous a setup configuration to excite the correct mode.

The sliding units were to replace by two precision linear stages, as depicted in Fig. 1, which can be handled by a computer. It allows to run experiments including an adjustment of the quasi-parabolic (q.-p.) mirror system without any human attendance.

The proposed system has been validated by the excitation of the TE_{28,8}-mode at 140 GHz used for the

1 MW, CW gyrotrons for the stellarator W7-X at IPP Greifswald, Germany [5]. Recently, an upgraded 1.5 MW version of this gyrotron, with the possibility of operation also at 175 GHz, is under discussion. Therefore, a mode generator cavity for the TE_{28,10}/TE_{36,12}-cavity modes operating at 140/175 GHz, respectively, has been designed, fabricated and successfully tested [6]. The cavity of the generator contains an inner conductor and is especially designed for the low power measurement setup. Its design has been studied and optimized employing a scattering matrix code [7]. A frequency shift occurs due to the perforated midsection area. First results are shown in [6], where the operation frequency are determined at 140.155 GHz and 175.992 GHz. The remaining frequency shift of around 155 MHz can be eliminated by increasing the radius of the inner rod which leads to a lower eigenvalue and thus a lower frequency. The measured TE_{28,10} mode pattern at 140.01 GHz is shown in Fig. 2 and 3. The highest mode content is determined by 92.2 % and the counter-rotating amount is calculated to be 0.57 %. The designed quality factor is 2506 and is in very good agreement with the measured 2522. The adjustment of this mode was done using the old setup, as well. The comparison show, that a time saving of more than 94 % is achieved using the new setup with the advanced algorithm.

Recently, programs for the determination of the frequency, acquisition of the mode pattern and the mode pattern evaluation are running separately. In the future, those programs will run sequential and an already written intelligent algorithm makes the decision if the acquired mode pattern is matching to the theoretical one or not. The algorithm has two main functions, namely (i) finding the ideal position for the q.-p. mirror and (ii) the determination of the mode and its quality. Regarding point (ii), five techniques are

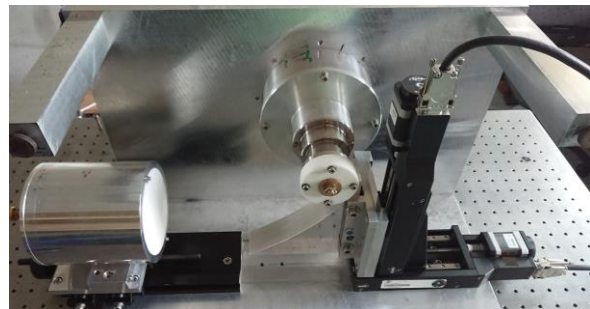


Fig. 1. Depiction of the mode generator setup.

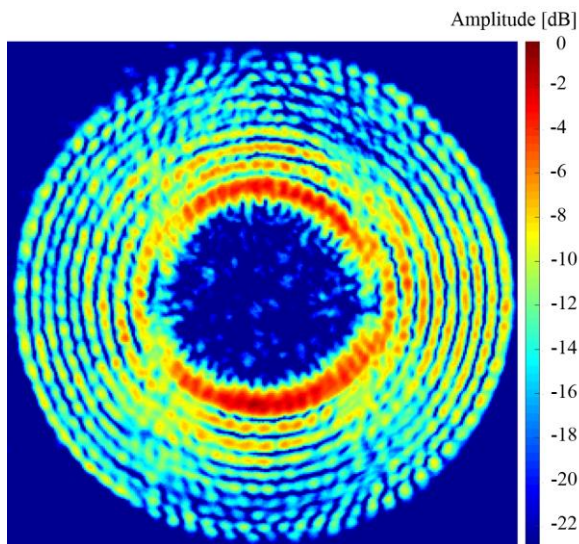


Fig. 2. Amplitude pattern of the TE_{28,10}-mode at 140.01 GHz with a resolution of the measurement arm of 0.2x0.2 mm.

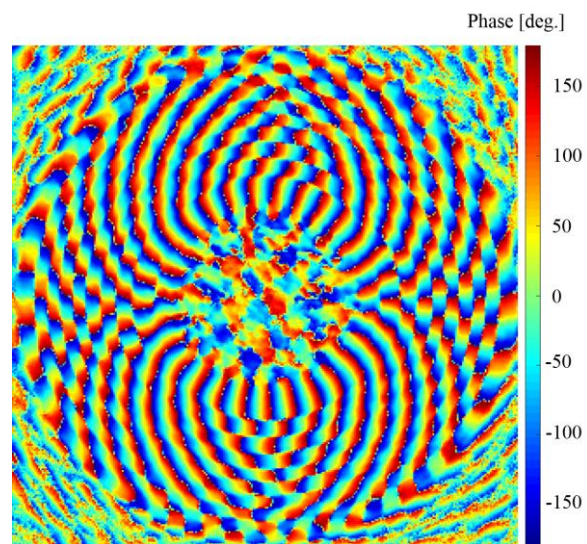


Fig. 3. Phase diagram of the TE_{28,10} mode pattern at 140.01 GHz with a resolution of the measurement arm of 0.2x0.2 mm.

implemented. It can determine the radial index by counting the number of rings and the azimuthal mode index by evaluating the phase jumps. Further, the scalar mode content, the quality factor and the amount of the counter-rotating mode are calculated.

Tolerance study of the quasi-parabolic mirror

The adjustment of the q.-p. mirror is the most important parameter for a correct excitation of the mode. A tolerance study has been started proving the required adjustment accuracy. The precision linear tables under use have a position error of < 25 μm/100 mm and a repetition failure (bidirectional) of < 15 μm. For this study, different q.-p. mirror positions are tested and the scalar mode content and the amount of the counter-rotating mode is calculated at each position and summarized in Tab. 1. Any deviation in x- and y-direction can be assumed and measured using the two precision linear tables. The values Δx and Δy are the differences between the actual and the ideal position. A deviation

Tab. 1. Summary of the tolerance study regarding different positions of the q.-p. mirror in respect to the ideal one.

ID	Δx [mm]	Δy [mm]	Scalar mode content [%]	counter-rotating mode [%]
1	0.0	0.0	92.2	0.57
2	-0.8	0.0	88.6	4.15
3	-0.8	+0.7	90.2	1.43
4	-0.4	0.0	91.0	1.25
5	-0.4	+0.7	92.0	1.13
6	0	+0.7	92.0	1.05
7	-0.2	-0.2	91.5	1.51
8	-0.2	0.0	91.1	1.35
9	-0.8	-0.2	92.1	1.00
10	-0.8	0.0	92.1	1.05

of Δx = 3 mm leads to a mode pattern where several modes are superimposed and no dominant mode could be identified. A deviation of Δx = 1.5 mm leads to a mode pattern where several modes are superimposed as well, but the TE_{28,10}-mode could be identified as dominant. Nevertheless, the quality is not sufficient. In general, a deviation of the ideal mirror position reduces the scalar mode content and increases the amount of the counter-rotating mode. But, the impact of a deviation of roughly 0.8 mm is not incredible high for this specific cavity, as can be seen in Tab. 1. In the next steps, further tolerance analysis will be made.

References

1. Rzesnicki, T. et al., 2.2-MW record power of the 170-GHz european pre-prototype coaxial-cavity gyrotron for ITER // *IEEE Trans. on Plasma Science*, Vol. 38, No. 6, pp. 1141-1149, 2010.
2. Alexandrov, N. L. et al., Low-power excitation of gyrotron-type modes in a cylindrical waveguide using quasi-optical techniques // *Int. Journal of Electronics*, 79, pp. 215-216, 1995.
3. Ruess, T. et al, 2018 status on the measurement capabilities for fusion gyrotrons at KIT/IHM // *30th Joint Russian-German Meeting on ECRH and Gyrotrons*, EPJ Web of Conferences (2018).
4. Losert, M., Jin, J. and Rzesnicki, T. RF beam parameter measurements of quasi-optical mode converters in the mw range // *IEEE Trans. On Plasma Science*, vol. 41, no. 3, 2013.
5. Braune, H. et al., Gyrotron operation during the first W7-X campaign – handling and reliability // in *Proc. IRMMW*, Copenhagen, Denmark, pp. 1-2, 2013.
6. Avramidis, K. A. et al., Studies towards an upgraded 1.5 MW gyrotron for W7-X // *20th Joint Workshop on Electron Cyclotron Emission (ECE) and Electron Cyclotron Resonance Heating (ECRH)*, Greifswald, Germany, May 2018.
7. Wagner, D., Pretterebner, J., Thumm, M., Design of coaxial gyrotron cavities using a scattering matrix code // *5th Joint Russian-German Meeting on ECRH and Gyrotrons*, pp. 555-565, 1993.

Gyrotron mm-wave radiation for dense plasma fluxes production from ECR discharge in a single solenoid

S.V. Golubev, R.A. Shaposhnikov, I.V. Izotov, R.L. Lapin, S.V. Razin,
A.V. Sidorov, V.A. Skalyga

Federal Research Center Institute of Applied Physics of the Russian Academy of Sciences, Nizhny Novgorod,
Russian Federation, shaposhnikov-roma@mail.ru

Electron-cyclotron resonance (ECR) ion sources are one of the most widespread types of systems for producing ion beams. Previous experiments in IAP RAS were aimed at creating sources of multiply charged ions with a high plasma density in such magnetic field configurations as open magnetic trap and cusp. It was demonstrated that in such systems the electron concentration can reach values $[10]^{13} \text{ [cm]}^{-3}$, electron temperature at the level of 100 eV, and the ion beam current has record values up to 500 mA [1-3]. System which is based on the ECR discharge in one solenoid magnetic fields has prospects for producing sources of singly charged ions and formation of plasma fluxes with large apertures as an alternative to existing magnetic plasma confinement systems. This paper is concerned with an experimental investigation the transversal plasma fluxes distribution and measurements of plasma parameters obtained in the ECR discharge in a single magnetic coil sustained by a powerful millimeter-wave gyrotron radiation.

The experiments were carried out at the IAP RAS on facility SMIS 37 (see fig.1), partly modified the single coil studies. Gyrotron radiation at the frequency of 37.5 GHz with the power up to 100 kW and pulse duration up to 1.5 ms was used for electron heating and discharge ignition. The microwave radiation is launched through a quasioptical system into the discharge chamber with diameter of 68 mm and 250 mm long placed inside pulsed magnetic coil. Magnetic field in the center of the coil varies from 1 to 4 T. ECR value of magnetic field for the frequency of external electromagnetic radiation 37.5 GHz is 1.34 T. The operating gas (hydrogen) was inlet into the discharge chamber in pulsed mode along the axis of the magnetic system through a gas-entry system integrated into the electrodynamic system for microwave radiation injection. To control neutral gas inlet the pressure in the gas buffer chamber above the gas valve was varied from 0.25 atm. up to 0.92 atm.

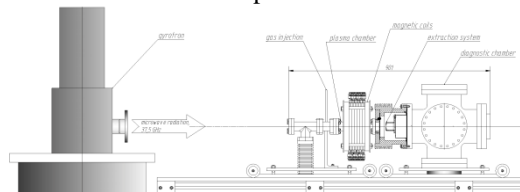


Fig.1 The scheme of experimental facility SMIS 37.

The first experiments were aimed to determine breakdown conditions in this system. At the first step experiments with a constant neutral gas injection were

performed to study the possibility of the discharge ignition and to determine a threshold microwave power for it at various pressures. Breakdown curve plotted according to the experimental data is shown in fig.2. Also it was demonstrated that discharge could be realized only if maximum magnetic field in the chamber is above ECR value.

The second part of the experiments was aimed to measurements of transverse profile of the plasma flux outgoing along the axis of magnetic system. During the experiments, the parameters of the system were optimized in such a way as to achieve the most homogeneous plasma flux radial distribution. The measurements were carried out using a Langmuir probe moved both in the radial and in the axial directions. As a result of experiments, the plasma flux profiles were measured at various distances from the center of the magnetic coil.

Example of the radial plasma flux distribution at the distances from the center of the magnetic coil of 31 cm, 21 cm, 12 cm, 10 cm and 8 cm at gyrotron power $Q=100$ kW and at the value of magnetic field at the center of the probe $B_c=2.16$ T is shown in fig. 3. The vertical axis represents the density of the plasma flux, the horizontal axis represents the radial coordinate.

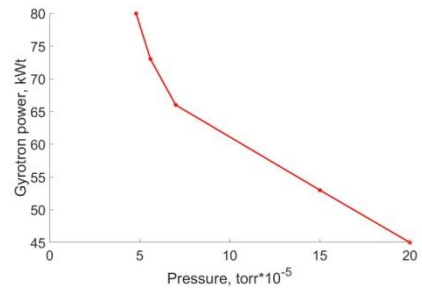


Fig. 2. Breakdown threshold curve for hydrogen

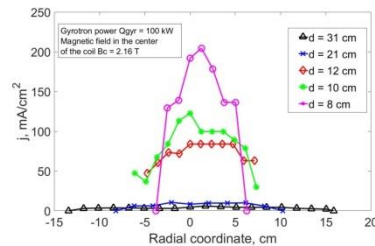


Fig 3. Plasma flux distribution in a cross section, d- distance between the probe and the centre of the coil.

The third part of the experiments was devoted to measuring the plasma parameters obtained as a result of the ECR discharge in the magnetic field of a single solenoid. During the experiments, the plasma density was measured at a distance of 31 cm from the center of the magnetic coil at different gyrotron powers, result is presented in fig. 4. It is clearly seen from the dependence that the plasma density in the discharge increases with the microwave power and reach values $[10]^{10} \text{ [cm]}^{-3}$. Measurements of the plasma density at various magnetic fields were also done. It is clear from the fig. 5 that plasma density increases with the growth of the magnetic field.

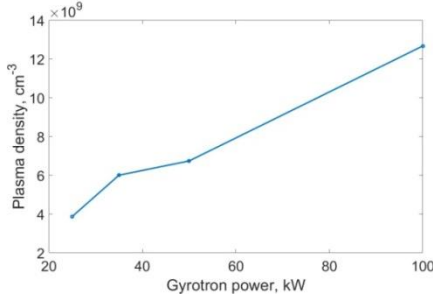


Fig. 4. Dependence of plasma density on the gyrotron power, $d = 31 \text{ cm}$

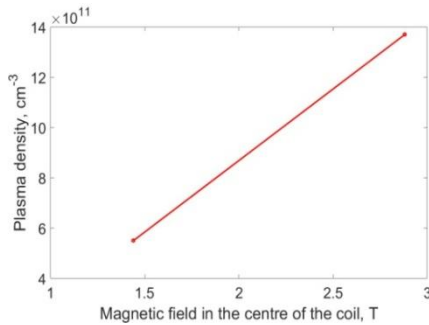


Fig 5. Dependence of plasma density on magnetic field.

The final part of the experiments was concerned with optimization of system parameters on purpose to obtain the maximum electron density in the discharge and to measure the current density of the ion beam. The maximum electron density in the center of the magnetic coil obtained in the experiments was $Ne_{max} = 2 \cdot 10^{13} \text{ cm}^{-3}$, and the electron temperature was in the range 10-30 eV. The ion beam current

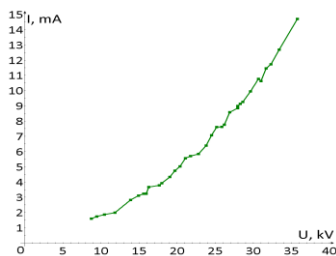


Fig 6. Ion beam current dependence on the extraction voltage.

reached 15 mA through a hole with a diameter of 1 mm, which corresponds to the ion current density of $j_{max} \approx 1.5 \text{ A/cm}^2$.

Conclusion

Experimental results obtained during the investigation of ECR discharge in one solenoid magnetic field demonstrated the possibility of producing wide-aperture plasma fluxes with a homogeneous radial distribution at different distances from the magnetic coil. It was also demonstrated that the plasma density increases with gyrotron power and magnetic field. As a result of the experiment parameters optimization plasma density of $Ne_{max} = 2 \cdot 10^{13} \text{ cm}^{-3}$ and the electron temperature at the level of $Te \approx 10\text{-}30 \text{ eV}$ were obtained. Density of ion current extracted through the 1mm hole reached record values $j_{max} \approx 1.5 \text{ A/cm}^2$. Thus, these experimental results demonstrate that such system has clear prospects for producing of a wide-aperture plasma fluxes with high current density.

Acknowledgments

Presented work was supported by the grant of Russian Foundation for Basic Research # 18-32-00419

References

1. S. Golubev, I. Izotov, S. Razin, A. Sidorov, V. Skalyga, A. Vodopyanov, V. Zorin, A. Bokhanov. High Current ECR Source of Multicharged Ion Beams. Nuclear Instruments and Methods in Physics Research B, v. 256, p. 537 – 542 (2007).
2. A. Sidorov, M. Dorf, A. Bokhanov, I. Izotov, S. Razin, V. Skalyga, V. Zorin, A. Balabaev, P Spädtke, J. Roßbach. Multi-aperture ion beam extraction from gas-dynamic electron cyclotron resonance source of multicharged ions. Review of Scientific Instruments, 79, 02A317 (2008).
3. V. Skalyga, I. Izotov, S. Razin, A. Sidorov, S. Golubev, T. Kalvas, H. Koivisto, and O. Tarvainen. High current proton beams production at Simple Mirror Ion Source 37. Review of Scientific Instruments, v. 85, no. 2, p. 02A702-1 – 02A702-3 (2014).

Study of mutual phase locking of two gyrotrons coupled with delay

A.B. Adilova¹, N.M. Ryskin^{1,2}

¹Saratov State University, Saratov, Russia, adilovaab@gmail.com

²Saratov Branch, Institute of Radio Engineering and Electronics, Saratov, Russia

Introduction

The most important application of high-power continuous-wave (CW) gyrotrons is electron cyclotron plasma heating for nuclear fusion [1]. For such application, a large number of gyrotrons should be used to obtain a very high power. For example, in ITER it is planned to use 26 gyrotrons with 1 MW power level. Providing coherence of radiation of large number of high-power microwave sources is a challenging task. One of the possible solutions is either injection locking by external master oscillator with stabilized frequency [2],[3] or mutual phase locking [4].

In this paper, we present the results of theoretical analysis and numerical simulation of mutual phase locking of two coupled gyrotrons.

Modified quasilinear model

In [5], we developed a basic theory of mutual phase locking of two limit-cycle oscillators coupled with delay. The delay in coupling provides essential features of the pattern of synchronization. In particular, it is very sensitive to the phase shift of the coupling signal propagating between two counterparts. However, the analysis presented in [5] is valid only in the case of weak coupling and small frequency mismatch. In [6], we considered a more general model of two coupled gyrotron oscillators, which are assumed identical except a small frequency mismatch. The model is described by two delay-differential equations (DDE)

$$\begin{aligned} \frac{dA_1}{dt} + i\frac{\Delta}{2}A_1 + A_1 &= I_s\Phi(A_1) \cdot A_1 + \rho e^{-i\psi}A_2(t-\tau), \\ \frac{dA_2}{dt} - i\frac{\Delta}{2}A_2 + A_2 &= I_s\Phi(A_2) \cdot A_2 + \rho e^{-i\psi}A_1(t-\tau). \end{aligned} \quad (1)$$

Here, $A_{1,2}$ are slow amplitudes, Δ is normalized frequency mismatch, Φ is the complex gain factor, I_s is the normalized beam current parameter, ρ is the coupling strength, $\tau = \omega_0 t_d / 2Q$ is the normalized delay time t_d , $\psi = \omega_0 t_d$. In the quasi-linear theory [7], the complex gain factor is obtained as a polynomial expansion $\Phi = \alpha - \beta|A|^2 - \gamma|A|^4 - \dots$ as a result of approximate solution of the electron motion equations. However, this approximation is valid only at a slight excess of the start-oscillation current and, consequently at low efficiency. Therefore, to extend the range of validity of the model, we obtain $\Phi(|A|^2)$ by fitting the numerical solution of the equations of time-domain gyrotron theory with fixed Gaussian profile of the RF field [7].

Numerical simulation in a wide range of parameters confirms the basic pattern of synchronization re-

vealed in [5]. The results of simulation for the DDE model (1) and time-domain gyrotron theory with fixed Gaussian profile of the RF field [7] are in good agreement with each other.

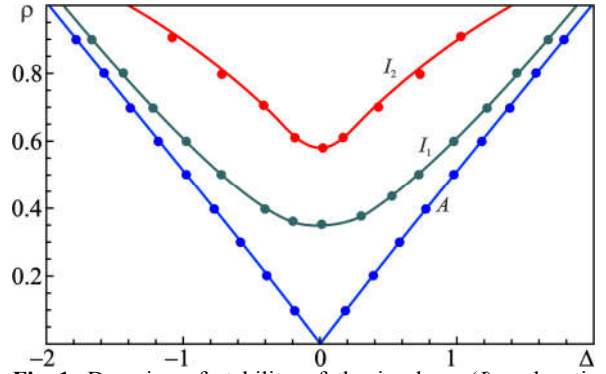


Fig. 1. Domains of stability of the in-phase (I) and anti-phase (A) mode of synchronization on the Δ, ρ plane for $I_s = 0.05$, $\psi = 0.4\pi$, and $\tau = 3.0$.

The study of mutual phase locking of two gyrotrons in the soft-excitation mode ($\Delta_H = 0.4$) [6] revealed that the delay in coupling strongly affects the pattern of phase-locking regimes. In particular, it is very sensitive to the phase shift of the coupling signal propagating between two counterparts.

Numerical simulation in a wide range of parameters confirms the basic pattern of synchronization revealed in [5]. With the increase of the delay, there appear new modes of synchronization, i.e. the multistability becomes more pronounced. Fig. 1 illustrates the situation when there exist two in-phase and one anti-phase modes.

In addition, in Fig. 1 the stability domains calculated according the time-domain gyrotron theory with fixed Gaussian profile of the RF field [7] are shown with circles. They are in good agreement with the results of simulation for the DDE model (1).

Synchronization of two gyrotrons in the hard excitation mode

Maximum efficiency in a gyrotron is usually attained in a hard excitation mode [7]. Thus, we studied synchronization of two coupled gyrotrons with Gaussian profile of the RF field with the parameters $\mu=15$, $I_s = 0.06$, $\Delta_H = 0.53$ when the orbital efficiency is nearly 70%.

The system of two mutually coupled gyrotrons demonstrates a behavior which has much common with dynamics of a single gyrotron oscillator driven by an external signal [2]. In [2], we found a number of differences from the well-studied pattern of synchronization of the generator with soft excitation.

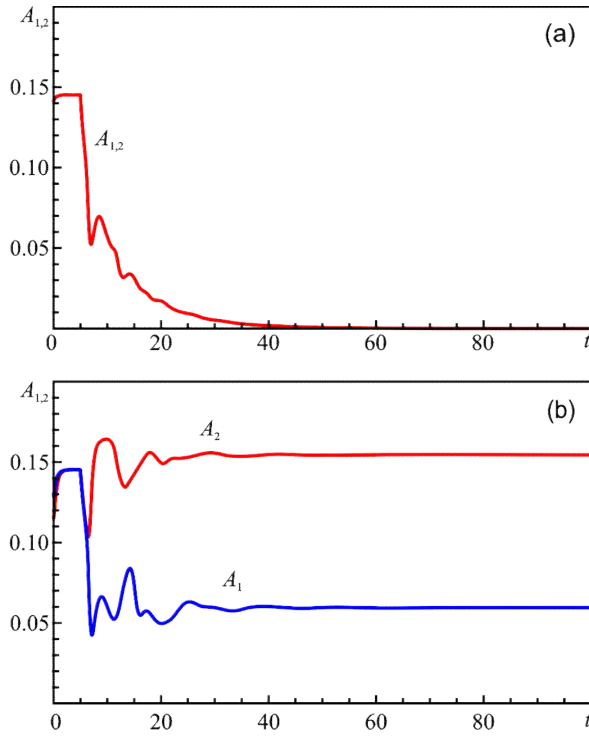


Fig. 2. Time histories of the amplitudes at $\mu=15$, $\Delta_H = 0.53$, $I_s = 0.06$, $\rho = 0.5$, $\psi = 0.15\pi$, $\tau = 5$.

In particular, since bistability presents in the autonomous system, it also appears in the non-coupled system. The synchronization mode with high efficiency establishes only if the initial perturbation is large enough that is typical for systems with hard self-excitation. Moreover, for certain values of the parameters, the synchronization mode turns out to be extremely sensitive to the initial phase of the oscillations and an external signal may cause a breakdown into the low-amplitude mode instead of synchronization. In Fig. 2, examples of the time histories for a sufficiently large coupling are presented. When both gyrotrons start from the same initial amplitudes (Fig. 2(a)), the oscillations are excited in both gyrotrons and the efficiency reaches its maximum value. However, at $t = 5$ the signal from one gyrotron starts to affect the other one and vice versa. As a result, the oscillations of both gyrotrons are completely suppressed. Under somewhat different initial condition, only one of the gyrotrons suppresses the other, as is shown in Fig. 2(b).

On the contrary, coupling of the gyrotrons may lead to the excitation of one gyrotron by another. Fig. 3 illustrates the case when the initial amplitude of the second gyrotron is zero. In the hard excitation regime, this is a stable state. However, when the signal from the first gyrotron enters the resonator of the second one, the oscillation of the second gyrotron starts to grow and finally the synchronization mode is established.

Synchronization of coupled multimode gyrotrons

Finally, we considered mutual synchronization of two multimode gyrotrons. The simulation shows that in this case instead of oscillation quench there occurs excitation of a spurious mode.

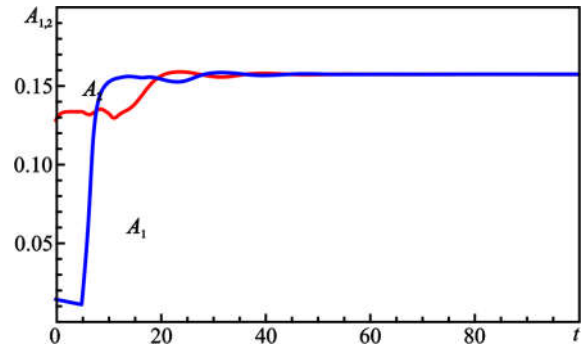


Fig. 3. Time histories of amplitudes of gyrotrons at $\rho = 0.3$, $\psi = 0.4\pi$, $\tau = 5$.

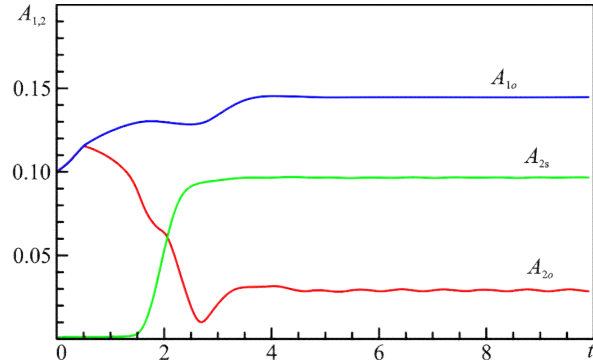


Fig. 4. Time histories of amplitudes ($A_{1,0}$ - operation mode in the first gyrotron, $A_{2,0}$ and $A_{2,s}$ - operation and spurious modes in the second gyrotron) at $\rho = 0.5$, $\psi = 0.4\pi$, $\tau = 0.5$.

This is illustrated by Fig. 4 where time histories of the operating modes in two gyrotrons are plotted (cf. Fig. 2(b)). Or, on the contrary, at different initial conditions build-up of the synchronization mode may occur while the spurious modes in both gyrotrons are completely suppressed.

Acknowledgment

This work is partly supported by the Russian Foundation for Basic Research grant No. 18-02-00839.

References

1. Thumm M. Recent advances in the worldwide fusion gyrotron development // IEEE Trans. Plasma Sci., 2014. V. 42, no. 3, pp. 590-599.
2. Yakunina K.A., Kuznetsov A.P., Ryskin N.M. Injection locking of an electronic maser in the hard excitation mode // Phys. Plasmas. 2015. V. 22, No 11. 113107.
3. Bakunin V.L., Denisov G.G., Novozhilova Y.V. Zones of frequency locking by an external signal in a multimode gyrotron of a megawatt power level // Radiophys. Quantum Electron., 2016. V. 58, No. 12. P. 893-904.
4. Rozental R.M., Ginzburg N.S., Glyavin M.Yu., Sergeev A.S., Zotova I.V. Mutual synchronization of weakly coupled gyrotrons // Phys. Plasmas. 2015. V. 22, No. 9. 093118.
5. Usacheva S.A., Ryskin N.M., Phase locking of two limit cycle oscillators with delay coupling // Chaos. 2014. V. 24, No. 2. 023123.
6. Adilova A.B., Gerasimova S.A., Ryskin N.M., Synchronization of delay-coupled gyrotron oscillators // EPJ Web of Conferences. 2017. V. 149. P. 04029.
7. Nusinovich G.S. Introduction to the Physics of Gyrotrons. Johns Hopkins University Press, Baltimore, 2004.

High power THz-range Wave generation based on Transformation of Plasma Waves Pumped by High-current Relativistic Electron Beam

A.V. Arzhannikov^{1,2}, V.V. Annenkov^{1,2}, V.S. Burmasov^{1,2}, I.A. Ivanov^{1,2}, A.A. Kasatov^{1,2}, S.A. Kuznetsov^{1,2}, M.A. Makarov¹, K.I. Mekler¹, S.V. Polosatkin^{1,2}, V.V. Postupaev^{1,2}, A.F. Rovenskikh¹, D.A. Samtsov^{1,2}, S.L. Sinitsky^{1,2}, V.F. Sklyarov^{1,2}, V.D. Stepanov^{1,2}, I.V. Timofeev^{1,2}, and E.P. Volchok^{1,2}

¹Budker Institute of Nuclear Physics Russian Academy of Science, Novosibirsk, Russia, arzhan1@ngs.ru

²Novosibirsk State University, Novosibirsk, 630090, Russia

Introduction

The beam-plasma interaction system allows one to generate high-power sub-mm waves (frequency interval 0.1–1 THz) by usage of mechanism of plasma wave transformation [1]. This way gives possibility to achieve multi megawatt power with the promptly varying frequency that can be necessary for various practical applications. The original project of a sub-mm wave based on transformation of plasma waves pumped by a kA-current relativistic electron beam is developed at the GOL-PET facility. We present novel results on the study of mechanisms of sub-mm wave emission by the processes of plasma wave transformation in electromagnetic one in case of the strong beam-plasma interaction.

Facility and results of experiments

To study the conditions associated with the generation of electromagnetic radiation, the specialized facility GOL-PET was constructed. The GOL-PET facility consists of an open magnetic trap with a multiple-mirror or uniform magnetic field of mean value $B = 4.2$ T and length $L = 2.4$ m between the end mirrors, see Fig. 1. The end mirrors have a strong field up to $B = 8$ T. A plasma column with the density $n_e \approx (0.2 \div 5) \times 10^{15}$ cm⁻³ and a diameter of 7 cm is created by a longitudinal high-current discharge. U-2 accelerator producing a high current relativistic electron beam (REB) is mounted at one end of the trap. It produces the beam with the current $I \sim 10$ kA, the pulse duration 6 μ s at the electron kinetic energy $E_e \approx 0.8$ MeV. The REB is injected into the end of the plasma column and where the beam diameter is 4 cm at the magnetic field 4 T. The radial profile of the plasma density is measured in 9-dots over the column diameter at a distance $z = 0.83$ m from the entrance mirror by diagnostics based on Thomson scattering. Dynamics of the average plasma density is measured by Michelson interferometer at $z = 1.16$ m. Pulsed current transformers measure the electron beam current at different axial points. Electron energy of REB is determined according with accelerator voltage in the U-2 diode. The transfer of energy from REB to plasma is calculated from results of measurements of diamagnetism of the plasma column. The 8-channel sub-mm polychromator, as well as a number of single detectors with bandpass filters at their entrance are utilized to study properties of radiation emitted by plasma [2].

Previous experiments showed that the changes of the power value of the emitted electromagnetic waves correlated with the variation in the efficiency of plas-

ma heating by the electron beam. [1-3]. In a previous series of experiments on the simultaneous registration of radiation power emitted along the axis of the plasma column and in its perpendicular direction conducted at varying the plasma density from 10^{14} up to 10^{15} cm⁻³, we observed that the emission in the transverse direction was only at relatively low plasma densities ($n_e < 5 \times 10^{14}$ cm⁻³). For higher value of plasma density, the emission in the band above 300 GHz was observed along the axis of the device only. Just as in the earlier experiments on the GOL-3, the EM-wave emission mainly exists simultaneously with the increasing of the plasma diamagnetism.

A series of experiments for measuring the temporal dynamics of radiation spectra emitted along the axis carried out for the plasma density higher than 5×10^{14} cm⁻³. It was done by the 8-channel polychromator with semiconductor diodes for the frequency interval from 0.1 up to 0.5 THz. For the interval 0.5 \div 0.9 THz the measurements were done by single plasmonic detectors and an additional 2-channel system of cryogenic sensors. Experiments showed that at plasma density $5 \times 10^{14} \div 10^{15}$ cm⁻³ the spectral composition of the emission along the axis of the plasma column depended on radial gradient of the plasma density [2, 3]. The increase of the gradient caused to strongly increasing the spectral power density in the frequency band 150 \div 300 GHz. An example of signals from various sensors for one of the pulses of the GOL-PET facility (#1945) in case of the strong plasma density gradient (greater than 10^{15} cm⁻⁴) is presented in Fig. 2. The signal of the spectral power density from the diodes in the interval 150 - 300 GHz is dumped in 50 times for presenting here. Taking into account, this dumping factor we can say that the power in the spectral interval 150 \div 300 GHz is 25 kW/(sr·cm²) and the spectral power density is greater than its value in the interval 400 \div 800 GHz approximately in two orders of the value.

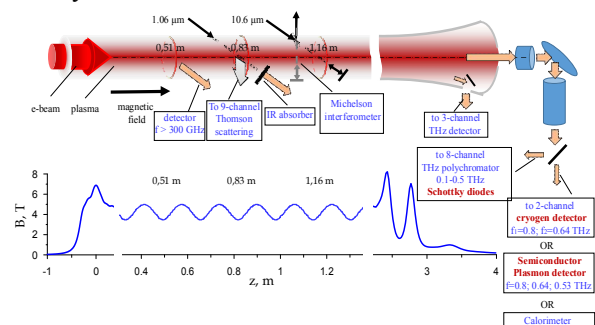


Fig. 1. Schematic of experiments at the GOL-PET facility

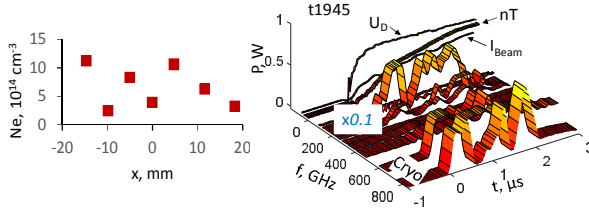


Fig. 2. Results of measurements in pulse #1945 at the GOL-PET facility. Left – plasma density distribution from 8-channel Thomson scattering system; right – signals from various sensors. U_D – diode voltage of the accelerator (MeV), I_{Beam} – beam current (10 kA), nT – plasma pressure from diamagnetic loop, other signals – radiation power in frequency selective detectors in Watts.

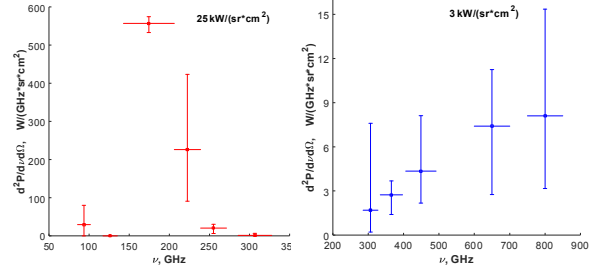


Fig. 3. Spectral composition of the plasma emission along the axis in case of strong plasma density gradient in transverse direction

Short analysis of measurement results

The signals in the frequency band $125 \div 250$ GHz are interpreted as radiation near the plasma frequency, Fig.3 (spectral band in left side of the picture). Such radiation can be produced through the linear mode conversion of upper-hybrid branch of plasma oscillations in region with plasma density gradients [4]. The observed width of the spectral line corresponds to the limited range of plasma density $(3-6) \times 10^{14} \text{ cm}^{-3}$. It means that intense beam-driven oscillations are localized near the bottom of density wells visible in Fig. 2 (left). If the plasma density in such a narrow well is modulated in the longitudinal direction due to, for example, the modulation instability, sub-luminal beam-driven modes can resonate with slow waveguide electromagnetic modes [5]. Then, these waveguide modes escape from the local density wells in the predominantly longitudinal direction via regular longitudinal inhomogeneity of plasma density on the scale of the magnetic field corrugation (10 cm). As to the high-frequency band $400 \div 800$ GHz, Fig.3 (spec-

tral band in right side), on our opinion, is a result of the coalescence of two upper hybrid plasma waves into electromagnetic ones [6-8]. Since the sub-mm wave emission at the plasma density higher than $5 \times 10^{14} \text{ cm}^{-3}$ is realized along the axis, we suppose that additional feature exists for longitudinal redirection of electromagnetic waves in the GOL-PET device. Note that the tendency to this redirection is qualitatively reproduced in theory [7].

Conclusion

It is found for the plasma density $(0.5 \div 1.0) \times 10^{15} \text{ cm}^{-3}$ that the radiation spectrum of the flux propagating along the axis of the beam-plasma system is mainly concentrated in two clearly distinct regions with the high level of spectral power density. The first region is located in the frequency interval $f_1=0.15 \div 0.25$ THz, the second one is in the interval $f_2=0.4 \div 0.8$ THz. The emission observed in the frequency interval f_1 has the power in the flux on a megawatt level and is interpreted as result of the linear conversion of the upper-hybrid branch of plasma oscillations to the electromagnetic radiation in regions of strong plasma density gradients. We interpret the emission in the interval f_2 as result of merging of these two plasma oscillations into the electromagnetic wave at a high level of plasma turbulence.

This work is supported by the Russian Foundation for Basic Research (grant 18-02-00232).

References

1. *A. V. Arzhannikov, et al.*, // Transactions of Fusion Science and Technology, 2013, vol. 63, pp. 82-87.
2. *I. A. Ivanov, et al.*, // AIP Conf. Proc., 2016, vol.1771, p.070009, doi.org/10.1063/1.4964233.
3. *A.V. Arzhannikov, et al.*, // AIP Conf. Proc., 2016, v.1771, p.070004, doi.org/10.1063/1.4964228.
4. *I.V. Timofeev, V.V. Annenkov and A.V. Arzhannikov* // Phys. Plasmas 2015, vol.22, p.113109.
5. *C.Miao, J.P.Palastro, and T.M. Antonsen* // Physics of Plasmas, 2017, vol.24, p.043109, doi.org/10.1063/1.4981218.
6. *I.V.Timofeev* // Phys. Plasmas 2012, vol.19, p.044501.
7. *A.V.Arzhannikov and I.V.Timofeev* // Plasma Phys. Control. Fusion, 2012, vol.54, p.105004.
8. *A. V. Arzhannikov et al.*, // IEEE Trans. Terahertz Sci. Technol., 2016, vol. 6, no 2, pp.245–252.

Prospective THz Gyrotrons for High-Field Magneto-Resonance Spectroscopy

V.L. Bratman^{1,2}, A.E. Fedotov², Yu.K. Kalynov², and V.N. Manuilov^{2,3}

¹Ariel University, Ariel, Israel, v_bratman@yahoo.com

²Institute of Applied Physics of Russian Academy of Sciences, Nizhny Novgorod, Russia

³Nizhny Novgorod State University, Nizhny Novgorod, Russia

Abstract

A high-harmonic Large Orbit Gyrotron and a low-voltage gyrotrino placed inside a spectrometer cryomagnet enable greatly simplify terahertz systems for magneto-resonance spectrometers. Large Orbit Gyrotrons provide a powerful third-harmonic generation at frequencies of 1 THz and 0.394 THz in pulsed and CW regimes, respectively, at significantly lower magnetic fields than conventional gyrotrons. According to simulations the gyrotrino with the voltage of 1.5 kV and frequency of 0.264 THz can generate a power of tens of watts; a possibility to operate at such a low voltage is demonstrated in the existing gyrotron with three-electrode magnetron-injection gun.

Introduction

THz medium power gyrotrons are in high demand for high-field DNP-NMR spectroscopy. However, only few installations are now equipped with such fairly expensive generators. Large Orbit Gyrotrons (LOGs) and gyrotrininos may make this method accessible for many laboratories due to the considerable simplification of the gyrotron magnetic system.

Conventional gyrotrons commonly operate at the fundamental or second cyclotron harmonics. The latter allows using simpler cryomagnets with a half-value of the magnetic field. A greater effect can be achieved in LOGs, capable of selective operation even at the third and fourth harmonics due to applying an axis-encircling electron beam [1-5], in contrast to a hollow poly-axis beam in a conventional gyrotron.

Another option is integration of a compact gyrotrino in single cryomagnet with an NMR spectrometer [6, 7]. This is based on the proximity of the electron cyclotron frequency and the frequency of the paramagnetic resonance in a sample. The integration eliminates the need for an additional cryomagnet and a long THz transmission line with high losses. An exact frequency matching can be achieved at a very low gyrotron voltage, namely 1-2 kV [6], or at special profiling the cryomagnet field [7].

High-Harmonic Large Orbit Gyrotrons

In a LOG cavity (Fig. 1), an axis-encircling electron beam can excite only co-rotating modes with azimuthal indices equal to the number of the resonant cyclotron harmonic [1-5]. This strong selection rule prevents the excitation of most of parasitic modes and makes it possible to operate at higher harmonics.

At the Institute of Applied Physics, LOGs, are being studied in parallel with conventional gyrotrons, for more than 20 years to obtain higher frequencies at lower magnetic fields. First experiments were carried out at high-current electron accelerators with moderately relativistic electron energy of (250 – 400) keV. These LOGs selectively generated high output powers at harmonics $s=2-5$ and frequencies from 20 GHz up to 0.4 THz [5]. At relativistic energy, electron-wave coupling at high harmonics can be stronger than at the fundamental resonance, but a problem of neighboring harmonics discrimination is fairly complex. In addition, use of relativistic energy decreases the cyclotron electron frequency and reduces the frequency gain.

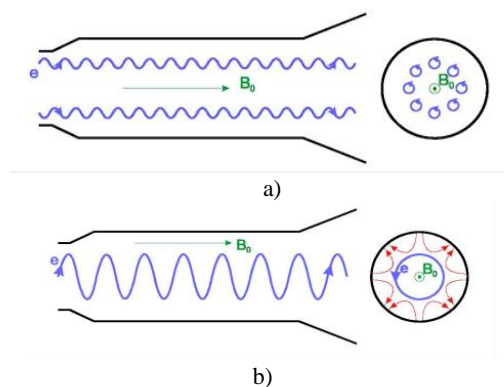


Fig. 1. Electron beams in conventional gyrotron (a) and high-harmonic Large Orbit Gyrotron (b)

The further progress in development of LOGs was associated with reducing the operation voltage that enables replacing the accelerators by simpler high-voltage modulators, as well as with increasing the radiation frequencies. In the 80-kV LOG (Fig. 2a) [4], a stable single-mode second- and third-harmonic generation with a power of 0.3–1.8 kW was obtained in 10- μ s pulses at four frequencies in the range of 0.55–1.00 THz at magnetic fields 10.5–13.6 T. A relatively low efficiency of this generator $\sim 1\%$ was caused by great Ohmic losses in a long gyrotron cavity at THz frequencies. This LOG was used for scientific applications and for testing novel versions of THz cavities [5] aimed to enhance efficiency by decreasing Ohmic losses, as well as to make possible the fourth-harmonic operation.

An important step in LOG progress is a development of a 30 kV/0.7 A gyrotron [5] with a 5 T cryomagnet designed for a CW operation (Fig. 2b). In this oscillator, an electron beam with a large pitch-factor of 1.5 is formed in a cusp gun and then the transverse electron velocity increases in an increasing

magnetic field. The main scope of this setup is operation at the second, third and fourth harmonics at the

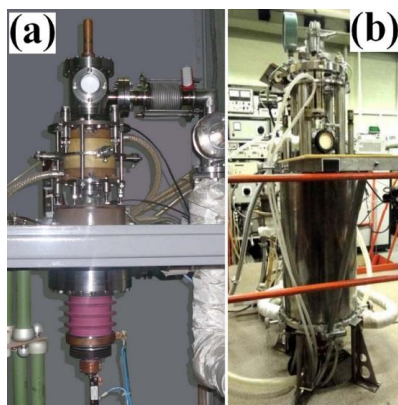


Fig. 2. LOGs with parameters 1 THz/80 kV (a) and 0.394 THz/30 kV (b).

typical DNP frequencies of 0.26 THz, 0.39 THz, and 0.52 THz with the power level of hundreds of watts.

In a good accordance with simulations, experimental zones of excitation of the second-harmonic $TE_{2,5}$ and third-harmonic $TE_{3,7}$ modes are well separated by magnetic field. Generation with parameters 800 W/ 0.267 THz and 300 W/ 0.394 THz is obtained at the fields $B=5.02$ T and $B=4.93$ T, respectively. Competition of these two modes is observed at intermediate magnetic fields. An increase in operating magnetic field up to 6.3 T and in the electron voltage up to 45 kV should allow achieving frequencies up to 0.65 THz at the fourth cyclotron harmonic [5].

Gyrotrino

Integration of a THz generator and an NMR spectrometer in single cryomagnet requires the exact matching of the DNP and gyrotron frequencies. Because of relativistic dependence of the cyclotron frequency on electron energy this is possible at an extremely low voltage of 1-2 kV only [6]. The very possibility of operating at a such low voltage was verified in an existing CW gyrotron [8]. A three-electrode magnetron injection gun of the gyrotron was initially designed for a higher voltage; to obtain an acceptable electron pitch factor for the low voltage, a high positive potential was applied to a modulating anode while keeping a negative cathode potential in order to increase the transverse particle velocity in the emitter region and decrease the longitudinal velocity in a region between the anode and the cavity. As a result, a stable generation with the frequency of 0.25 THz was observed at whole range of electron energies in the gyrotron cavity from 15 keV down to 1.5 keV.

According to simulations [10], a gyrotrino with an operating $TE_{6,2}$ mode, a voltage of 1.5-1.8 kV, a current of 200 mA, a pitch factor of 1.2 and a small cavity length can provide a power up to 15 W at the frequency of 0.264 THz with a required magnetic field about of 9.42 T (Fig. 3b). Since the gyrotron cavity is very close to the sample, a short transmission line is needed, that reduces the radiation losses and decreases

a required THz power. A magnetic field disturbance induced by the low-voltage electron beam at the sam-

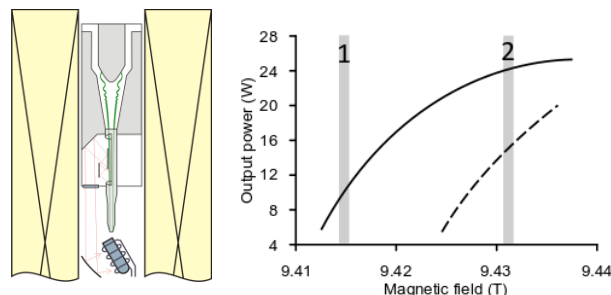


Fig. 3. a) Gyrotrino in cryomagnet of NMR spectrometer; b) calculated power vs. magnetic field for 1.5 kV / 200 mA (solid line) and 2 kV / 150 mA (dotted). Lines 1 and 2 show two regimes of gyrotron-DNP frequency matching.

ple is about of 10^{-8} and can be neglected. To save a limited space in the uniform magnetic field region, the radiation output from the gyrotron cavity can be directed toward the electron gun (Fig. 3a). Due to lack of space, the electron beam is to be collected in a cavity cut-off narrowing in a strong field [10].

The gyrotrino project was supported by Russian Science Foundation under grant No. 16-12-10445. Authors are grateful to M.Yu. Glyavin, A.P. Fokin, I.V. Osharin, and N.A. Zavolsky for collaboration.

References

1. Jory, H. Investigation of electronic interaction with optical resonators for microwave generation and amplification // Varian Associates, Palo Alto, CA, USA, R&D Tech. Rep. ECOM-01873-F. 1968.
2. McDermott, D.B., Luhmann, Jr, N.C., Kupiszewski, A., and Jory, H.R. Small-signal theory of a large-orbit electron-cyclotron harmonic maser // Phys. Fluids. 1983. V. 26. No. 7. P. 1936–1941.
3. Lawson, W., Destler, W.W., and Striffler, C.D. High-power microwave generation from a large-orbit gyrotron in vane and hole-and-slot conducting wall geometries // IEEE Trans. Plasma Sci. 1985. V. 13. No. 6. P. 444–453.
4. Bratman, V.L., Kalynov, Yu.K., and Manuilov, V.N. Large-orbit gyrotron operation in the terahertz frequency range // Phys. Rev. Lett. 2009. V. 102. No. 24. P. 245101.
5. Bandurkin, I.V., Bratman, V.L., Kalynov, et al. Terahertz Large-Orbit High-Harmonic Gyrotrons at IAP RAS: Recent Experiments and New Designs // IEEE Trans. Electron Devices. 2018. V. 65. No. 6. P. 2287–2293.
6. Bratman, V.L., Fedotov, A.E., Kalynov, Yu.K., and Samoson, A. THz Gyrotron and BWO Designed for Operation in DNP-NMR Spectrometer Magnet // J. Infrared, Millimeter, and THz Waves. 2013. V. 34. P. 837.
7. Sirigiri, J.R., Maly, T. Integrated high-frequency generator system utilizing the magnetic field of the target application // U.S. Patent No. 8,786,284, 22. Jul. 2014.
8. Glyavin, M.Yu., Denisov, G.G., Zapevalov, et al. High power terahertz sources for spectroscopy and material diagnostics // Phys.-Usp. 2016. V. 59. P. 595.
9. Bratman, V.L., Fedotov, A.E., Fokin, A.P., et al. Operation of a sub-terahertz CW gyrotron with an extremely low voltage // Physics of Plasmas. 2017. V. 24. P. 113105.
10. Bratman, V.L., Fedotov, A.E., Kalynov, et al. Numerical study of a low-voltage gyrotron (“gyrotrino”) for DNP/NMR spectroscopy. // IEEE Transactions on Plasma Science. 2017. V. 45. No. 4. P. 644.

Fast Magnetic Measurements Of 8.6 m Undulator

I. V. Davidyuk^{1,2}, Ya. I. Gorbachev¹, O. A. Shevchenko¹

¹ Budker INP SB RAS, Novosibirsk, Russia, daveduke@outlook.com

² Novosibirsk State University, Novosibirsk, Russia

Abstract

The design of the large-aperture variable-period undulator (VPU) developed for the Novosibirsk free electron laser (FEL) is shortly described. High amplitude of on-axis field is achieved due to the arc shape of the magnet blocks and poles of the undulator. To conduct magnetic measurements and fine tuning of the undulator as well as to perform real time position tracking of magnet blocks, pulsed wire technique was adopted.

Introduction

A permanent magnet variable-period undulator with large (1.4) ratio of the aperture to the minimum period and possibility to change the number of poles was designed to upgrade the first stage FEL of the Novosibirsk FEL facility. The Novosibirsk FEL is a source of radiation in the THz range. The new undulator will replace the existing insertion device section which consists of two 4-meter-long undulators and the three-pole buncher. That will shift long-wave border of the tuning range from 200 μm to 450 μm . A comparison of parameters of former and new undulators is given in the following table:

Parameter	EM undulators	VPU
Period, cm	12	10 – 16
Gap (inner diameter), cm	8	14
Number of periods	2×32	50 – 80
Radiation wavelength, μm	90 – 240	82 – 450
Deflection parameter	0 – 1.1	0.45 – 1.9
Full length, cm	2×400	860

The idea of a VPU with free moving poles was proposed in [1]. At the minimum period l_{min} , the developed undulator is a conventional hybrid device with neodymium magnets and poles made of soft steel with large permeability. All poles in the undulator are split into halves, and so the undulator is two arrays (upper and lower) of separate removable blocks. Each block is $l_{\text{min}}/2$ long and consists of a magnet embraced by two pole halves and the whole structure is set in an aluminum frame. The pairs of blocks in upper and lower arrays are connected and placed on a carriage that can move freely along the undulator, see Fig. 1. Adjacent magnets in an array always have antiparallel longitudinal magnetizations, so they experience strong repulsion from each other. Due to repulsion force and the low-friction between guide rail and carriages, the undulator period can be changed via shifting the terminal blocks. This procedure, which changes the overall length of the undulator, is performed by pushers that can be remotely controlled. More details about similar undulator can be found in [2].

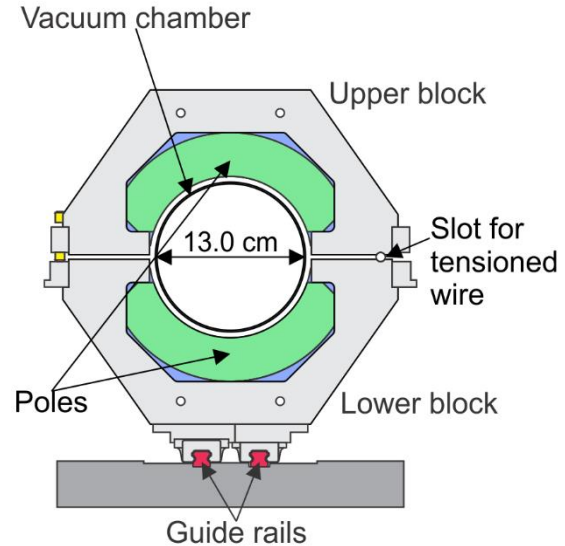


Fig. 1. Front view of the undulator

Obviously blocks in the undulator can create inhomogeneous distribution which may lead to phase errors between the radiation field and the electron transverse motion. The construction of the undulator provides possibility to make in situ measurements of magnetic field distribution in real time to monitor blocks' position errors and calculate the radiation spectrum via pulsed wire method. Slot for the stretched wire in undulator block is shown in Fig. 1.

The pulsed wire technique for magnetic measurements was proposed in [3] and since then it has been used for measurements of field when undulator gap cannot fit the support of the Hall probe or to speed-up the tuning of the undulator [4]. This method allows several measurements per second, thus it would significantly reduce the time of magnetic investigation of the developed 8.6 meters long VPU for the first FEL of Novosibirsk FEL facility.

Measurement system

The basic components of the measurement setup are a wire stretched along the axis of investigated magnetic field, a current pulse generator and a detector of the wire displacement. When current is passing through the wire it interacts with the magnetic field. Flexural waves that travel through the wire towards detector contain information about transverse field profile in the region of interest.

Theoretical analysis of this technique is presented in [5] where the stretched wire is treated as a thin rod in order to take dispersion into account. The expression for wire displacement at the detector position $z = 0$

reads:

$$x(0, t) = \frac{1}{2\sqrt{\mu T}} * \int_{t-\tau}^t I(t-t') \int_0^{v_0 t'} B_{eff}(z) dz dt', \quad (1)$$

where μ is the mass per unit length of the wire, T is the tension in the wire, τ is current pulse duration, v_0 is $\sqrt{T/\mu}$ and B_{eff} is defined by the following expression:

$$B_{eff}(z) = \int_{-\infty}^{\infty} A(k) e^{-i\frac{\omega(k)z}{v_0}} dk, \quad (2)$$

where $A(k)$ is the Fourier transform of the magnetic field in the path of the current and $\omega(k)$ is the dispersion relations for the flexural waves in the wire [5]. Using above expressions one can correct effects of dispersion, current pulse form averaging and restore the magnetic field distribution from the data obtained by the detector.

An experimental setup was constructed in order to adopt the technique. A beryllium copper wire with a diameter of 200 μm and length of 10 m was stretched by applying tension close to yield point. A capacitor based current pulse generator can generate pulses with duration of 50 μs and amplitude of 10 A. A homemade optocoupler is used as the wire position detector, it is based on fd-24k photodiode and provide 0.14 mV/ μm gradient. Since the size of the undulator do not allow avoiding intersection of the main signal and reflections by elongation of the wire and the period of the undulator can be changed during operation of the FEL it was decided to use dampers based on oil drops, see [6], placed on the ridges of an automated pantograph.

Several trial launches of the system were performed, see example in Fig. 2.

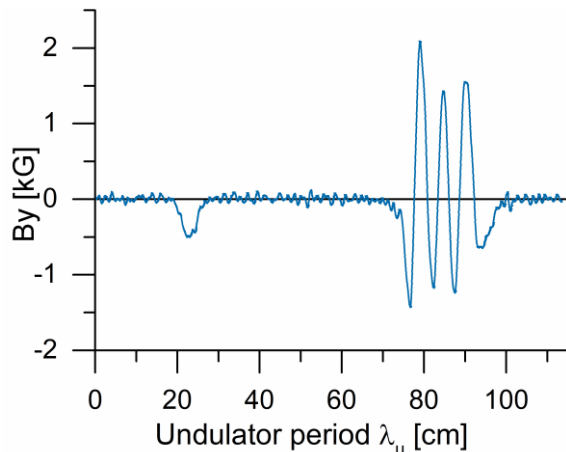


Fig. 2. Test measurement

The field distribution was reconstructed from the measured first integral data by differentiating, no filter was applied.

Discussion and conclusion

The described experimental setup is under active development now. Test measurements of reference magnet and VPU short prototype were conducted, see Fig. 2, and obtained results indicate that detector sensitivity should be improved in order to obtain larger signal to noise ratio.

The task to commission a pulsed wire measurements setup over 10 m long has not been challenged yet. It is yet to be determined whether

complete compensation of signal distortion effects e.g. wire sagging influence, attenuation and dispersion is possible during postprocessing. Alternatively, complementary components, like wire supports and additional detector, could be applied to minimize the influence of distortion effects.

Currently authors attempt to increase the sensitivity of the detector and suppress impact from external noises in order to acquire clean data.

Acknowledgements

The work was supported by the Russian Science Foundation (project No. 14-50-00080).

References

1. Vinokurov N.A., Shevchenko O.A., Tcheskidov V.G. Variable-period permanent magnet undulators // Phys. Rev. Spec. Top. - Accel. Beams. 2011. V. 14. No. 4. P. 040701.
2. Davidiuk I.V., Shevchenko O.A., Tcheskidov V.G., Vinokurov N.A. Modeling and designing of variable-period and variable-pole-number undulator // Phys. Rev. Accel. Beams. 2016. V. 19. No. 2. P. 020701.
3. Warren R.W. Limitations on the use of the pulsed-wire field measuring technique // Nucl. Instruments Methods Phys. Res. Sect. A Accel. Spectrometers, Detect. Assoc. Equip. 1988. V. 272. No. 1–2. P. 257–263.
4. Fan T.C., Lin F.Y., Hwang C.S., Hsu I.C. Pulsed wire magnetic field measurements on undulator U10P // PACS2001. Proceedings of the 2001 Particle Accelerator Conference (Cat. No.01CH37268). Chicago: IEEE, 2001. P. 2775–2777.
5. Kumar V., Mishra G. Analysis of pulsed wire method for field integral measurements in undulators // Pramana. 2010. V. 74. No. 5. P. 743–753.
6. Varfolomeev A.A. et al. Wire method for magnetic field measurements in long undulators // Nucl. Instruments Methods Phys. Res. Sect. A Accel. Spectrometers, Detect. Assoc. Equip. 1995. V. 359. No. 1–2. P. 93–96.

Frequency control in subterahertz gyrotrons

A. Bogdashov, A. Fokin, A. Fedotov, M. Glyavin, M. Morozkin, Yu. Novozhilova, M. Proyavin, R. Rozental, A. Sedov, A. Tsvetkov, I. Zotova and G. Denisov

Institute of Applied Physics of the Russian Academy of Sciences, Nizhny Novgorod, Russia, ap.fokin@mail.ru

Subterahertz gyrotrons are promising for application in different fields of science and technology, like spectroscopy [1], media diagnostics [2] and materials processing [3]. Many of the application require the possibility of precise frequency tuning or stabilization. In this paper we present the experimental investigation of different ways of frequency control in medium-power continuous-wave gyrotrons carried out in the Institute of Applied Physics RAS. The capabilities and limitations of different methods are presented.

Magnetic field variation

The magnetic field variation provides the biggest range of frequency tuning. Excitation of different transverse modes with close caustic radius enables step frequency tuning in range up to 200 GHz [4]. The fine frequency tuning with band of up to 6 % of carrier frequency can be obtained by consequent excitation of high-order longitudinal modes. It is possible due to the use of a short cavity with low Q-factor and operation at low transverse modes in order to increase the electron-wave coupling. The proof of concept experiment on low frequency (using the 12 GHz gyrotron setup) demonstrated the 4% tuning band without any special optimization of the system (see Fig. 1). Based on this concept the project of the 200 GHz gyrotron with 1 kW output power and 10 GHz band was developed [5].

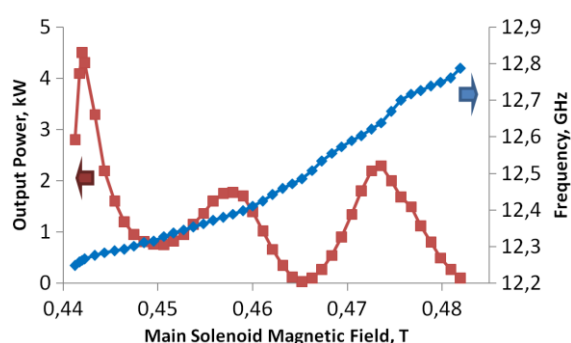


Fig. 1 The gyrotron output power and frequency vs. magnetic field

The frequency tuning speed of such method is limited by the parameters of the cryomagnets, mainly the maximum current variation rates, which are less than 0.1% of maximum field per minute. The possible solution is to apply the additional coil either in the cathode region or at the cavity. The latter approach was tested and demonstrated the possibility of operating mode switching with sweeping frequency up to 2 kHz. The same method can be applied for fast

power modulation with frequency up to 10 kHz (Fig. 2), which is limited by auxiliary coil inductance and alternating field screening [6].

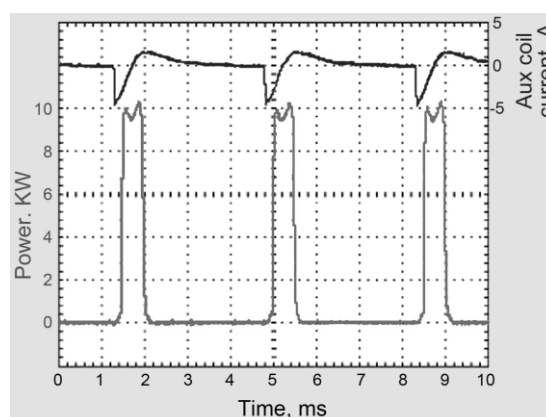


Fig. 2 Oscillograms of auxiliary coil current (top) and gyrotron output power (bottom)

Cavity temperature variation

In the recent experiments, the possibility of tuning the frequency of the 0.26 THz gyrotron [7] by more than 1 GHz was demonstrated by the simultaneous changing of the magnetic field of the main solenoid and the temperature of the cavity coolant. The measured frequency sensitivity of 4 MHz/°C allowed to tune the frequency in more than 200 MHz range and close the power gap between different longitudinal modes (Fig. 3).

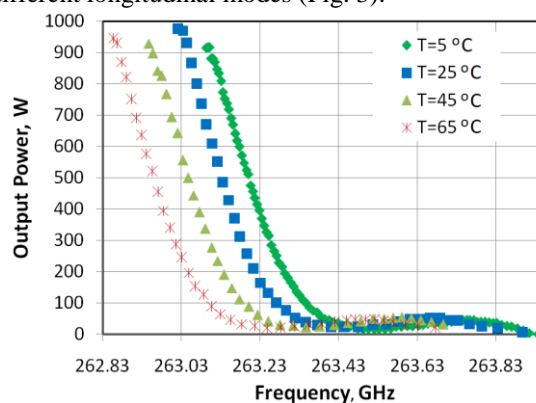


Fig. 3. Output power vs. frequency for different cavity coolant temperatures

Voltage variation

The fastest way of frequency control is the variation of the voltage at one of the electrodes of the magnetron-injection gun or the potential of the gyrotron cavity [8, 9]. The modulation of cathode voltage requires complex and expensive power supply; the speed of cavity voltage variation is limited

by big capacitance, so the most effective way of frequency control is the anode voltage variation.

For this purpose, the special control unit was developed, that allowed voltage variation in range of 1 kV with speed more than 1 kV/ μ s. The control system based on this unit opened up the possibility of frequency tuning in 20 to 50 MHz range with up to 200 kHz modulation frequency. Application of the system for frequency stabilization by phase-lock loop against reference oscillator allowed to achieve the spectrum width of the gyrotron radiation of 1 Hz [10].

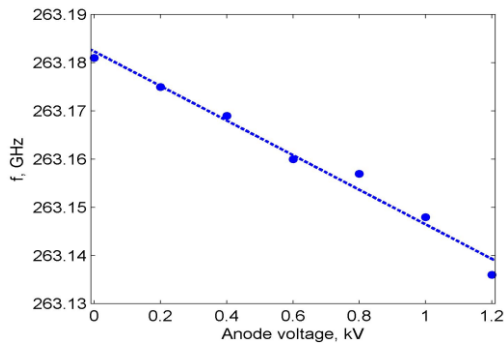


Fig. 4. Radiation frequency of a gyrotron vs. anode voltage

External signal and reflections

The presence of external signal or the power reflected from the load can be used for power and frequency control [11]. Experiments on influence of the signal, reflected from distant non-resonant load [12] show the possibility of frequency stabilization, while proof of concept experiments with mobile reflector demonstrate the means of slow power and frequency control (Fig. 5)

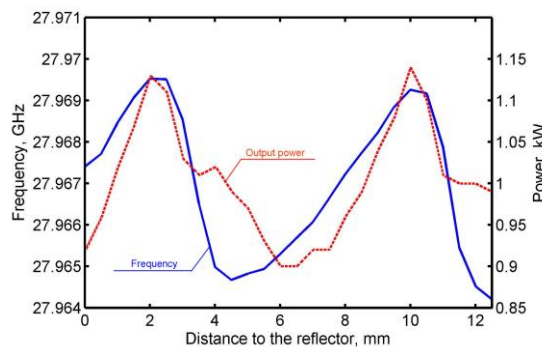


Fig. 5. Output power and frequency vs. distance to the non-resonant reflector

Conclusion

The IAP RAS gyrotron research team developed and tested a number of approaches to frequency control in sub-THz gyrotrons, including excitation of high-order longitudinal modes, cavity temperature sweeping, anode voltage variation and use of reflections. Beyond the scope of this work are mechanical means

of frequency tuning, for example [13], which are surely promising, but their use in sub-THz frequency range is limited by the precision requirements.

Investigated approaches open up new prospects for the successful development of new medium power THz band gyrotrons with unique capabilities for modern applications

The work was supported by Russian Foundation for Basic Research grant № 17-02-00183

References

- Blank M, Rosay M, Engelke F Instrumentation for solid-state dynamic nuclear polarization with magic angle spinning NMR // J. Magn. Reson., 2016, V. 264 P. 88-98
- Yamaguchi, Y. et al., High-power pulsed gyrotron for 300 GHz-band collective Thomson scattering diagnostics in the Large Helical Device // Nuclear Fusion, 2015, V. 55 013002
- Vodopyanov, A. et al., Application of the 263GHz/1 kW gyrotron setup to produce a metal oxide nanopowder by the evaporation-condensation technique // Vacuum, 2017, V. 145, P. 340-346
- Idehara, T. et al., A novel THz-band double-beam gyrotron for high-field DNP-NMR spectroscopy // Review of Scientific Instruments, 2017, V. 88, 094708
- Fedotov, A.E. et al., Frequency Tunable sub-THz Gyrotron for Direct Measurements of Positronium Hyperfine Structure // Journal of infrared, millimeter and terahertz waves, 2018, V. 39, No. 10, P. 975–983
- Glyavin, M.Yu., Luchinin, A.G., Morozkin, M.V., Ka-band 10 kW CW gyrotron with the wide-band fast frequency sweep // Rev. Sci. Instrum., 2012, V. 83, 074706
- Glyavin M.Y. et al. Experimental tests of 263 GHz gyrotron for spectroscopy applications and diagnostic of various media // Review of Scientific Instruments, 2015, V. 86, No. 5, P. 054705
- Idehara, T., Mitsudo, S., Ogawa, I. Development of High-Frequency, Highly Stable Gyrotrons as Millimeter to Submillimeter Wave Radiation Sources // IEEE Trans. Plasma Sci., 2004, V. 32, P. 910–916
- Golubiatnikov, G.Y. et al. Gyrotron frequency control by a phase lock system // Tech. Phys. Lett., 2006, V. 32, P. 650
- Fokin, A. et al., High-power sub-terahertz source with a record frequency stability at up to 1 Hz // Scientific Reports, 2018, V. 8, 4317
- Novozhilova, Yu. et al., Gyrotron frequency stabilization under the influence of external monochromatic signal or wave reflected from the load: Review // Izvestiya VUZ, Applied Nonlinear Dynamics, 2017, V. 25, No. 1, P. 4-34
- Glyavin, M.Yu. et al., Frequency Stabilization in a Sub-Terahertz Gyrotron With Delayed Reflections of Output Radiation // IEEE Transactions on Plasma Science, 2018, V. 46, No. 7, P. 2465 – 2469
- Sabchevski, S, Idehara, T. Resonant Cavities for Frequency Tunable Gyrotrons // Int J Infrared Milli Waves, 2008, V. 29, P. 1–22

Problems of Amplifier Klystron Advancing into the Terahertz Band

A.D. Grigoriev^{1,2}

¹Saint Petersburg State Electrotechnical University “LETI”, St. Petersburg, Russia, adgrigoriev@mail.ru,

²“Svetlana-Electronpribor” JSC

Electromagnetic oscillations and waves of the terahertz band have some important preferences compared with their neighbors. But lack of power coherent sources impedes wide application of these waves in radar and telecommunication systems.

Amplifier klystrons due to their high efficiency and relatively small dimensions are considered as one of the most perspective power sources of submillimeter and terahertz radiation. For example, the CPI Inc. (Canada) produces a number of Extended Interaction Klystrons (EIK) with working frequencies from 94 to 280 GHz and output pulse power from 3 to 0.03 kW [1]. In Russia, the “Svetlana” JSC produces the 8-mm wavelength amplifier klystron with output power 6 kW.

In spite of these advances, design and manufacturing of terahertz amplifier klystrons encounter a number of serious problems, namely:

- Very high current density of the electron beam;
- High cathode current density;
- Low cavities impedance;
- Small gap length and consequently little threshold voltage.
- Small collector area and dissipated heat.

To overcome these problems some techniques were proposed [2]. Among them are using of extended interaction (multigap) cavities, sheet electron beams and cathodes with high current density. But to obtain desirable effect the designer have to choose thoroughly the main device parameters starting from project input data.

The main input data for amplifier klystron design are its working frequency f_0 , output power P_{out} , bandwidth Δf and amplification factor G . Basing on these data, the designer have to estimate device efficiency η , which can change from 10 to 80 %. The more is working frequency and bandwidth, the less is efficiency.

When efficiency is estimated, one can calculate electron beam current $I_0 = P_{out}/(\eta U_0)$, where U_0 – accelerating voltage. Increasing of the voltage leads to decreasing beam current density, increasing gap length and optimal value of the cavity R/Q ratio. As a rule, such values cannot be achieved in a single gap cavity, so multigap cavities have to be used. Besides, one has to use complicated power sources.

Decreasing accelerating voltage, vice versa, decrease demanding R/Q ratio, but increases beam current. Large magnetic field is needed to transfer such beam through the interaction region. And cathodes with high current density have to be used.

The efficient way to overcome these difficulties is using a sheet electron beam. With a given beam current a sheet beam with cross-section $w \times d$ has current density approximately w/d times less than a pencil

beam with diameter d . But, cavities designed for interaction with a sheet beam have R/Q ratio much less than cavities for a pencil beam.

The mentioned considerations were taken into account in the project of 95 GHz high power klystron proposed by the “Svetlana-Electronpribor” JSC in collaboration with LETI. The pulsed output power of the device is no less than 1 kW, relative bandwidth $\geq 1\%$ and amplification factor ≥ 45 dB. After examining parameters of the existing devices, efficiency of the klystron was set at 10 % level. It is rather low value, but taking in account possible manufacturing difficulties, this value seems reasonable.

The accelerating voltage was set to 10 kV, which is rather low compared with, for example, CPI EIKs with $U_0 = 20 \dots 25$ kV. Chosen value helps us to design klystron cavities and obtain demanded bandwidth. The beam current in our case have to be 1 A. A pencil beam with such current has current density more than 5 Ka/cm^2 , which is unreal, so we chose sheet current with $1 \times 0.1 \text{ mm}^2$ cross-section.

Three-gaps cavities composed from a section of wide comb slow wave system were chosen as an input and idle resonators and four-gaps cavity of the same type – as an output resonator. The working mode of the all cavities is 2π because this mode well separated from the neighboring ones and has positive electron load, preventing self-oscillations.

To find optimal cavities configuration we used computer simulation code RFS [3], based on vector finite element method. Calculated cavity parameters are given in the table, where eigenfrequency f_0 , Q -factor, R/Q ratio, interaction factor M and relative electron load Ge/G_0 are listed.

Cavity type	f_0 , GHz	Q_0	R/Q , Ohm	M	G_{er}
Input & idle	94.3667	1120	83.1	0.654	0.3
Output	95.0617	1310	112	0.65	0.2

Fig. 1 shows the computer cavity models with main dimensions. Input and output cavities are coupled with waveguides by slots in their sidewall. Ceramic rods are used for cavity tuning (not shown on Fig. 1).

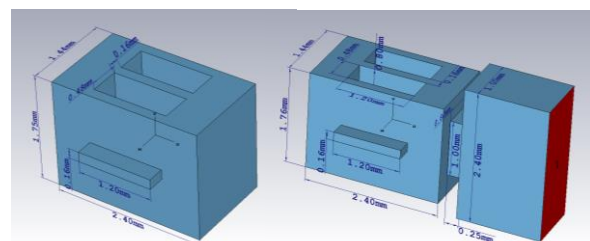


Fig. 1. Computer models of the input cavity (left) and output cavity with waveguide (right).

Input and output cavities frequency charts are shown on Fig. 2 for beam current 0.8 A and accelerating voltage 10 kV. As can be seen, the output cavity coupling slot provides bandwidth about 1 GHz, i. e. almost 1 %.

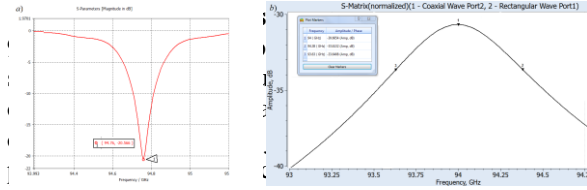


Fig. 2. Input (a) and output (b) cavities frequency charts.

The model of the klystron interaction region is shown on Fig. 3. The model contains 6 cavities, their eigen frequencies were tuned according to the skirtron scheme, where eigen frequencies of all intermediate (idle) cavities are higher than f_0 . Input cavity eigen frequency is lower than f_0 , and output cavity frequency is equal to f_0 . Electron gun, collector and magnetic focusing system are not shown.

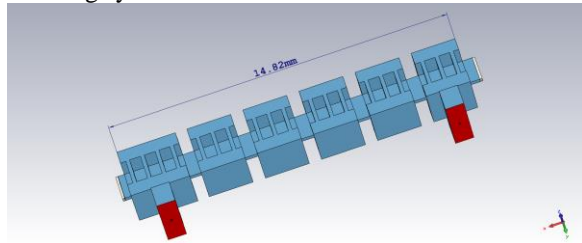


Fig. 3. Model of the klystron interaction region.

Field-particle interaction was modeled by Particle-in-Cell (PIC) method. Total number of particles in the interaction region was 26500, simulation time 15 ns, which was sufficient to reach stationary regime. Fig. 4. Shows calculated amplitude chart of the klystron at the central frequency. Klystron amplification factor changes from 60 dB for small signal regime to nearly 50 dB for the saturation point. These values are greater than targeted one.

Output power as a function of frequency at the input power level 8 mW is depicted on Fig. 5. The -3 dB bandwidth is 380 MHz, which is somewhat less than needed, but we hope that implementation of output filter circuit would give 500 MHz, or 0.5 % from carrying frequency.

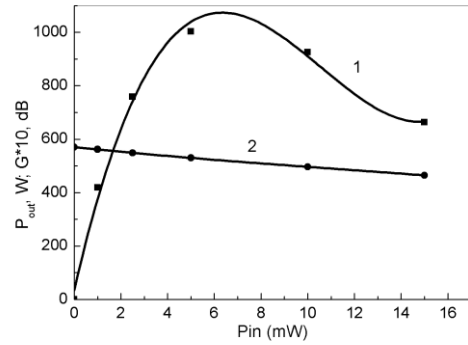


Fig. 4. Output power (1) and amplification factor (2) vs input power

The project confirmed the possibility of design and manufacturing 3-millimeter wavelength power klystron, using existing technological equipment.

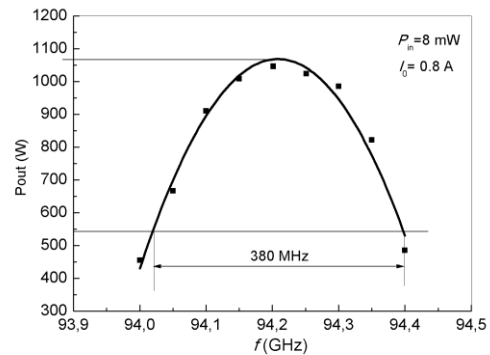


Fig. 5. Output power vs frequency

References

1. <http://citeseerx.ist.psu.edu/viewdoc/download?doi=10.1.1.734.2121&rep=rep1&type=pdf>.
2. Cariotakis, G. High power klystrons: theory and practice at the Stanford Linear Accelerator Center // SLAC-PUB 10620. 2005. 138 pp.
3. Grigoriev A. D., Salimov R.V., Tikhonov R.I. Cellular handsets antenna modeling by vector finite element method // Journal of communication technology and electronics. 2012, V.57, No 3, pp 261-270.

A

Electron-optics systems with decreased life-time of trapped electrons for terahertz gyrotrons

V.N.Manuilov^{1,2}, A.L.Goldenberg¹, M.Yu.Glyavin¹, K.A.Leshcheva^{1,2}

¹Institute of Applied Physics, Russian Academy of Sciences, N. Novgorod, Russia

²Lobachevsky State University of Nizhni Novgorod, N. Novgorod, Russia, e-mail: manuilov@rf.unn.ru

One of the most promising applications of novel gyrotrons is a high resolution spectroscopy [1]. For this goal, scientific society needs sources with rather low microwave power (typically, from 10W up to 1 KW) and frequencies 0.3-1.0 THz or even more. For the consumer, low operating voltage is preferable. Such frequency range can be obtained mainly at the second or even third cyclotron harmonic due to present cryomagnets limitations. Same time with frequency value, frequency tunability is very important for spectroscopy applications. It is a well known, that in a "short" cavity with a reduced length of homogeneous section (and, correspondently, lower Q-factor) tuning range becomes bigger. Unfortunately, decreasing of cavity length proportionally reduce the normalized length of the interaction space and, finally, push down gyrotron efficiency. Efficiency can be restored or even increase by rise of the electron pitch-factor g (ratio of gyration and longitudinal velocities) from 1.1-1.3 (at present tube) to 1.7-2.0. But in such case increase a number of electrons, reflected from the magnetic mirror (fig.1), that causes the beam instabilities. Suppression of this effect is possible by decreasing of the life-time of trapped electrons [2]. An effective way to eject trapped electrons is to install on the second anode in the triode gun the longitudinal ribs (fig.2).

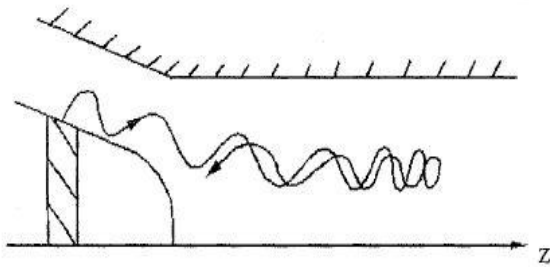


Fig. 1. The reflection of electrons from a magnetic mirror

The principle of extraction in a such gun is based on the particle drift in the crossed electric and magnetic fields. In traditional configuration of the above mentioned electron-optic system, such ribs intercept not only reflected particles, but also essential part of the primary electron beam, passed from the cathode to the cavity. To combine the small intersection of the primary beam with quick (during 1-2 longitudinal oscillations in the trap) catch of trapped electrons it is necessary to use the sectioned cathode, where emission takes place only from some sections spaced apart from azimuth angle, and/or special complex geometry of the ribs.

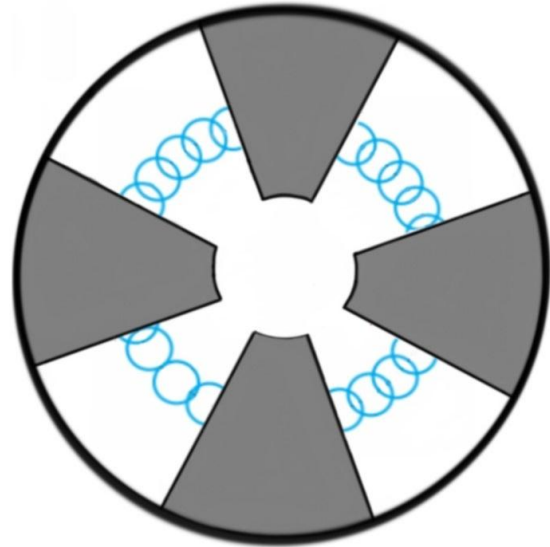


Fig. 2. The longitudinal ribs in the triode gun

In the report the preliminary geometry estimations of the sectioned electron-optic system are performed, including the profile and position of the ribs. Two versions of electron-optic system for low-voltage (16-20 kV) gyrotrons operating at the frequencies 10 GHz and 300 GHz are considered. The numerical simulation of both systems is performed. The possibility to catch the trapped electrons during first 1-2 longitudinal oscillations in the trap is shown. Same time reasonable thermal load on the longitudinal ribs is obtained, good enough for CW operation. So, proposed system looks promising for the formation of the stable helical electron beam and looks reasonable for future gyrotrons for spectroscopy applications.

The reported study was funded by RFBR according to the research project № 18-32-00142

References

1. J.H.Booske, R.J.Dobbs, C.D.Joye, C.L.Kory, G.R.Neil, G.Park, J.Park, R.J.Temkin. Vacuum electronic high power terahertz sources. // IEEE Trans. on Terahertz Science and Technology, 2011, V.1, No.1. pp.54-75
2. E. V. Ilyakov, I. S. Kulagin, V. N. Manuilov, A. S. Shevchenko Experiments on the formation of an intense helical electron beam under conditions of picking-up of the electrons reflected from the magnetic mirror // Radiophysics and Quantum Electronics, 2007, Volume 50, Issue 9, pp. 713-719.

Development of the Prototype of High Power Sub-THz Gyrotron for Advanced Fusion Power Plant (DEMO)

M.Morozkin¹, G.Denisov¹, E.Tai², E.Soluyanova², A.Sedov¹, A.Fokin¹, A.Kuftin¹, A.Tsvetkov¹, M.Bakulin², E.Sokolov², V.Malygin¹, M.Proyavin¹, V.Zapevalov¹, O. Mocheneva, and M.Glyavin¹

¹Institute of applied physics RAS, Nizhny Novgorod, Russia, morozkin@ipfran.ru

²Gycom Ltd., Nizhny Novgorod, Russia,

Next stage of the development of controlled nuclear fusion systems after the ITER project in accordance with the European Fusion Roadmap [1] is a demonstrational reactor DEMO, which should be the first thermonuclear reactor generating electrical energy. The parameters of the gyrotrons in the electron cyclotron heating system of the plasma of this reactor are not yet definitively specified, but frequencies of about 230-250 GHz and power up to 2 MW are discussed with an efficiency of more than 60% (full efficiency with energy recovery).

At present, most of the participants of the ITER project, which are involved in creating electron-cyclotron plasma heating systems, have already begun developing prototypes of radiation sources that meet the requirements of the DEMO project [2]. In the Institute of Applied Physics and Gycom Ltd. for these purposes, a prototype gyrotron with a frequency of 250 GHz and a radiation power of up to 200 kW in continuous mode was designed and tested (see fig. 1), intended for use in advanced fusion installations.



Fig. 1. Photo of the gyrotron in the cryomagnet.

The main factor limiting the output power in gyrotrons for plasma heating is the limitation of thermal loads on the cavity. Therefore, to increase the output power, it is necessary to increase the dimensions of the interaction space and use high-order modes. However, for the prototype gyrotron with an operating frequency of 250 GHz, the maximum size of the resonator and the electron-optical system was limited by the magnetic system. To generate the cyclotron frequency at the first harmonic, a magnetic field of more than 9.5 T is required, which is available in the cryomagnet at the IAP RAS, which has a warm bore of 100 mm in diameter. The warm bore diameter determined the dimensions of the electronic optics and

cavity taking into account the technical requirements for cooling systems.

As a result, to ensure stable generation at the selected frequency, the TE_{19,8} mode was selected as the working mode with a cavity radius of 9.34 mm.

Investigation of the coupling factors of the electron beam with the modes of the cylindrical cavity made it possible to determine the optimum radius of the electron beam in the cavity, which simultaneously provides both a large coupling coefficient with the working mode and the smallest coupling with parasitic modes. Due to the close coupling factors of the working mode TE_{19,8} and the parasitic modes TE_{18,8} and TE_{20,8}, the optimal radius of the electron beam is $R_{beam} = 3.93$ mm, which differs slightly from the radius of maximum coupling coefficient with the working mode $R_{opt} = 3.85$ mm.

To ensure the effective interaction of the electron beam with the high-frequency field, the cavity length was optimized. The choice of length is determined by the compromise between the increase in the efficiency of the interaction of electrons with the RF field and the limitation of ohmic losses in the walls of the cavity (see Fig. 2). As a result of modeling, the length of the homogeneous section was chosen to be $L = 10$ mm.

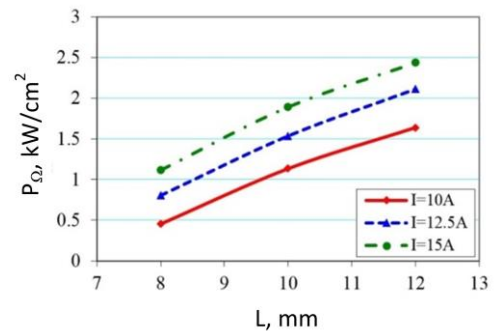
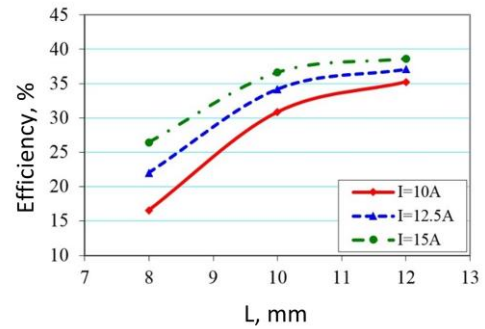


Fig. 2. Dependence of the efficiency and the density of ohmic losses on the length of a homogeneous part of the cavity

The calculated parameters of the developed gyrotron are given in the following table.

Main parameters of the gyrotron

Operating frequency, GHz	250
Operating mode	TE _{19,8}
Cyclotron harmonic	1
Accelerating voltage U_0	55 kV
Depressed collector potential	30 kV
Magnetic field in the cavity	9.6-9.7 T
Beam current (nominal in CW mode)	12 A
Beam current (pulsed mode)	20 A
Cavity radius	9.34 mm
Cavity length (homogeneous part)	10 mm
Beam radius inside cavity	3.93 mm
Pitch factor, not less than	1.1

The tube is equipped with an internal quasi-optical wave beam converter which provides a transformation of the operating mode into a Gaussian TEM₀₀ beam and couples it radially to the vacuum window. The converter consists of a shaped waveguide, a quadratic mirror, four flat mirrors, and a synthesized mirror, which allows directing the wave beam in the output window.

The first experimental tests of the developed gyrotron were carried out at the IAP RAS on a high-frequency gyrotron setup equipped with a dry cryomagnet Jastec JM1D10T100 with a warm bore of 100 mm in diameter and a magnetic field of up to 10 T. Due to the limitations of the power sources existing in the IAP RAS, the first experiments were carried out in a pulsed mode. For this tests a removable BN output window with a diameter of 66 mm was manufactured and installed. The thickness of the window was chosen to be about 3.1 mm in order to minimize the reflections at the operating frequency of 250 GHz. The pulse duration in the experiment was 20-40 μ s with a repetition frequency of 10 Hz. The power was measured with a water calorimetric dummy load equipped with thermal sensors in the inlet and outlet nozzles, the calibration was carried out with a heater in the circuit of a calorimeter with a known power of 100 W. The output power of the gyrotron was calculated on the basis of the measurement of the steady-state average power in the pulsed mode, taking into account the duty cycle of 2500.

The frequency of the output radiation was measured using a resonant-cavity wave meter. The registered value of 249.74 GHz has been obtained at the following operating parameters: accelerating (cathode) voltage $U_0 = 55$ kV, beam current $I_b = 12.5$ A, and magnetic field $B = 9.625$ T. These results are in agreement with the simulation data.

Reduction of the thermal load on the resonator during operation in the pulsed mode made it possible to test gyrotron with parameters exceeding the nominal design values. Thus, with an increase in the electron beam current, it was possible to reach a power of 330 kW at a beam current of 20 A and an accelerating voltage of 55 kV. The obtained experimental results are shown in Figures 3 and 4.

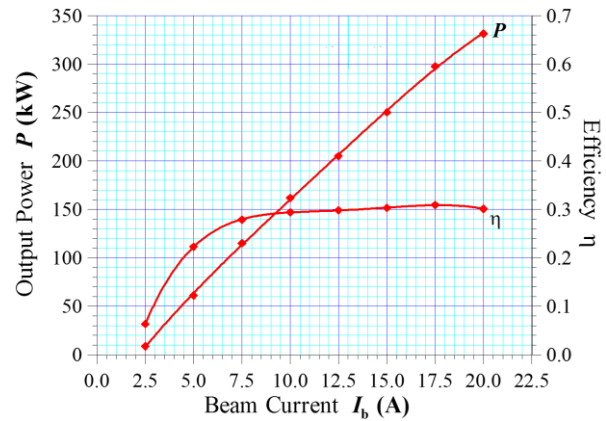


Fig. 3. Dependence of the output power and efficiency on the beam current, $U_0 = 55$ kV.

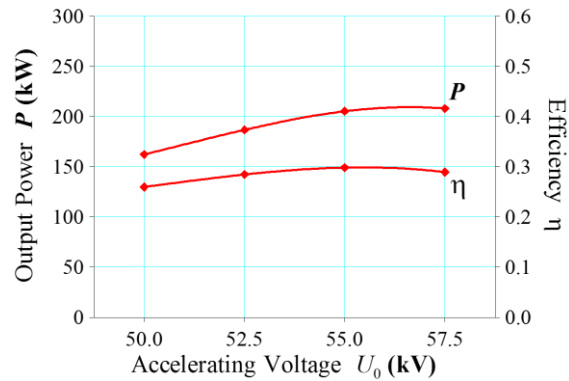


Fig. 4. Dependence of the output power and efficiency on the accelerating voltage, $I_b = 12.5$ A.

Measurements of the transverse distribution of the microwave beam formed by the built-in quasi-optical gyrotron converter were made, and the content of the TEM₀₀ wave (Gaussian beam) was estimated. The measurement was performed according to the thermal imaging technique [3] in several cross sections during the propagation of a wave beam. As the analysis showed, the content of a Gaussian wave beam in the reconstructed wave beam is 98.6%.

Thus, the tested 250-GHz gyrotron showed output parameters close to the calculated ones: the power of 220 kW at a beam current of 12.5 A (corresponds to the beam current in a continuous mode) and 330 kW at a beam current of 20 A. The generation efficiency was about 30% (without energy recovery), the content of the TEM₀₀ wave in the output beam is 98.6%.

This work was supported by Russian scientific fund, grant 14-12-00887.

References

1. <https://www.euro-fusion.org/eurofusion/roadmap/>
2. J. Jelonnek et al. Design considerations for future DEMO gyrotrons: A review on related gyrotron activities within EUROfusion // Fusion Eng. Des. 2017. V. 123, P. 241–246.
3. S. O. Kuznezov, V. I. Malygin Determination of gyrotron wave beam parameters // Int. J. Infrared Millimeter Waves 1991. V. 12, No. 11, P. 1241–1252.

Thermal regimes and THz generation from BSCCO mesas

L.S. Revin¹, E.A. Vopilkin¹, A.L. Pankratov¹, S.A. Kraev¹,
A.A. Yablokov¹, S.A. Churin¹, A.B. Kulakov²

¹Institute for Physics of Microstructures of Russian Academy of Sciences, Nizhny Novgorod, Russia, alp@ipmras.ru

²Institute of Solid State Physics of RAS

At present, the question of creating generators of subTHz and THz ranges based on $\text{Bi}_2\text{Sr}_2\text{CaCu}_2\text{O}_{8+x}$ (BSCCO) mesastructures is of great interest [1]. BSCCO is a high-temperature superconductor with strong anisotropy, which leads to the appearance of an internal Josephson effect [2]. In other words, CuO layers represent a series of Josephson chains formed on an atomic scale. The first success in observing of electromagnetic radiation from BSCCO structures was achieved in 2007 [3]. The observed radiation had a power of the order of $0.5 \mu\text{W}$ and a frequency up to 0.85 THz. Since that time the radiation power has been increased to a value of hundreds of microwatts [4]. These achievements make it possible to use BSCCO mesostructures as sources for noise spectroscopy [5, 6].

In our group the technology of electrolytic build-up of a BSCCO/Cu heterostructures is worked out, representing copper covering over a thin layer of gold, that allows to get rigid single BSCCO mesastructures with a good heatsink. To obtain the described samples, we used a BSCCO single crystal, fabricated at ISSP RAS, of several microns thick with lateral dimensions of several millimeters. On one of its surfaces, a layer of 50 nm thick gold was deposited by thermal deposition. After this a layer of copper with thickness of about 30 microns was electrolytically built up on top of the gold layer. Then a layer of 50 nm thick gold was deposited on BSSCO second surface by thermal deposition. After that, using the original method of fast chemical etching [7], developed in our team, the cylindrical single mesastructures were fabricated. The obtained sample was glued to the copper holder, Fig. 1, after which it is taped to the contact pads and installed in a cryostat.

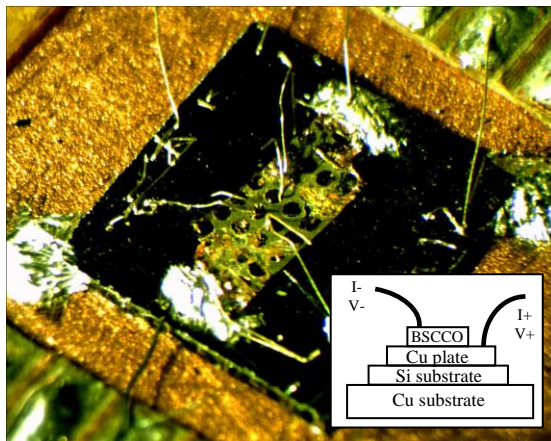


Fig. 1. Photo of the mesas connected by wires. Inset: Schematic view of the Si substrate with BSCCO sample, attached to the copper holder

To measure the radiated power, the room temperature detector (Golay cell) together with the horn and infrared filters were used, Fig. 2. Although the obtained samples were not intended for effective power radiation, since antennas and lenses were not supposed, the level of the expected signal was sufficient. The calculated diagram had maxima at 45° from the plane and only a small amount of radiation was detected outside the cryostat window with the holder parallel to the cryostat plate.

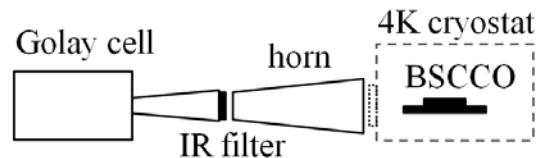


Fig. 2. Schematic of the experimental setup

In Fig. 3 the current-voltage characteristic of BSCCO mesa is presented, forward and backward branches are measured. The shape of the curve indicates the presence of Josephson generation in the structure. On the forward branch there are transitions from the superconducting state to the resistive one both of the individual junctions of the layered superconductor and of the entire structure. On the backward branch there is an area of negative differential resistance, which indicates the presence of a "hot spot" inside the mesastructure, the heating region of the structure, which is the channel for synchronization of electromagnetic waves in the superconductor-insulator-superconductor layers.

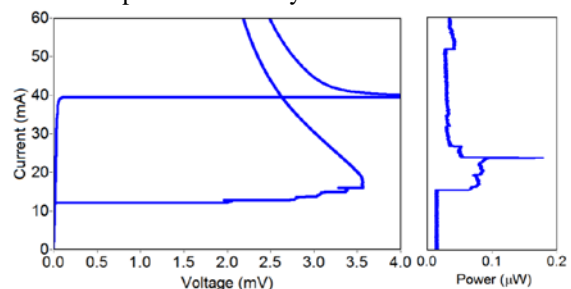


Fig. 3. The voltage and received power as a function of bias current

As a result, the statistics of the obtained structures were processed, and the characteristics of the samples were compared with the world level. Thus, the critical current density of the obtained samples $J_c = 30 - 70 \text{ A/cm}^2$ is close to the literature data $J_c = 80-250 \text{ A/cm}^2$. The gap voltage in terms of one junction $V_g =$

0.6 - 0.7 mV is also close to the literature data $V_g = 1 - 1.4$ mV.

Experiments on detecting the radiation from BSCCO sample allow to obtain a signal of the order 0.05–0.08 μ W. Radiation was observed at the plate temperature of 18 K when the substrate was attached to a copper holder by a rubber glue. Conversely, when the substrate was attached by indium, no radiation was observed, presumably due to a too-low holder temperature at a better heat sink or not enough over-heating due to a too-efficient heat sink.



Fig. 4. Photo of BSCCO single crystal fabricated by Bridgman technique

Recently, first BSCCO single crystal samples have been fabricated at IPM RAS by Bridgman technique, having a plain surface of order 3 by 10 mm, see Fig. 4. The samples have been measured in a cryostat and critical temperature of 84K has been achieved for oxygen annealed samples, see Fig. 5. Currently, new BSCCO single mesas with Cu sublayer from these single crystals are under fabrication.

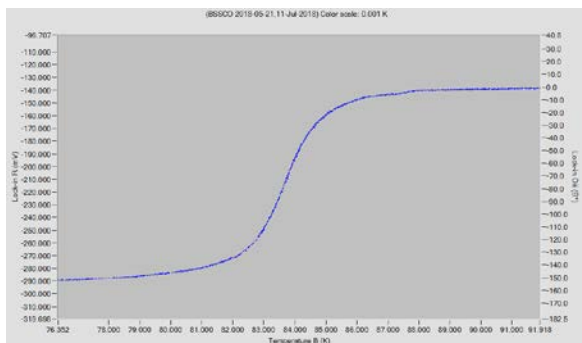


Fig. 5. Measurement of BSCCO single crystal critical temperature

In conclusion, we report on the progress of the wet etching method for the fabrication of BSCCO mesastructures, making it possible to obtain samples with a large thickness on the order of 1-15 μ m. The current-voltage curves of BSCCO mesas are measured at different plate temperatures and there is a significant dependence on the thermal interface. It is possible to determine the power (of the order of 0.1 μ W) outside the cryostat by a room temperature detector. BSCCO single crystals, having critical temperature of 84K were fabricated by Bridgman technique.

The work is supported by RSF (project 16-19-10478).

References

1. Welp, U., Kadowaki, K., Kleiner, R., Superconducting emitters of THz radiation // Nat. Photonics. 2013, Vol. 7, pp. 702
2. Kleiner R., Steinmeyer, F., Kunkel G., Mueller P., Intrinsic Josephson effects in Bi2Sr2CaCu2O8 single crystals // Phys. Rev. Lett. 1992, Vol. 68, p. 2394.
3. Ozyuzer, L., Koshelev, A.E., Kurter, C., Gopalsami, N., et al Emission of Coherent THz Radiation from Superconductors // Science 318, 2007, p. 1291.
4. Yamaki, K., Tsujimoto, M., Yamamoto, T., Furukawa, A., Kashiwagi, T., Minami, H., Kadowaki, K., High-power terahertz electromagnetic wave emission from high-Tc superconducting Bi2Sr2CaCu2O8+ δ mesa structures // Opt. Express. 2011. Vol. 19, P. 3193.
5. Revin, L.S., Vaks, V.L., Koshelets, V.P., Wang, H., // EPJ Web of Conferences. 2017, Vol. 132, P. 03042.
6. Sobakinskaya, E.A., Vax, V.L., Kinev, N.V., Koshelets, V.P., Wang, H., // Proc. 1st Russian Microwave Conf. 2013, p. 1015.
7. Vopilkin E.A., Chiginev A.V., Revin L.S., Tropanova A.N., Shuleshova I.Yu., Okhapkin A.I., Shovkun A.D., Kulakov A.B., Pankratov A.L., Quick and reliable technology for fabrication of stand-alone BSCCO mesas, // Supercond. Sci. Technol. 2015, Vol. 28, P. 045006.

Development of powerful long-pulse Bragg FELs operating from sub-THz to THz bands based on linear induction accelerators: recent results and projects

N.Yu. Peskov¹, N.S. Ginzburg¹, A.M. Malkin¹, A.S. Sergeev¹, V.Yu. Zaslavsky¹,
A.K. Kaminsky², S.N. Sedykh², I.I. Golubev², S.M. Golubykh², A.P. Kozlov², A.I. Sidorov²,
A.V. Arzhannikov³, D.A. Nikiforov³, S.L. Sinitsky³, D.I. Skovorodin³ and A.A. Starostenko³

¹Institute of Applied Physics RAS, Nizhny Novgorod, Russia, peskov@appl.sci-nnov.ru

²Joint Institute for Nuclear Research, Dubna, Russia,

³Budker Institute of Nuclear Physics RAS, Novosibirsk, Russia

Introduction

To date, a series of successful experiments on the realization of powerful high-efficiency free-electron masers (FEMs) has been carried out in collaboration between JINR (Dubna) and IAP RAS (N.Novgorod) based on linac LIU-3000 0.8 MeV / 200 A / 250 ns. The use of high-selective Bragg resonators of new types allowed stable regime of narrow-band generation to be obtained in these experiments up to W-band at multi-MW powers [1, 2]. The radiation parameters achieved allows JINR-IAP FEM to be used in several applications including testing of components for high-gradient accelerators, biology-medical studies, physics of nanoparticles, etc [3].

The aim of present work is advance of powerful long-pulse FELs into the THz frequencies. Such project is initiated based on the linear induction accelerators, which are developing in the BINP RAS (Novosibirsk) 5 - 20 MeV / 2 kA / 200 ns. In this paper, we discuss the basic parameters of such FELs and the results of their computer simulations. As a microwave system capable to provide stable narrow-band operation in strongly oversized interaction space in these FELs, we consider so-called advanced Bragg structures with the feedback loop involving propagating and quasi-cutoff waves (Fig. 1) [4, 5].

JINR-IAP FEM operating from Ka- to W-band

The JINR-IAP FEM is driven by induction linac LIU-3000 (JINR). A reversed guide magnetic field configuration is used in the FEM, which possesses low sensitivity to the initial beam spread and, as a result, provides high-efficiency interaction. For operation from Ka- to W-bands, helical wigglers having periods from 6 cm to 3 cm correspondingly were constructed. Enhance in amplitude of the transverse magnetic field in short-period wigglers alongside with refining its transverse homogeneity was achieved by optimization of the currents distribution in the wiggler winding. To improve the quality of helical electron beam formation at short wavelengths, the slowly up-tapered wiggler entrance was optimized as well [2].

For operation in different parts of the millimeter wavelength band a series of combined two-mirror Bragg resonators, consisted from the up-stream high-selective advanced Bragg reflector and down-stream weakly-reflecting conventional Bragg reflector (Fig.1a), was elaborated. Resonators of such type

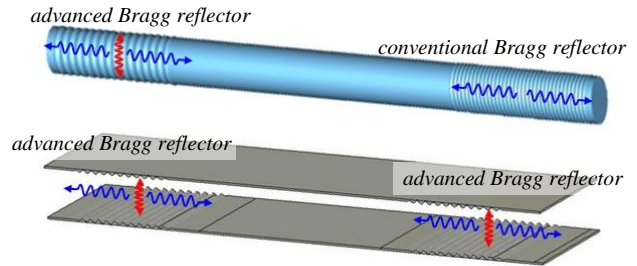


Fig. 1. Different schemes of Bragg resonators: (a) combined two-mirror resonator based on advanced and conventional Bragg reflectors of cylindrical geometry and (b) two-mirror resonator consisted from two advanced Bragg reflectors of planar geometry. The partial wave-fluxes in both reflectors are shown by the arrows.

allow decrease in Ohmic losses associated with excitation of the cut-off mode. For operation at 30 GHz, combined Bragg resonator was constructed with the oversized parameter $\varnothing/\lambda \sim 2$ and included advanced Bragg reflector with a feedback loop formed by two counter-propagating $TE_{1,1}$ waves and cutoff $TE_{1,2}$ wave. Resonator for V-band (60 GHz) was composed with advanced up-stream Bragg reflector having feedback loop $TE_{1,1} \leftrightarrow TM_{1,2} - \text{cutoff} \leftrightarrow TE_{1,1}$ at the oversize parameter $\varnothing/\lambda \sim 3$. For W-band (80 GHz) advanced Bragg reflectors based on excitation of the feedback cutoff wave of $TE_{1,5}$ -type were designed to provide an effective FEM operation at oversize parameter $\varnothing/\lambda \sim 5$ (Fig. 2). In accordance with the 3D simulations, effective narrow-band reflections were demonstrated in “cold” test of novel Bragg structures. In all resonators described above the reflection band in advanced Bragg structures was measured 0.5 - 0.7 GHz with maximum power reflection up to 80 - 90%, while the conventional structures had $\sim 60\%$ reflection in much broader band of 2.5 - 3 GHz.

In the proof-of-principle experiments at LIU-3000 a narrow-band operation of novel scheme of FEM-oscillators was obtained under design parameters. At Ka-band, stable single-mode operation at the frequency of 30.2 GHz was observed in accordance with simulations. The output power amounted up to 20 MW (efficiency about 15 - 20%) with the spectrum width of 6 - 7 MHz (measured by heterodyne technique) close to the theoretical limit (Fig. 3).

In the experiments at V- and W-band, the radiation spectrum was measured by means of cut-off filters set with the accuracy of about 1 GHz. Both FEM demonstrated the oscillation frequency belonging to the designed feedback loop of the hybrid resonator in

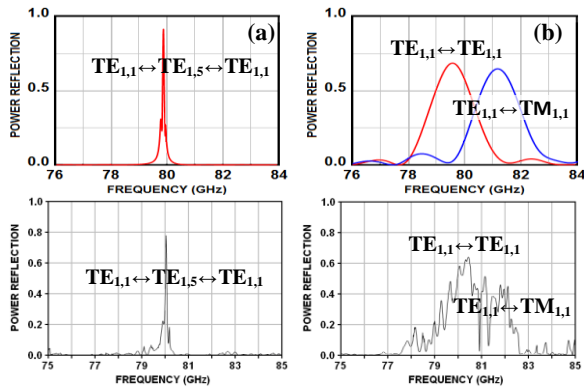


Fig. 2. Results of 3D simulations (top) and “cold” tests of Bragg structures of different types at W-band. Frequency dependence of reflection of (a) advanced ($l_{adv} = 12$ cm) and (b) conventional ($l_{con} = 8$ cm) reflectors.

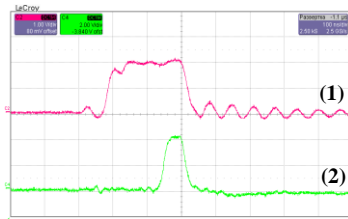


Fig. 3. Results of the JINR-IAP FEM experiments in W-band. Typical oscilloscope traces of (1) beam current and (2) output RF-pulse (100 ns / div.).

the vicinity of 59 GHz and 80 GHz correspondingly. In the resonators of optimal geometry the output power (measured by calorimeter) in both frequency regions amounted to 5 - 7 MW when the beam current was about 70 - 100 A (Fig. 3), which corresponded to the electron efficiency of up to 10 - 12%.

Project of powerful Bragg FEL for THz-band

Further increase of the radiation frequency in the JINR-IAP FEM is restricted by the wiggler period and electron beam energy. To advance FEL of this type into THz frequencies, it is attractive to exploit more powerful induction linac, which was elaborated currently at BINP RAS (the LIU-2 accelerator) [6]. This accelerator generates electron beam with the current of kA-level and energy of 2 - 5 MeV (with the possibility to increase electrons energy up to 20 MeV).

Based on this beam, we initiated new project of multi-MW long-pulse THz FEL. In fact, the use of the beam with specified particles energy allows realization of the FEL in the range 1 - 10 THz using the wiggler of 3 - 6 cm period. For the realized beam current of ~ 1 - 2 kA, the radiation power is estimated on the level of 10 - 100 MW even under the electron efficiency of 1 - 0.1% (which, obviously, would decrease with increase of the radiation frequency).

Results of simulation of the FEL driven by 5 MeV / 1 kA electron beam generated by the LIU - 2 are presented in Fig. 4. This beam is focused by the guide magnetic field of ~ 0.15 T (in reversed configuration) and operating transverse electron velocities in the beam are pumped by the wiggler having 4 cm spatial period. For this FEL-oscillator we consider two-mirror resonator consisting of advanced Bragg reflectors of planar geometry (Fig.1b). Simulations demonstrated that Bragg structures of such type

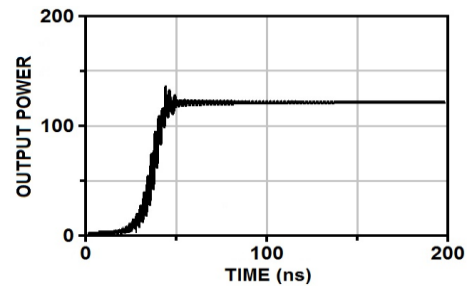


Fig. 4. Results of simulations of THz-band FEL based on linac LIU-2 (BINP RAS).

possess high reflectivity and ensure selectivity of the resonator for the transverse size (gap) up to 20 wavelengths. This size is sufficient for usage with the intense relativistic electron beams. For operation at 1 THz, we designed the resonator with 6 mm gap and the Bragg structures of 20 cm (up-stream) and 10 cm (down-stream) long having corrugation of the 0.3 mm period and 10 - 15 μ m depth, a regular section of 50 - 70 cm long between them. According to the simulations, under design parameters the electron efficiency could achieve 2 - 3% and the output power reaches up to 50 - 100 MW. The Ohmic losses in this case do not exceed 25 - 30% from the radiated power.

Summarizing, novel conception of powerful THz-band Bragg FEL is developed. Original feature of this concept (in comparison with the others for now operating THz FEL) is the possibility to use electron beams with high-current (kA-level) and long-pulse (hundreds ns) duration. Such beams would allow achieving record levels of the radiation power of 10 - 100 MW and pulse energy up to 10 J for the THz-band. Operability of key components of electrodynamic system for such FEL - advanced Bragg resonators - was demonstrated in the proof-of-principle experiments up to W-band under oversized parameter $\Phi/\lambda \sim 5$.

This work is partially supported by the Russian Foundation for Basic Research (grant # 18-02-40009).

References

1. A.K. Kaminsky, E.A. Perelstein, S.N. Sedykh, *e.a.* Demonstration of powerful 30-GHz FEM operation with resonant load // *Tech. Phys. Lett.* 2010. V.36 No.5 P.37.
2. N.Yu. Peskov, N.S. Ginzburg, A.K. Kaminsky, *e.a.* Powerful FEM-oscillators with advanced Bragg resonators operating in a single mode regime from Ka- to W-band // *Proc. of the 41th Int. Conf. on IR, MM and THz Waves, Copenhagen, Denmark, 2016, p.F2E.01.*
3. N.S. Ginzburg, I.I. Golubev, A.K. Kaminsky, *e.a.* Experiment on pulse heating and surface degradation of a copper cavity powered by powerful 30 GHz free electron maser // *Phys. Rev. Accel. Beams* 2011. V.14. No.4. P.041002.
4. N.S. Ginzburg, A.M. Malkin, N.Yu. Peskov, *e.a.* Improving selectivity of free electron maser with 1D Bragg resonator using coupling of propagating and trapped waves // *Phys. Rev. Accel. Beams* 2005. V.8. P.040705.
5. N.S. Ginzburg, V.Y. Zaslavsky, I.V. Zotova, *e.a.* Terahertz Free-Electron Lasers with Bragg structures based on coupling between travelling and quasi-cutoff waves // *JETP Lett.* 2010. V.91. No.6. P.266.
6. P.V. Logachev, G.I. Kuznetsov, A A Korepanov, *e.a.* LIU-2 linear induction accelerator // *Instruments and Experimental Techniques.* 2013. V.56. No.6. P.672.

Generation of Ultra-Short Microwave Pulses in a Tunable Gyrotron with Subsequent Compression

R.M. Rozental¹, I.V. Zotova¹, N.S. Ginzburg¹, V.P. Tarakanov^{2,3}

¹ Institute of Applied Physics RAS, Nizhny Novgorod, Russia, rrz@appl.sci-nnov.ru

² Moscow Engineering Physics Institute, Moscow, Russia

³ Joint Institute for High Temperatures, RAS, Moscow, Russia

Generation of ultrashort electromagnetic pulses is of interest for many applications. A well-known method for obtaining such pulses is based on the compression of a frequency-modulated signal in a dispersive medium [1]. In principle, as such media, one can use regular waveguides. However, in this the frequency range optimal for compression is very close to the critical frequency, where the dispersion of the wave is most pronounced. This creates problems for ensuring matching in the operating band of the input chirped source. In [2,3] for solution of this problem, the compression in the helical waveguides is proposed. But in high-frequencies band such systems are rather complicated for manufacturing.

In this paper we suggest the two-stage scheme of generation of multi kilowatts subnanosecond microwave pulses based on a gyrotron matching directly with a compression section in the form of a regular waveguide. It is well-known, that gyrotrons typically have a rather narrow band of frequency tuning ($\sim 0.1-0.3\%$). However, as it was shown in [4], significant widening of the generation band in gyrotrons can be achieved with using of a shortened interaction space due to the weaker sensitivity to the velocity spread in the electron beam. The required frequency tuning of 5% can be provided due to excitation of several axial modes.

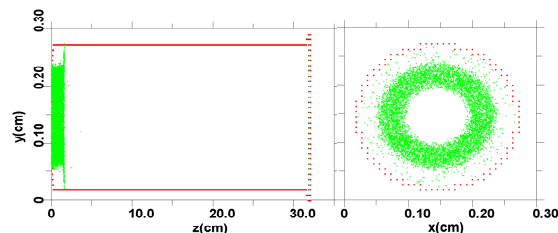


Fig. 1 Geometry of the interaction region.

Further, results of particle-in-cell simulations of such a system are presented based on the KARAT code [5]. In Fig.1 the geometry of the interaction region is shown, where the first section with an electron beam corresponds to a gyrotron with rather short resonator, while the second one is the section of compression. The Ohmic losses were taken into account. The electron beam with the current of 2 A, excites the TE_{21} mode at the frequency of about 200 GHz. The operating voltage due to variation of an accelerating voltage from 90 to 15 kV, the operating frequency of a gyrotron varies from 200 to 210 GHz in the pulse with a duration of 12 ns (Fig.2a). The radiation power at the output of a gyrotron doesn't exceed 8 kW. In

the second stage, the radiation is compressed in a regular waveguide connected directly to the gyrotron resonator. As a result, the output radiation represents the subnanosecond pulse with power of 80 kW.

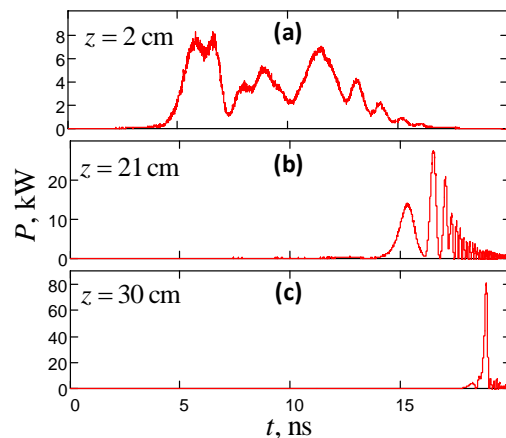


Fig. 2. Evolution of the radiated pulse in the section of compression.

This research was performed within the framework of the RFBR project No. 18-08-00717.

References

1. Petelin, M. Microwave pulse compressors // Proc. Int. Workshop on Strong Microwaves in Plasmas. 1997. V. 2. P. 903.
2. Samsonov, S.V., Phelps, A.D.R., Bratman, V.L., Burt, G., Denisov, G.G., Cross, A.W., Ronald, K., He, W., Yin, H. Compression of Frequency-Modulated Pulses using Helically Corrugated Waveguides and Its Potential for Generating Multigigawatt rf Radiation // Phys. Rev. Lett. 2004. V. 92. No.11. Art.no. 118301.
3. Bratman, V.L., Denisov, G.G., Kolganov, N.G., Mishakin, S.V., Samsonov, S.V., Cross, A.W., He, W., Zhang, L., McStravick, M.C., Whyte, G., Young, A.R., Ronald, K., Robertson, C.W., Phelps, A.D.R. Generation of 3 GW microwave pulses in X-band from a combination of a relativistic backward-wave oscillator and a helical-waveguide compressor // Phys. Plasmas. 2010. V. 17. No. 11. Art.no. 110703.
4. Fedotov, A.E., Rozental, R.M., Zotova, I.V., Ginzburg, N.S., Sergeev, A.S., Tarakanov, V.P., Glyavin, M.Yu., Idehara T. Frequency Tunable sub-THz Gyrotron for Direct Measurements of Positronium Hyperfine Structure // J Infrared Milli Terahz Waves. 2018. V. 39. No. 10. P. 975.
5. Tarakanov, V.P. Code KARAT in simulations of power microwave sources including Cherenkov plasma devices, vircators, orotron, E-field sensor, calorimeter etc. // EPJ Web of Conferences. 2017. V. 331. Art.no. 04024.

Gyrotrons with Shortened Cavities as Tunable Sources of Powerful Sub-Terahertz Radiation for Spectroscopic Applications

M.Yu. Glyavin, A.E. Fedotov, R.M. Rozental, I.V. Zotova, A.S. Zuev,
V.N. Manuilov, M.Yu. Tretyakov, D.S. Makarov

Institute of Applied Physics RAS, Nizhny Novgorod, Russia, zotova@appl.sci-nnov.ru

Studies of forbidden resonance transitions are among the most complicated and most interesting problems in molecular gas spectroscopy. Typical transitions of this type are quadrupole transitions. Such transitions should be found in the spectra of all molecules, but currently only single vibrational-rotational lines of nonpolar molecules such as H₂, N₂, CO₂, etc. can be detected. The intensity of quadrupole transitions is very small. Therefore, an extraordinary sensitivity of the spectrometers is required for their observation and analysis. Most part of the spectrometers detecting radiation transmitted through a gas or re-emitted by a gas, have reached a sensitivity close to their theoretical limit. Only spectrometers using the method of radioacoustic detection of radiation absorption (RAD) by gases can provide a reserve of increasing sensitivity due to an increase in the power of the probing radiation [1]. Implementation of this idea requires the development of a CW coherent frequency-tunable radiation source.

In this paper, we discuss the possibility of developing powerful (>100 W) subterahertz gyrotron with frequency tuning band of about 3-5%, which is aimed to be used for RAD spectroscopy of quadrupole transitions of CO₂ at the frequency of 163 GHz. As it was demonstrated in [2], significant widening of the generation band in gyrotrons can be achieved with using of a shortened interaction space due to the weaker sensitivity to the velocity spread in the electron beam. At the same time, the shortening of the resonator will require increasing the current of the gyrotron electron beam. However, the required current value can be substantially reduced by going to operation at low transverse modes due to the growth of the electron-wave coupling coefficient. With a certain optimization, such approaches can provide a sufficiently wide band of gyrotron generation.

Further, results of PIC simulations are presented with using the KARAT code [3]. For 15 keV/0.4 A electron beam with pitch factor of 1 the TE₁₃ mode, counter-rotating with electron motion in the guiding magnetic field, was chosen as an operating one. In Fig.1 the geometry of magnetron-injection gun (MIG) with above indicated parameters are presented. The gyrotron resonator was formed by a section of a circular waveguide bounded by a cutoff narrowing at the cathode end and a smooth widening at the collector end. The radius and the length of the regular part of resonator was 0.25 cm and 2.5 cm, correspondingly.

The simulations evidence that for the velocity spread of 20% the radiation power exceeds 100 W in the entire frequency tuning band of 4.1 GHz (2.5%)

(Fig.2). For magnetic fields from 5.87 to 6.35 T, stationary single-mode excitation of the operating TE₁₃ mode takes place. For magnetic field values outside this region, the excitation of the parasitic transverse TE₄₂ and TE₃₂ modes occurs, which limits the further increase in the bandwidth.

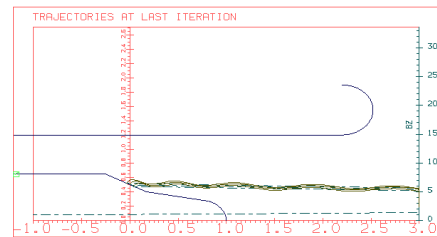


Fig. 1 Geometry of the MIG cathode part for a 163 GHz frequency-tunable gyrotron.

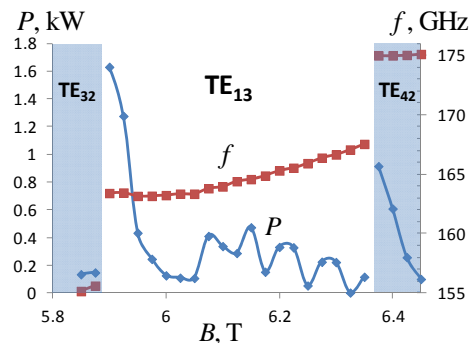


Fig. 2 Results of PIC simulations. Dependence of output power and operating frequency on the guiding magnetic field.

The work is supported by the Russian Science Foundation under grant No. 18-12-00394.

References

1. Koshelev, M.A., Tsvetkov, A.I., Morozkin, M.V., Glyavin, M.Yu., Tretyakov, M.Yu. Molecular gas spectroscopy using radioacoustic detection and high-power coherent subterahertz radiation sources // J. Mol. Spectrosc. 2017. V.331. P. 9–16.
2. Fedotov, A.E., Rozental, R.M., Zotova, I.V., Ginzburg, N.S., Sergeev, A.S., Tarakanov, V.P., Glyavin, M.Yu., Idehara T. Frequency Tunable sub-THz Gyrotron for Direct Measurements of Positronium Hyperfine Structure // J Infrared Milli Terahz Waves. 2018. V. 39.
3. Tarakanov, V.P. Code KARAT in simulations of power microwave sources including Cherenkov plasma devices, vircators, orotron, E-field sensor, calorimeter etc. // EPJ Web of Conferences. 2017. V. 331. Art.no. 04024.

Rogue-waves generation in the terahertz region

R.M. Rozental, N.S.Ginzburg, A.M. Malkin, A.S. Sergeev, V.Yu. Zaslavsky, I.V. Zotova

Institute of Applied Physics RAS, Nizhny Novgorod, Russia, rrz@appl.sci-nnov.ru

One of the promising schemes of high-power terahertz radiation generators are gyrotrons with planar configuration of interaction space [1]. In such a configuration, by reducing the distance between the plates of the cavity, it is possible to obtain a large current parameter sufficient for occurrence of rogue waves – ultrashort pulses with a peak power exceeding the power of the unperturbed electron beam [2].

For description of rogue waves in gyrotron the self-consistent time-domain model was used:

$$i \frac{\partial^2 a}{\partial Z^2} + \frac{\partial a}{\partial \tau} = \frac{i I_0}{2\pi} \int_0^{2\pi} \frac{\hat{p}_\perp}{\hat{p}_\parallel} d\theta_0,$$

$$\left[\frac{\partial}{\partial Z} + \frac{g^2}{4} \frac{\partial}{\partial \tau} \right] p_\perp + i \frac{p_\perp}{p_\parallel} \left(\Delta - 1 + |p_\perp|^2 + \frac{p_\parallel^2 - 1}{g^2} \right) = i \frac{a}{\hat{p}_\parallel} + \frac{\beta_{\perp 0}^2}{2} \frac{\partial a}{\partial Z}$$

$$\left[\frac{\partial}{\partial Z} + \frac{g^2}{4} \frac{\partial}{\partial \tau} \right] p_\parallel = -g^2 \frac{\beta_{\perp 0}^2}{2} \operatorname{Re} \left(\frac{\partial a}{\partial Z} \frac{p_\perp^*}{p_\parallel} \right)$$

where $a(Z, \tau)$ – normalized amplitude of the operating wave; Z, τ – normalized coordinate and time; $p_{\perp, \parallel}$ – normalized particle moments, I_0 – current parameter, Δ – initial mismatch between the wave cutoff frequency, g – initial pitch-ratio.

In simulations we assumed that the 300 GHz gyrotron excited by the planar electron beam with energy of about 200 keV, current density of about 2 kA/cm and pitch-factor of about 1.0 at the lowest TE mode of the planar waveguide. With this parameters the value of the dimensionless current parameter $I_0 \approx 1$, which is enough for the radiation of rogue waves.

All processes were analyzed over a time interval of several tens of nanoseconds, which corresponds to the typical pulse duration in electron guns based on explosive emission cathodes. Simulation showed that in a sufficiently wide range of magnetic fields in the system, it is possible to generate rogue waves with a peak power of several hundred megawatts (Fig.1).

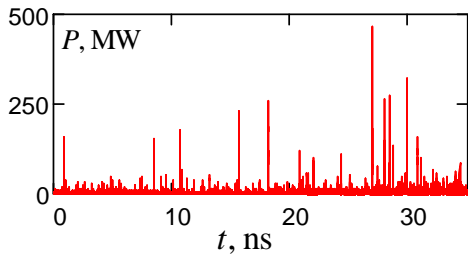


Fig. 1. The time dependence of the output power for simulation of planar gyrotron based on the averaged equations.

The obtained results have been confirmed by direct PIC simulations at KARAT code [3]. In the simulation, pulses of a duration of the order of 10 ps were obtained with a peak power reaching hundreds of megawatts (Fig.2a). The total width of the emission spectrum reached 150 GHz (Fig. 2b).

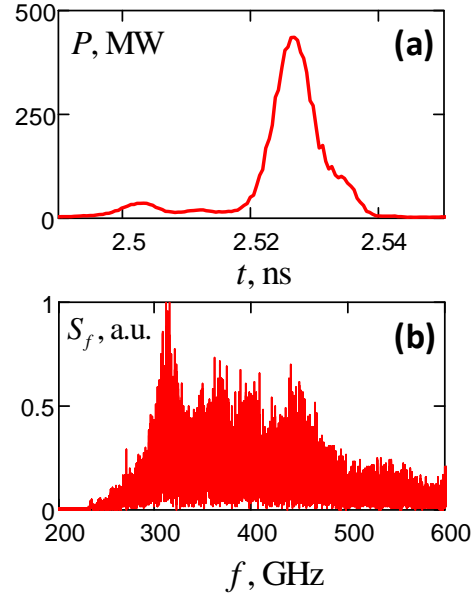


Fig. 2. Results of PIC simulation: (a) – a typical form of an rogue wave; (b) is the total spectrum of the output radiation.

This research was performed within the framework of the RFBR project No. 17-08-01077.

References

1. Zaslavsky, V.Yu., Ginzburg, N.S., Glyavin, M.Yu., Zheleznov, I.V., Zotova, I.V. Three-dimensional particle-in-cell modeling of terahertz gyrotrons with cylindrical and planar configurations of the interaction space // Phys. Plasmas. 2013. V. 20. Art.no. 043103
2. Ginzburg, N.S., Rozental, R.M., Sergeev, A.S., Fedotov, A.E., Zotova, I.V., Tarakanov, V.P. Generation of Rogue Waves in Gyrotrons Operating in the Regime of Developed Turbulence // Phys. Rev. Lett. 2017. V.119. Art. no. 034801.
3. Tarakanov, V.P. Code KARAT in simulations of power microwave sources including Cherenkov plasma devices, vircators, orotron, E-field sensor, calorimeter etc. // EPJ Web of Conferences. 2017. V. 331. Art.no. 04024.

Development and Modeling of Miniaturized Traveling-Wave Tubes in Millimeter and Sub-THz Bands

Nikita M. Ryskin^{1,2}

¹Saratov Branch, V.A. Kotel'nikov Institute of Radio Engineering and Electronics RAS, Saratov, Russia

²Saratov State University, Saratov, Russia, RyskinNM@info.sgu.ru

1. Introduction

Development of compact vacuum-tube millimeter- and THz-band sources with 10-100 W output power would have a great potential for numerous applications such as high-data-rate wireless communications, security, spectroscopy, biomedical applications, etc. Among the vacuum tubes, microfabricated analogs of traveling-wave tube (TWT) amplifiers are the most promising. Over 50-W output power in G-band (0.22 THz) has recently been demonstrated [1,2].

Slow-wave structure (SWS) is a core part of a TWT serving to slow the electromagnetic wave down to the electron beam velocity. In this paper, we present the results of recent studies aimed at modeling and development of medium power TWTs with various SWS suitable for operation in millimeter and sub-THz frequency bands. Different types of TWTs are considered, such as folded-waveguide TWT, TWTs with sheet electron beam and dual-grating SWS, and TWTs with planar meander-line SWS on a dielectric substrate.

2. Folded-waveguide TWT

TWT with folded-waveguide (FW) SWS has numerous advantages due to its high coupling impedance, reasonably wide (~30%) bandwidth, relatively simple structure compatible with existing microfabrication technologies, thermal and mechanical robustness, and simple input/output coupling.

We designed and simulated FW TWTs operating at Q-band (38-54 GHz), V-band (48-90 GHz), and G-band (175-275 GHz). Electromagnetic parameters of the SWSs were calculated by using ANSYS HFSS simulator. FW SWS circuits at Q- and V-band were fabricated using CNC-milling machine. In Fig. 1, a picture of the 50-pitch Q-band SWS with input/output couplers is shown. Cold-test electromagnetic measurements of *S*-parameters of the circuits were performed using Keysight Technologies PNA N5227A vector network analyzer. Good transmission characteristics were measured. In particular, return loss (*S*₁₁) is less than -10 dB and transmission loss (*S*₂₁) is about -2 dB in the most part of the passband. Experimental measurements are in good agreement with numerical simulations using ANSYS HFSS.

In addition, small-signal and large-signal gain regimes of Q- and V-band FW TWT amplifiers driven by a 50-mA, 15-kV electron beam were simulated using the 1-D parametric code [3]. Parameters of the tubes were obtained, for which 30-40 dB small-signal gain and nearly 100 W saturated power are attained.

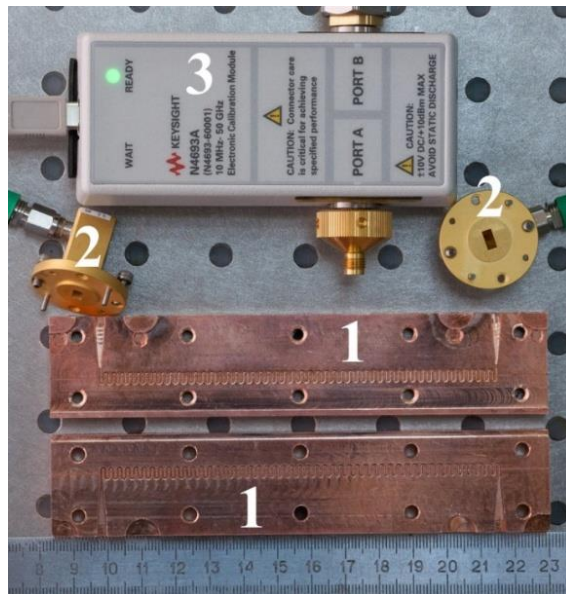


Fig. 1. Photo of the Q-band folded-waveguide SWS sample. 1 – folded waveguide; 2 – coax to waveguide adapters; 3 – electronic calibration module (ECal module)

3. Sheet-beam TWT dual-grating SWS

Using high-aspect-ratio sheet electron beams allows substantial reduce of current density and facilitates beam focusing and transportation in a narrow beam tunnel. In [3,4], we studied feasibility of a 0.2-THz sheet-beam TWT amplifier with a staggered grating SWS. An electron gun with a 0.7×0.1 mm² thermionic cathode producing intensive sheet electron beam with over 120 A/cm² current density has been developed [3,4]. However, such a gun can operate only in a short-pulse mode with 10 us pulse duration and 2000 off-duty cycle. At the same time, the required focusing magnetic field is as high as 1.12 T.

In order to overcome the problems mentioned above, we designed the electron-optic system (EOS) with a converging sheet electron beam having 10-times compression in vertical direction using the method of synthesis described in [5]. This allows a significant reduce of the beam thickness as well as of the cathode load and focusing magnetic field (0.8 T). Schematic of the electron gun is presented in Fig. 2. The design was verified by 3-D simulation using LORENTZ-3SEM simulator [6]. The results are in a fairly good agreement, except that the beam thickness obtained in 3-D analysis is somewhat higher than expected (~75 um) that can be attributed to thermal and angle spread of the emitted electrons.

The gun was fabricated and up to 140-mA beam current was measured.

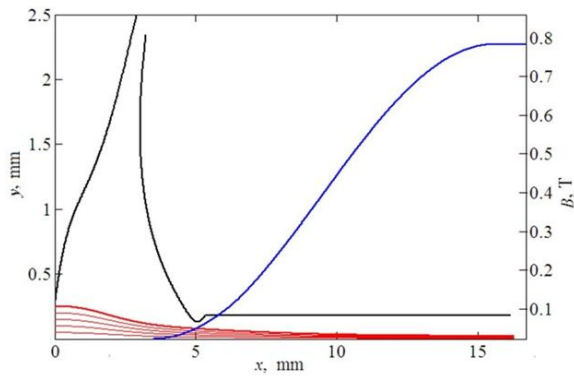


Fig. 2. Configuration of the gun electrodes, particle trajectories, and the magnetic field profile

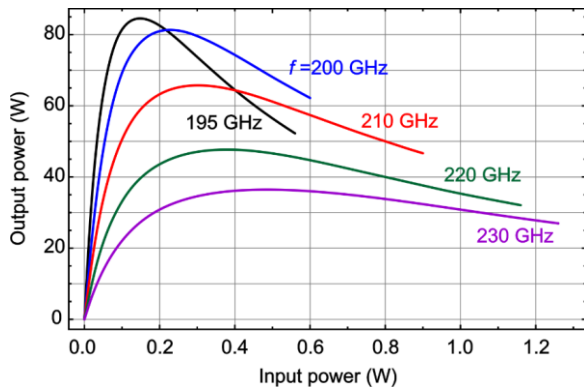


Fig. 3. Output power versus input power of the sheet-beam TWT at different frequencies

Performance of the TWT with 0.1-A, 20-kV sheet beam and dual-grating SWS was simulated. Parameters of the SWS were the same as in [3,4] except the beam tunnel height, which was reduced from 200 μm to 150 μm , owing to reduced beam thickness. This results in significant increase of the coupling impedance and the gain factor. For the 40-mm-length TWT circuit, over 30-dB small-signal gain was observed in the simulations (instead of ~ 20 dB in [3]). In Fig. 3, output power versus input power at different frequencies is plotted. Saturated power over 80 W is observed, which is close to [3]. However, the saturation is attained at the input power about 0.1 W, which is nearly 10 times less than in [3].

4. TWT with planar microstrip meander-line SWS

In order to reduce the tube size and dimensions, as well as the dc voltage, planar microstrip meander-line SWS on dielectric substrates have been proposed. We fabricated SWS circuits in V- and W-band using the novel technology utilizing magnetron sputtering and laser ablation methods [7]. Several samples of V-band and W-band meander SWS circuits on quartz substrates were fabricated. The strip thickness was increased up to 10 μm that should increase robustness of the circuits. In Fig. 4, photo of the 50-pitch SWSs with matching elements at both ends is shown.

Cold-test measurement of the electromagnetic parameters shows good transmission characteristics. Measured transmission loss of the structure did not exceed -2.5 dB.

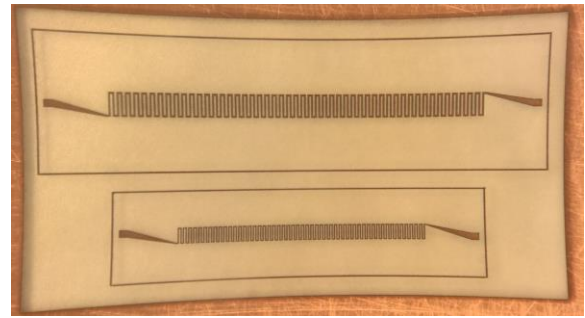


Fig. 4. Photo of the V- and W-band meander SWS samples fabricated by laser ablation

The developed SWSs provide high slow-down factor ($c/v_{ph} \sim 7 \div 9$) and thus are suitable for operation with a low-voltage ($3 \div 5$ kV) electron beam. Small-signal and large-signal gain characteristics of the TWT driven by a 100-mA sheet electron beam were simulated. For a 1-cm-length SWS, the peak gain is about 15-20 dB. Owing to strong dispersion of the meander-line SWS, the bandwidth of the amplifier is rather narrow (2–3 GHz). However, the central frequency may be easily tuned in a wide range by varying the beam voltage. The simulations predict over 60 W output power at saturation.

Acknowledgment

This research is supported by Russian Science Foundation under Grant # 17-12-01160.

References

1. Joye C.D., Cook A.M., Calame J.P., Abe D.K., et al. Demonstration of a high power, wideband 220-GHz traveling wave amplifier fabricated by UV-LIGA // IEEE Trans. Electron Devices. 2014. V. 61, No. 6, P. 1672–1678.
2. Baig A., Gamzina D., Kimura T., Atkinson J. et al., Performance of a nano-CNC machined 220-GHz traveling wave tube amplifier // IEEE Trans. Electron Devices. 2017. V. 64, No. 6, P. 2390-2397.
3. Karetnikova T.A., Rozhnev A.G., Ryskin N.M., Fedotov A.E., Mishakin S.V., Ginzburg N.S. Gain analysis of a 0.2-THz traveling-wave tube with sheet electron beam and staggered grating slow wave structure // IEEE Trans. Electron Devices. 2018. V. 65, No. 6, P. 2129-2134.
4. Karetnikova T.A., Rozhnev A.G., Ryskin N.M., Torgashov G.V. et al. Modeling a subterahertz traveling-wave tube with a slow-wave structure of the double grating type and a sheet electron beam // J. Commun. Technol. Electron. 2016. V. 61, No. 1, P. 50–55.
5. Yu.G. Gamayunov, E.V. Patrusheva. Synthesis of systems formation of converging sheet electron beams at partial magnetic shielding of the cathode // J. Commun. Technol. Electronics. 2017. Vol. 62, No. 11, 1291-1297.
6. Karetnikova T.A., Navrotsky I.A., Danilushkin A.V. Design and simulation of a 0.2-THz traveling-wave tube with a converging sheet electron beam // Proc. 19th International Vacuum Electronics Conference (IVEC 2018). 24-26 Apr. 2018, Monterey, CA, USA. P. 161-162.
7. Ryskin N.M., Rozhnev A.G., Starodubov A.V., Serdobintsev A.A., et al. Planar microstrip slow-wave structure for a low-voltage V-band traveling-wave tube with a sheet electron beam // IEEE Electron Device Lett. 2018. V. 39, No. 5, P. 757-760.

High-harmonic gyrotrons with irregular microwave systems

A.V. Savilov, I.V. Bandurkin, M.Yu. Glyavin, Yu.K. Kalynov, Yu.S. Oparina, I.V. Osharin, N.A. Zavolsky

Institute of Applied Physics RAS, N. Novgorod, Russia, savilov@appl.sci-nnov.ru

A natural way to increase the gyrotron frequency is the use of operation at higher cyclotron harmonics. However, at moderate voltages, the intensity of the electron-wave coupling decreases rapidly with the increasing harmonic number. Due to this fact, the danger of excitation of parasitic close-to-cutoff waves at lower harmonics becomes a serious problem. This is true especially in low-relativistic gyrotrons with low output powers (and, therefore, low operating currents) at least due to two reasons. First, low-harmonic waves possess bigger electron-wave coupling factors. Second, longer operating cavities are required, in general, to excite high-harmonic operating waves. The latter results also in extremely high diffraction Q -factors for the operating near-cutoff waves and, therefore, a great share of ohmic losses. In this work, we describe several schemes of cavities with short irregularities designed to improve operation of low-relativistic high-harmonic gyrotrons.

Cavities with decreased ohmic losses

A method to combine a long-length interaction region of a high-harmonic gyrotron and a relatively low diffraction Q factor was proposed in Refs. [1,2]. This method is based on the use of a sectioned system (Fig. 1 a) with a klystron-like character of the electron-wave interaction: particles interact with a near-cutoff wave only in the input and output cavities (sections 1 and 3), whereas the drift region (section 2) provides coupling between these cavities as well as bunching of electrons (Fig. 1). The diffraction Q factor in such a scheme is determined mainly by the sum of lengths of the two cavities, $Q_{\text{dif}} \propto (L_1 + L_3)^2$. At the same time, the starting current is determined by the total length of the system, $(L_1 + L_2 + L_3)$. This scheme was realized in the pulsed large-orbit 80 kV gyrotron [3]. Selective excitation at the third harmonic was achieved at a magnetic field close to 10.2 T. The output rf signal with a power of 100–250 W at a frequency of 0.74 THz corresponded to the transverse mode $TE_{3,5}$. According to simulations, the share of the ohmic losses in this experiment was relatively low (20%–25% of the rf wave power emitted from the electron beam) as compared to the first regular-cavity experiment under this third-harmonic gyrotron [4].

A different method for decreasing the diffraction Q -factor of the operating gyrotron mode is proposed in works [5,6]. This is based on exciting a higher axial mode (possessing a relatively low diffractive Q -factor) in the gyrotron-type regime (i.e. at the electron-wave resonance condition $\omega \approx N\Omega$ without Doppler terms). This method is based on the use of a periodically sectioned cavity; every two sections are

separated by a short phase corrector providing the π -shift of the wave phase (Fig. 2). This approach is used to provide operation at the fourth cyclotron harmonic in the 30 keV/0.7A CW large-orbit gyrotron [7] based on a 5 T cryomagnet. The main scope of this setup is to provide operation at the second, third, and fourth cyclotron harmonics at the frequencies 0.26 THz, 0.39 THz, and 0.52 THz, respectively, with the output power level of hundreds of Watts. In first experiments, the use of a regular 19 mm cavity provided selective excitation of the mode $TE_{2,5}$ at the second harmonic (0.267 THz) and of the mode $TE_{3,7}$ at the third harmonic (0.394 THz) at slightly different magnetic fields. However, the 0.52 THz fourth-harmonic gyrotron requires a long (50–60 wavelengths) operating cavity, so that the diffraction Q -factor of the lowest axial mode (over 100,000) is much greater than the ohmic Q -factor ($\sim 10,000$), and the share of ohmic losses exceeds 90%. This leads to as low output efficiency of this gyrotron as 0.2%. We designed a cavity consisting of 5 sections and based on the excitation of the mode $TE_{4,5}$ with 5 axial variations (Fig. 2). Although the cavity is relatively long (~ 90 wavelength), sectioning makes possible to reduce the diffraction Q -factor of the operating wave down to $\sim 30,000$, and to reduce the share of ohmic losses down to $\sim 60\%$. This provides an increase in the output wave efficiency up to $\sim 1\%$ (the output power is ~ 100 W).

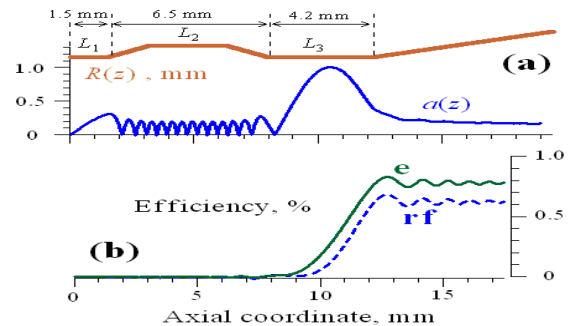


Fig. 1. (a): Sectioned cavity of the third-harmonic large-orbit gyrotron. (b): Results of simulation of the operation at a frequency of 0.74 THz; electron efficiency (e) and rf wave efficiency (rf) versus the axial coordinate.

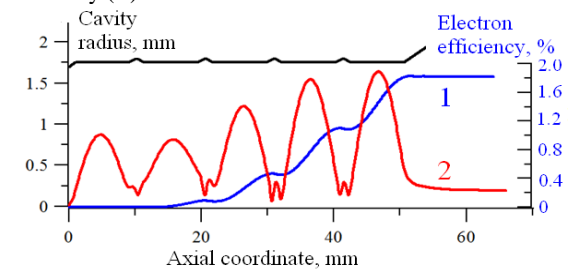


Fig. 2. Large-orbit fourth-harmonic gyrotron: cavity shape, the calculated electron efficiency versus the axial coordinate, and the spatial rf-wave structure of the operating mode corresponding to the 5th axial mode.

Selective irregularities

A method for suppression of the fundamental-harmonic parasitic waves in second-harmonic gyrotrons based on a simple principle [8] can be used in low-power short-wavelength gyrotrons with a weak electron-wave interaction and, therefore, with long (tens wavelengths) operating cavities. This method is based on the use a quasi-regular cavity with either one or several short irregularities (phase correctors). Evidently, the phase incursion of a near-cutoff wave inside the irregularity is proportional to the frequency, $\phi(\omega) \sim \omega$. For the operating second-harmonic wave, $\phi(\omega) = 2\pi$ and, therefore, such an irregularity does not effect on the excitation of this wave. As for fundamental-harmonic near-cutoff parasitic waves, their phase shift on the same corrector is twice smaller, π (Fig. 3 a). The π -shift of the phase changes the “sign” of the electron-wave coupling (shifts decelerated electron to the accelerating phase of the wave); this lead to a significant degradation of the interaction of electrons with the parasitic waves. This method is valid only for low-mode resonators, when the corrector does not provide scattering of the waves into lower transverse modes. In the case of operation at high radial modes, this approach can be developed by the use of the mode transformation effect (Fig. 3 b) [9]. If the operating high-harmonic mode is $TE_{m,n}$ then the radius of the widening corresponds to the cutoff $TE_{m,n+1}$ wave at the same frequency. Thus, the operating $TE_{m,n}$ wave is converted into the $TE_{m,n+1}$ wave inside the widening with no transformation losses. However, the irregularity is not resonant for the parasitic near-cutoff fundamental-harmonic waves, and a significant reduction of the diffraction Q-factors of these waves is provided due to their scattering. Using this approach, we designed a selective cavity for a pulsed 60 keV gyrotron to achieve second-harmonic excitation of a very developed mode ($TE_{63,15}$) at a frequency of ~ 1.2 THz.

One more approach is based on reducing the cavity length due to the use of a special output irregularity [10]. The irregularity increases the Q-factor of the operating high-harmonic wave due to the reflection, but it almost does not reflect parasitic fundamental-harmonic waves (Fig. 3 c). In addition, the irregularity spoils the axial structure of the parasitic wave. This approach can provide a significant increase in the starting current of parasitic close-to-cutoff waves with no considerable effect on the generation of the operating high-harmonic wave.

The work is supported by the Russian Science Foundation, project # 17-19-01605.

References

1. Savilov, A. V. High-harmonic gyrotron with sectioned cavity // Appl. Phys. Lett. 2009. V. 95, P. 073503.
2. Bandurkin, I. V., Kalynov, Y. K., Savilov, A. V. High-harmonic gyrotron with sectioned cavity // Phys. Plasmas. 2010. V. 17. No. 8. P. 073101.

3. Bandurkin, I. V., Kalynov, Y. K., Savilov, A. V. Experimental realization of the high-harmonic gyrotron oscillator with a klystron-like sectioned cavity // IEEE Trans. Electron Devices. 2015. V. 62. No. 7. P. 2356-2359.

4. Bratman, V. L., Kalynov, Y. K., Manuilov, V. N. Large-orbit gyrotron operation in the terahertz frequency range // Phys. Rev. Lett. 2009. V. 102, No. 24. P. 245101.

5. Bandurkin, I. V., Kalynov, Y. K., Osharin, I. V., Savilov, A. V. Gyrotron with a sectioned cavity based on excitation of a far-from-cutoff operating mode // Phys. Plasmas. 2016. V. 23. N. 1. P. 013113.

6. Bandurkin, I.V., Kalynov, Y.K., Makhalov, P.B., Osharin, I.V., Savilov, A.V., Zhelezov, I.V. Simulations of sectioned cavity for high-harmonic gyrotron // IEEE Trans. Electron Devices. 2017. V. 64 (1). P. 300.

7. Bandurkin, I.V., Bratman, V.L., Kalynov, Y.K., Osharin, I.V., Savilov, A.V. Terahertz large-orbit high-harmonic gyrotrons at IAP RAS // IEEE Trans. Electron Devices. 2018. V. 65. P. 2287.

8. Bandurkin, I. V., Kalynov, Y. K., Osharin, I. V., Savilov, A. V. A method for suppression of spurious fundamental-harmonic waves in gyrotrons operating at the second cyclotron harmonic // Phys. Plasmas. 2016. V. 23. No. 5. P. 053116.

9. Bandurkin, I. V., Glyavin, M.Y., Kuzikov, S.V., Makhalov, P.B., Osharin, I. V., Savilov, A. V. Method of providing the high cyclotron harmonic operation selectivity in a gyrotron with a spatially developed operating mode // IEEE Trans. Electron Devices. 2017. V. 64. P. 3893.

11. Oparina, Yu.S., Savilov, A.V. Improvement of mode selectivity of high-harmonic gyrotrons by using operating cavities with short output reflector // J. IR MM THz Waves 2018. V. 39. P. 595.

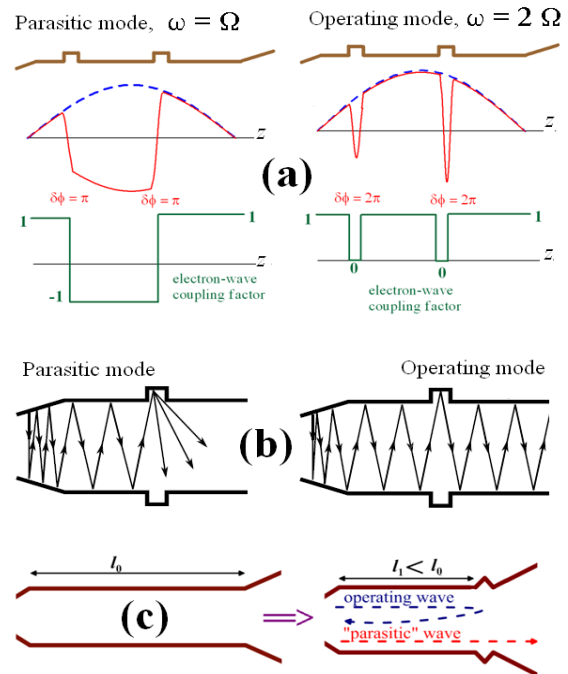


Fig. 3. Gyrotron cavities with selective irregularities. (a): Phase corrector, which provides the 2π phase incursion for the operating second-harmonic wave, and the π phase incursion for the parasitic fundamental-harmonic wave. (b): An irregularity providing scattering of the parasitic near-cutoff wave. (c): Shortening of the gyrotron operating cavity by the use of the reflecting output irregularity.

THz radiation of stabilized dense electron bunches

A.V. Savilov¹, I.V. Bandurkin¹, I.S. Kurakin¹, Yu.S. Oparina¹,
V.L. Bratman^{1,2}, N. Balal², Yu. Lurie²

¹ Institute of Applied Physics RAS, N. Novgorod, Russia, savilov@appl.sci-nnov.ru
² Ariel University, Ariel, Israel

Laser-driven photo-injectors are capable to form very compact and dense electron bunches with a particles energy of 3-6 MeV, picosecond and subpicosecond duration, and charge of the order of 1 nC. When moving in the periodic field of the undulator with a period of a few centimeters, such bunches can generate coherent radiation in the near-terahertz range. The power and duration of such a generation is limited due to an increase in the axial length of the electron bunch under the action of the Coulomb repulsion, which under normal conditions does not allow for the effective implementation of such a scheme for dense nC bunches [1]. Therefore, a special methods of stabilization of the axial length of the operating bunch during its motion over a long enough electron-wave interaction region should be used. The report describes two such methods, namely, the so-called “negative-mass” stabilization and the radiative compression of electron bunches.

Negative-mass stabilization and compression

The negative-mass regime of the electron motion is realized in a combination of periodic undulator field and relatively strong homogeneous axial magnetic field (Fig. 1 a). The cyclotron frequency corresponding to the axial field should be slightly higher than the undulator bounce-frequency of the particle. In this case, the Coulomb field inside the bunch leads not to repulsion of electrons but to their mutual attraction [1]. This effect is a result of an abnormal dependence of the velocity of undulator oscillations of electrons on the cyclotron frequency (Fig. 1 b). Let us consider a particle moving in the front of the bunch (Fig. 1 c). The Coulomb field accelerates this electron, and its relativistic cyclotron frequency decreases. The electron approaches the undulator-cyclotron resonance, which is accompanied by a resonant increase in its transverse velocity; this leads to decrease in the axial electron velocity.

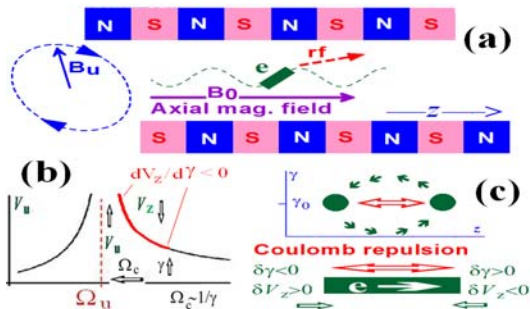


Fig. 1. (a): Electron motion in the combined helical undulator and uniform axial fields. (b) Characteristic dependence of the transverse electron velocity on the cyclotron frequency. (c) Coulomb attraction and oscillations of electrons in the “negative-mass” regime.

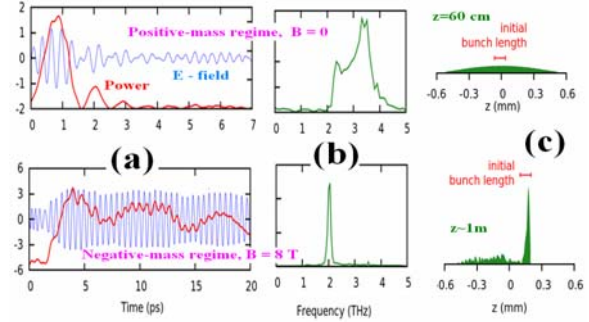


Fig. 2. (a): Radiated wave field and power (red) in the “positive-mass” and “negative-mass” regimes. (b): Spectra of the radiated rf signal. (c): Axial distributions of the charge in the bunch after the 60 cm trip in the positive-mass regime and after the 1m trip in the negative-mass regime.

Thus, increasing the energy of the particle causes it to slow down in the longitudinal direction. The opposite situation takes place for the particle moving in the tail of the bunch; this particle is decelerated by the coulomb field, and this leads to an increase in the axial velocity. Overall, the Coulomb interaction of particles leads to compression of the bunch in the longitudinal direction. Such a behavior of electrons can be regarded as a consequence of its effective mass being negative [2,3], and this is very similar to the negative-mass effect in cyclotron masers [4-7].

Numerical simulations show [1,8] that in a certain range of parameters, significant improve of the radiation characteristics is possible when using the described scheme. Figure 2 illustrates an example, where an electron bunch with the particles energy of 5.5 MeV scatters the undulator field having a period of 2.5 cm into the wave with a frequency of about 2 THz. In this case, the resonant cyclotron frequency corresponds to the axial field of about 5 T, and effective negative mass regime is realized at magnetic fields near 8 T and the undulator field amplitude of about 0.2 T (Fig. 2). Simulations predict generation of a 20 ps rf pulse with a power of ~ 10 MW. According to simulations [8], the negative-mass regime can provide axial stabilization of extremely dense (with charges up to several nC) picosecond bunches. A prototype of the negative-mass undulator with a 8 T axial magnetic field is designed and tested in the experiment [9]. There is also an interesting option to use this regime for the axial compression of dense bunches by their own Coulomb fields, when the undulator is used not for the radiation but for providing the negative-mass electron motion only [10]. Since in this situation there is no goal to achieve THz radiation, undulators with longer periods can be used, and a lower magnitudes of the axial magnetic field are required to provide the negative-mass electron motion.

Radiative compression

An alternative compression method can be the undulator super-radiative radiation of a long-wavelength wave in an auxiliary long-period undulator [11]. A relatively long electron bunch propagates in a simple (with no axial magnetic field) helical undulator inside a waveguide (Fig. 3 a) and radiates a short wave packet propagating with a group velocity equal to the electron axial velocity (Fig. 3 b). Since the wavelength of the radiated wave is longer than the bunch length, the emission has the spontaneous coherent character. Such emission results in axial compression of the bunch (Fig. 3 c). This is due to the fact that in the situation described above the phase of the radiated wave is correlated in a certain way with the electron bunch phase, namely, there is a $\pi/4$ shift between the bunch center and maximum of the decelerating wave phase (Fig. 3 d). In the case of a bunch being four times shorter than the wavelength, the bunch is compressed in the radiated field, because the front of the bunch is placed in the maximum of the decelerating wave phase whereas the tail is placed close to the “zero” wave field.

This effect can be used for creation of a “bicolor” THz source based on the spontaneous emission from a short bunch, so that the super-radiation of the auxiliary long-wavelength wave is used to compress the bunch down to a size shorter than the wavelength of the short-wavelength wave. Figure 4 illustrates an example, where a 0.1 nC 3 MeV 0.6 mm bunch moves in two undulators ($\lambda_{u,1}=2.3$ cm and $\lambda_{u,2}=1.1$ cm). At the first stage, electron oscillations in the first undulator lead to the spontaneous coherent radiation of the long-wavelength ($\lambda_1=1.2$ mm) compressing wave. During this process, the bunch is compressed several times. This makes possible the spontaneous coherent radiation of the short-wavelength ($\lambda_2=0.3$ mm) wave in the second undulator with a relatively high ($\sim 10\%$) electron efficiency.

The work is supported by IAP RAS Project 0035-2014-0012, Russian Foundation for Basic Research (Project 18-32-00351 and 16-02-00794), and the Israeli Ministry of Science, Technology and Space.

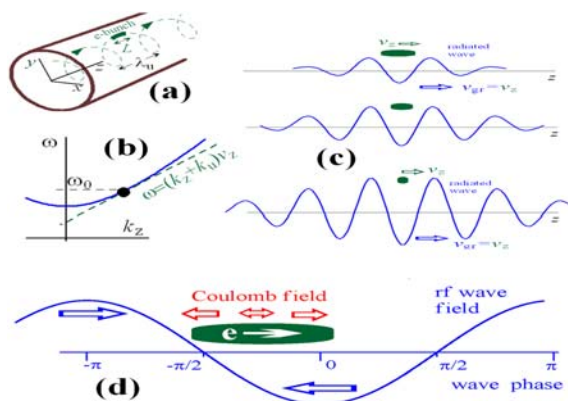


Fig. 3. (a): Electron bunch moving along a helical undulator. (b): Dispersion diagram of the operating waveguide mode. (c) Super-radiative radiation and the bunch compression. (d): Bunch phase with respect to the wave.

References

1. Balal, N., Bandurkin, I. V., Bratman, V. L., Magory, E., Savilov, A. V. Negative-mass mitigation of Coulomb repulsion for terahertz undulator radiation of electron bunches // Appl. Phys. Lett. 2015. V. 107. P. 163505.
2. Freund, H. P., Sprangle, P. Unstable electrostatic beam modes in free electron-laser systems // Phys. Rev. A. 1983. V. 28. P. 1835.
3. Ginzburg, N. S., Peskov, N. Yu. Non-linear theory of relativistic ubitrons with electron beams formed in an adiabatically increasing undulator field and a uniform longitudinal magnetic field // Tech. Phys. 1988. V. 58. P. 859.
4. Bratman, V. L. Instability of orbital motion in a layer of electrons rotating in a uniform magnetic field // Tech. Phys. 1976. V. 46. P. 2030.
5. Bondeson, A., Antonsen, T. Space-charge instabilities in gyrotron beams // Int. J. Electron. 1986. V. 61. P. 855.
6. Bratman, V. L., Savilov, A. V. Phase mixing of bunches and decrease of negative-mass instability increments in cyclotron resonance masers // Phys. Plasmas. 1995. V. 2. P. 557.
7. Savilov, A. V. Negative-mass instability in magnetron-injection guns // Phys. Plasmas. 1997. V. 4. P. 2276.
8. Lurie, Yu., Bratman, V. L., Savilov, A. V. Energy enhancement and spectrum narrowing in terahertz electron sources due to negative mass instability // Phys. Rev. AB. 2016. V. 19. P. 050704.
9. Balal, N., Bandurkin, I.V., Bratman, V.L., Fedotov, A.E. Helical undulator based on redistribution of uniform magnetic field // Phys. Rev. AB. 2017. V. 20. P. 122401.
10. Bandurkin, I.V., Kurakin, I.S., Savilov, A. V. Compression of a photoinjector electron bunch in the negative-mass undulator // Phys. Rev. AB. 2017. V. 20. P. 020704.
11. Bandurkin, I.V., Oparina, Y.S., Savilov, A.V. Super-radiative self-compression of photo-injector electron bunches // Appl. Phys. Lett. 2017. V. 110. P. 263508.

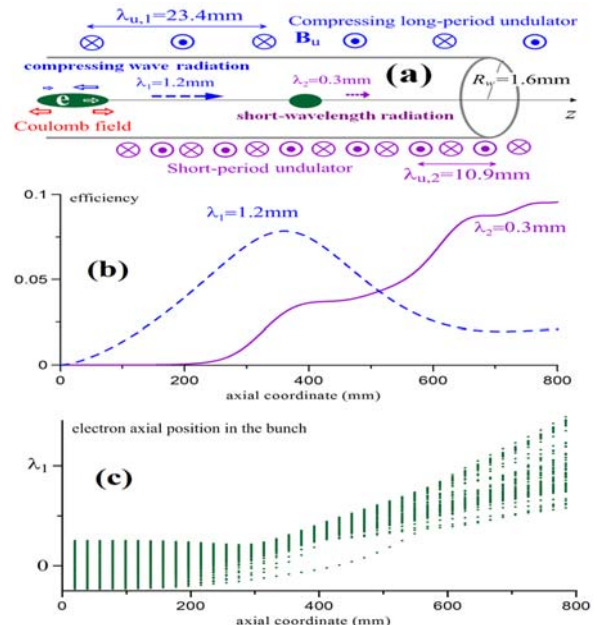


Fig. 4. (a): “Bicolor” THz source based on the spontaneous emission of two waves. (b): Efficiency of radiation of the two waves versus the axial coordinate of the bunch. (c): Evolution of axial distribution of electrons inside the bunch.

3D Printed Periodic Structures for Subterahertz Sources

D. I. Sobolev, M.D. Proyavin, N.Yu. Peskov, V.Yu. Zaslavsky, V.V. Parshin

Institute of Applied Physics, Nizhny Novgorod, Russia, nrtnm@mail.ru

Recent advances in 3D printing technology made it a favorable choice in many scientific applications, where large-scale production is not required. There are several different materials and printing methods available, which are more or less suitable for sub-terahertz devices. Selective laser sintering (SLS) printers can reach tolerances down to several microns, although these are on the expensive side, and in the case of metallic printing the surface roughness is unsatisfactory for radiation with millimeter and submillimeter wavelengths without additional finishing. Moreover, SLS printing of copper is very difficult due to its high reflection coefficient at commonly used laser wavelengths. Stereolithography (SLA) photopolymer printers have very high accuracy, but these plastics usually have high absorption in microwave and terahertz region. Fused-deposition modelling (FDM) printers are cheap, widely available and can use several well-known plastics with low absorption, such as nylon or HDPE, but the precision is less than for the former types.

To study the best possible solutions, we analyzed the dielectric permittivity and loss tangent of plastics used in different 3D printer types. Sample discs were printed and then placed inside the two-mirror resonator with high Q factor [1], and measurements were made for frequencies in 94-150 GHz range. Additional measurements were made for plastic waveguide inserts in 26-40 GHz range. Dielectric properties in different ranges have only a slight difference and can therefore be extrapolated to higher frequencies. Measurement results are collected in the table.

Plastic	Printer	Re ϵ	$\tan \delta$
Polyethylene terephthalate glycol (PETG) 1	FDM	2.31	$1.5 \cdot 10^{-3}$
PETG 2	FDM	2.47	$1.6 \cdot 10^{-3}$
Polylactic Acid (PLA)	FDM	2.27	$6.2 \cdot 10^{-3}$
Sterol-butadiene-sterol (SBS) 1	FDM	2.22	$1.6 \cdot 10^{-3}$
SBS 2	FDM	2.40	$1.3 \cdot 10^{-3}$
Visijet SL Clear	SLA	1.8	$3.5 \cdot 10^{-2}$
Visijet SL Flex	SLA	1.8	$3.5 \cdot 10^{-2}$
Visijet SL Hi-Temp	SLA	1.8	$3.5 \cdot 10^{-2}$
Polyamid	SLS	1.7	$3.5 \cdot 10^{-3}$

Sterol-Butadiene-Sterol has the best dielectric properties among the measured samples, and it was chosen to test the concept of two-dimensional planar Bragg resonator with chessboard-like grating, which can be used in distributed feedback lasers [2]. The parameters of Bragg structure were chosen in accordance with dielectric properties of the media and precision of FDM printers, which is acceptable for frequencies up to 100 GHz. Size of the square resonator is 180 mm, and average thickness is 2 mm. Grating periods in orthogonal directions are both equal to 4 mm, and grating depth is 0.4 mm. The 3D-printed structure is shown on Fig. 1.

The properties of this resonator were calculated in CST MWS for $\text{Re } \epsilon=2.4$ and $\tan \delta=2 \cdot 10^{-3}$, and the zone of effective scattering was near 60 GHz. To conduct the low-power measurement, the resonator had to be excited by a wave beam with a plane phase front, which was made by a planar quasioptical transmission line. The transmission line consists of two parallel metallic planes, parabolic mirror and single-mode waveguide ending in the focus of the mirror. After the reflection, the planar wave beam is very close to the TEM-mode of planar waveguide. The wave beam is transmitted through the resonator and then received into single-mode waveguide by the symmetrical quasioptical transmission line.

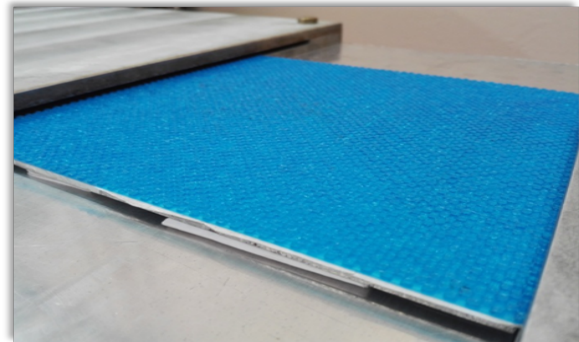


Fig. 1. Dielectric two-dimensional plane Bragg resonator printed from SBS plastic

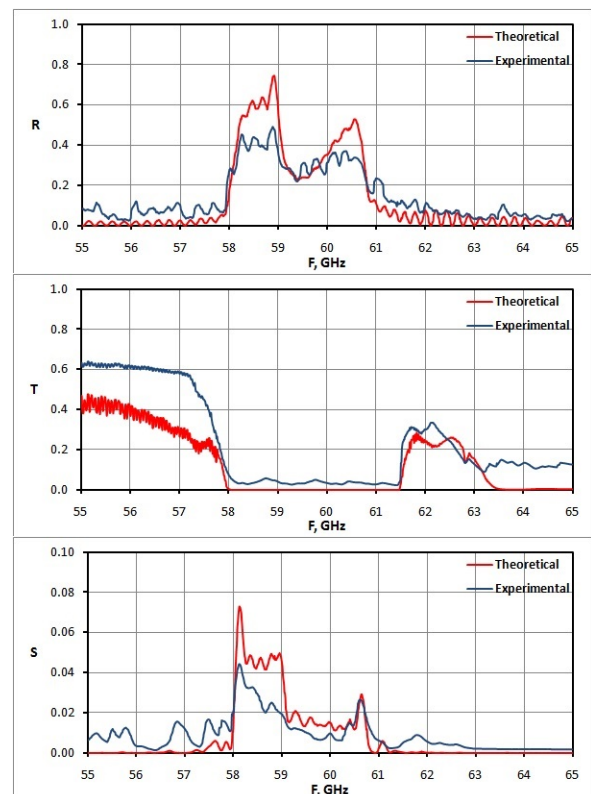


Fig. 2. Reflection (R), transmission (T) and orthogonal scattering (S) for dielectric two-dimensional plane Bragg resonator

Measurement results for reflection, transmission and orthogonal scattering are shown on the Fig. 2. There is a good agreement between calculations and experiment for both frequencies of the effective Bragg scattering and amplitudes of the scattering coefficients. The use of higher precision printers will allow manufacture of resonators suitable for submillimeter wavelengths.

Another promising field for printed dielectric structures is low-loss windows. Calculations basing on thermal and dielectric properties of printable plastics give the power of several tens of watts, which is sufficient for many applications, e.g. subterahertz gyrotron systems used for spectroscopy [3]. Window reflection can be minimized by the use of gratings of different shapes, like two-dimensional pyramidal or one-dimensional close to sinusoidal [4]. The shape of the grating requires fine details to be printed with high precision, and single-nozzle FDM printers flatten the top parts of the shape, which leads to the increase of the reflection. SLS plastic printers have significantly better precision. To compare different gratings, three discs were printed of polyamid: the first one has no gratings on the sides, the second one has pyramids with height 2 mm and base width 1 mm on both sides, and the third one has special one-dimensional periodic grating with height 3 mm and period 2 mm on both sides. The discs are shown on Fig. 3.

The low-power tests were conducted on the same resonator setup, which was used for the tests of dielectric properties. The measurements performed at frequencies 70-200 GHz show the significant reduction of reflection: both types of gratings effectively suppressed the reflection by more than 10 dB. This is sufficient for many subterahertz gyrotrons, and additional tests of mechanical and vacuum properties will be performed later.

This work was supported by RSCF grant 18-48-520022. Authors are grateful to DS Group for their help with manufacture of samples.



Fig. 3. Printed discs for antireflection grating tests: top – no gratings, middle – pyramidal gratings, bottom – one-dimensional gratings.

References

1. *Dryagin, Y.A. & Parshin, V.V.* A method to measure dielectric parameters in 5–0.5 millimeter wavelength band // *Int. J. Infrared Milli. Waves.* 1987. V. 13, No. 7. P. 1023-1032.
2. *Ginzburg, N.S., Peskov, N.Yu., Sergeev, A.S.* Dynamics of free-electron lasers with two-dimension distributed feedback // *Optics Commun.* 1994. V.112. P.151-156.
3. *Glyavin, M.Yu., Idehara, T., Sabchevski, S.P.* Development of THz gyrotrons at IAP RAS and FIR UF and their applications in physical research and high-power THz technologies // *IEEE Trans. Terahertz Sci. Techn.* 2015. V. 5, No. 5, P. 788-797.
4. *Vlasov, S. N., Kuposova, E. V.* Suppressing the reflection from an interface between dielectrics by corrugating their surfaces // *Techn. Phys.* 1993. V. 38, No. 7. P. 592-595.

Recent progress in development and application of sub-THz gyrotrons in University of Fukui

Y. Tatematsu

Research Center for Development of Far-infrared Region, University of Fukui, Fukui, Japan, tatemala@fir.u-fukui.ac.jp

I. Introduction

Till 2005, Research Center for Development of Far-Infrared Region, University of Fukui (herein referred to as FIR-UF) had developed gyrotrons to aim at increasing their frequency. For this purpose, the Gyrotron FU series were developed[1-3]. Fundamental, second and third harmonic oscillations were observed, and the breakthrough of 1 THz oscillation in gyrotron was achieved for the first time in the world[4].

Since 2006, gyrotrons have been developed in FIR-UF for the purpose of applications such as DNP-NMR spectroscopy[5,6], sintering and direct measurement of energy level of positronium hyperfine structure[7]. Gyrotrons developed for this purpose are Gyrotron FU CW series[8-13], Gyrotron FU CW G series[14-19] and pulsed gyrotrons[20-28].

II. Development of Gyrotron

Gyrotron FU CW I was developed in the collaboration between IAP, RAS and FIR-UF[10]. It was fabricated by Gycom. It was used for material processing and sintering. Some gyrotrons applying for DNP-NMR spectroscopies were developed, such as Gyrotrons FU CW II, IV, VI and VII[9,11-13]. For this application, the frequency tuning is necessary to adjust the sensitivity to maximum. With Gyrotron FU CW IV, a continuous frequency variation width of 6 GHz was observed[11]. The oscillation mode was fundamental TE_{12} mode. The mechanism of continuous frequency variation was explained as the interaction with gyro-backward waves.

Recently Gyrotron FU CW XA was developed. It is installed on an 8 T superconducting magnet. It is a linear type gyrotron without a built-in mode converter. The cavity is a normal hollow one with up and down tapers at the both ends of the straight section. The radius and length of the straight section of the cavity are 2.997 mm and 20 mm, respectively. Although this cavity was not specially designed for the purpose of frequency tuneability, frequency variations more than 1 GHz were measured with four modes, TE_{12} , TE_{13} , TE_{33} and TE_{14} , in this gyrotron. The frequency bands are 90, 140, 180, and 190 GHz, respectively[29].

For applications, conversion to Gaussian beam is necessary. About Gaussian beam output gyrotrons in FIR-UF, the Gyrotron FU CW I is the first, which was fabricated in Russia[10]. Gaussian beam output gyrotrons developed in FIR-UF are called as Gyrotron FU CW G series[14-19]. Gyrotron FU CW GI oscillates in 203 GHz frequency[14] and was used for direct measurement of the energy level of positronium hyperfine structure[7]. Gyrotrons FU CW GII and GIII oscillate in second harmonic[15-17]. Gyrotron FU

CW GIV showed frequency variations in two frequency ranges. The frequency varies with the widths of 5 GHz in 190 GHz band for the fundamental mode and of 3 GHz in 390 GHz band for the second harmonic mode[30].

Gyrotron FU CW GV is a multi-frequency gyrotron[18]. It is of sealed-off type and was constructed by New Japan Radio Company. It was installed on a 10 T magnet. The mode converter consists of a conventional Vlasov launcher and four mirrors. Although it was designed for the $TE_{10,6}$ mode, Gaussian beams were radiated in oscillations of ten modes. Their oscillation frequencies are from 162 GHz to 265 GHz about 10 GHz step. The transmittance of a window disk depends on the wave frequency. Some of them have low transmittance. To prevent the drop in transmittance due to the frequency-dependence, a distance variable double-disk window was adopted. With variation of the distance between the two disks, the transmittance of the electromagnetic wave periodically changed because of the wave interference. The transmittance can be almost one by setting with appropriate distances for every frequency.

In Gyrotrons FU CW VI and VII, frequency variation around 460 GHz was achieved in a second harmonic oscillation using a 10 T magnet[19].

We also developed pulsed high power gyrotron series[20-28]. They are developed in the purpose of a light source for the Collective Thomson Scattering (CTS) measurement in LHD, NIFS. First, we developed 400 GHz frequency, 2nd harmonic oscillation gyrotrons using 8 T superconductive magnet. However, for the required target power of 100 kW injection into the plasma, 2nd harmonic oscillation did not reach the goal power. So, we changed to 300 GHz gyrotron development using 12 T magnet in fundamental oscillation. With the beam voltage of 65 kV and current of 15 A, power of 320 kW and efficiency of 33 percent are achieved[28]. This gyrotron was moved to LHD of NIFS in July, 2018 and will be applied to CTS experiment.

III. Applications of Gyrotron

As examples of applications of sub-THz gyrotrons, there are sintering, DNP-NMR spectroscopy, positronium energy level measurement, CTS, pulsed ESR, millimeter wave discharge, light emission from crystals and study for safety data base of sub-THz radiation.

Gyrotron FU CW GI was applied for direct measurement of hyperfine structure of positronium[7]. This is a collaboration with Tokyo University. Positronium is a bound state of a positron and an electron. Ground-state positronium has two spin eigenstates,

ortho-state and para-state. The energy difference of the two states correspond to about 203.4 GHz. The measurements of the energy difference were done in the past, however, they were measurement used the Zeeman effect in a static magnetic field. It may be affected by the magnetic field, and the result has a slightly difference from the theoretically calculated values. So, we did directly measurement of the energy level using electromagnetic wave. The expected spectrum of the gamma ray annihilation probability is a function of frequency. So, for this measurement, a light source with frequency tunable between 201 to 206 GHz and high power more than 100 W with Gaussian beam output is necessary. However, frequency of a gyrotron is not widely continuously changed to keep high power. Therefore, to change the frequency, we changed the cavity itself. We prepared a lot of cavities whose diameters were slightly different each other. Changing the cavities, the intensity of gamma-ray produced by pair annihilation was measured. The energy difference of the hyperfine structure of positronium was measured with the central energy of 203.39 ± 0.11 GHz.

Another application of gyrotron is light emission from ZnO crystal[31]. This is a collaboration with Osaka University. Spectra of irradiation of a ZnO crystal by gyrotron exhibit a broad and asymmetric peak around 600 nm with a longer-wavelength tail. When the duty ratio of gyrotron irradiation increased, the peak emission intensity increases rapidly. Yellow light emitted from the ZnO crystal. The temperature was more than 1000 degree by the IR camera measurement. When heated up to 1250K using an electric heater without gyrotron irradiation, the crystal does not exhibit any visible emission. Therefore, this result indicates that the yellow emission of the gyrotron irradiated crystal is not a simple blackbody radiation but is caused by a combination of thermal effects and the gyrotron's sub-THz electric field.

When sub-THz wave from a gyrotron is radiated to nano-scale cages of $\text{Ca}_{12}\text{Al}_{14}\text{O}_{33}$ crystal, visible light was emitted from the crystal[32]. It was explained the mechanism of lightening that oxygen ions inside the cage rattle due to sub-THz wave and emit visible light. Conversion from THz wave to visible light is useful for THz range research to specify the wave position. This is a collaboration with Tokyo Institute of Technology and Hirosaki University.

Gyrotron is also applied for the study of safety data base of sub-THz radiation for eyes. This is a collaboration with Tokyo Metropolitan University and Kanazawa Medical University. They had the experiments at frequencies of 40, 75, 90 GHz irradiation so far. In the present experiment, we use electromagnetic wave with the frequency of 162 GHz, one of oscillation of Gyrotron FU CW GV. Sub-THz wave is irradiated into rabbit eyes, and the threshold of power or power density to cause injury on the eyes is being investigated.

A pulsed high power gyrotron of 303 GHz will be applied for CTS measurement in LHD, NIFS. The electromagnetic wave generated by a gyrotron is injected into plasma. From the observation of the scat-

tering wave, we can obtain the information of ion temperature. Due to the magnetic field distribution of LHD, 300 or 400 GHz is the best frequencies for CTS measurement in LHD.

IV. Summary

In FIR-UF, Gyrotron FU CW series, Gyrotron FU CW G series and pulsed gyrotron series have been developed for the purpose of various applications for the current decade and they have been and will be applied for various fields.

References

1. Idehara, T. *et al.*, Phys. Fluids **B 5**, 1377 (1993).
2. Hong, K. D. *et al.*, J. Appl. Phys. **74**, 5250 (1993).
3. Shimizu, Y. *et al.*, Phys. Plasmas **2**, 2110 (1995).
4. Idehara, T. *et al.*, Int. J. Infrared. Milli. Waves. **27**, 319 (2006).
5. Matsuki, Y. *et al.*, J. Mag. Res. **225**, 1 (2012).
6. Matsuki, Y. *et al.*, J. Mag. Res. **264**, 107 (2016).
7. Miyazaki, A. *et al.*, Prog. Theo. Exp. Phys. **2015**, 011C01 (2015).
8. La Agusu *et al.*, Int. J. Infrared. Milli. Waves. **28**, 315 (2007).
9. Idehara, T. *et al.*, Int. J. Infrared. Milli. Waves. **28**, 433 (2006).
10. Zapevalov, V. E. *et al.*, Radiophys. Quant. Electron. **50**, 420 (2007)
11. Chang T.-H. *et al.*, J. Appl. Phys. **105**, 063304 (2009).
12. Idehara, T. *et al.*, J. Infrared Milli. Terahertz Waves **31**, 763 (2010).
13. Idehara, T. *et al.*, J. Infrared Milli. Terahertz Waves **31**, 775 (2010).
14. Tatematsu *et al.*, J. Infrared Milli. Terahertz Waves **33**, 292 (2012).
15. Tatematsu *et al.*, J. Infrared Milli. Terahertz Waves **35**, 169 (2014).
16. Tatematsu *et al.*, J. Infrared Milli. Terahertz Waves **35**, 517 (2014).
17. Tatematsu *et al.*, Phys Plasmas **21**, 083113 (2014).
18. Tatematsu *et al.*, J. Infrared Milli. Terahertz Waves **36**, 697 (2015).
19. Idehara, T. *et al.*, J. Infrared Milli. Terahertz Waves **36**, 819 (2015).
20. Notake, T. *et al.*, Rev. Sci. Instrum. **79**, 732 (2008).
21. Notake, T. *et al.*, Plasma Fusion Res. **4**, 011 (2009).
22. Notake, T. *et al.*, Phys. Rev. Lett **103**, 225002 (2009).
23. Saito, T. *et al.*, Plasma Fusion Res. **7**, 1206003 (2012).
24. Saito, T. *et al.*, Phys. Plasmas **19**, 063106 (2012).
25. Yamaguchi, Y. *et al.*, Plasma Fus Res. **8**, 1205165 (2013).
26. Yamaguchi, Y. *et al.*, Nuclear Fusion **55**, 13002 (2015).
27. Yamaguchi, Y. *et al.*, J. Instrumentation **10**, C10002, (2015).
28. Saito, T. *et al.*, Plasma Fusion Res. **12**, 1206013-1-1206013-2, 2017.
29. Tatematsu *et al.*, 42nd IRMMW-THz, RA2.2, 2017.
30. Tatematsu *et al.*, 41st IRMMW-THz, H5P.21.13, 2016.
31. Kato, K. *et al.*, Appl. Phys. Lett. **111**, 031108 (2017).
32. Toda, Y. *et al.*, ACS Nano **11**, 12358 (2017).

Quasi-fractal PBG structures for Multi-Beam Devices

V. A. Tsarev¹, D. A. Nesterov², P. D. Shalaev³

¹Yuri Gagarin Saratov State Technical University, Saratov, Russia, tsarev_va@mail.ru

²Yuri Gagarin Saratov State Technical University, Saratov, Russia, enlucioro@gmail.com

³AO "NPP "Almaz", Saratov, Russia, p.d.shalaev@yandex.ru

Over the last years, the great attention of microwave vacuum tube and accelerator researchers therefore drawn to so-called photonic crystal resonator cavities, formed by a defect lattice (photonic band gap structure-PBG)[1-4].

Very strict requirements applied to the resonator systems used in such devices. They must have a high characteristic impedance $\rho = R/Q_0$ and increased (compared to the operating wavelength) dimensions. In addition, they must have a rigid and technological structure having a high unloaded Q-factor and a good heat-dissipating ability.

In the defect area it is appeared local electromagnetic waves (defect modes) similar to electromagnetic waves of ordinary cavity resonators.

The advantages of PBG are increased overall dimensions, high unloaded Q-factor, comparative simplicity of engineering implementation, as well as the possibility to suppress undesirable (parasitic oscillation).

Due to these advantages, the metal photonic band gap structure has potentialities in the areas of high-energy accelerators, multi-beams klystrons.

Up to the present moment, it was studied only one gap single defects and multiple defects of PBG for single-beam and multi-beam klystrons [5, 6]. This did not allow us to realize a large gain factor, a high efficiency and a wide band in such devices.

This paper presents the results of 3D computer simulations of a double-gap PBG resonator with enhanced impedance of interaction.

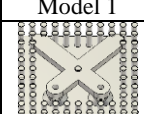
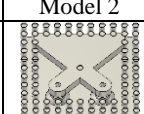
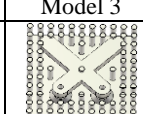
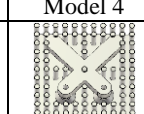
The transformation of the defect zone from two-dimensional to three-dimensional was accomplished by inserting an additional X-shaped quasi-fractal resonance element in the cross section in the central part of the interaction region (fig. 1). This transformation was performed by inserting an additional X-shaped quasi-fractal resonance element in transverse section in central part of the interaction area.

The interaction area is confined by side covers 1 with circular holes 2 for transition of two electron beams in longitudinal direction and in transverse direction by a conditional square 3 that defines boundary of the longitudinal rods location 4, which restrict two-dimensional defect area. The resonance rods 5, forming the additional X-shaped resonance element, are oriented on the diagonal of the conditional square in the two-dimensional photonic crystal. This element consisted of two similar triangles (ADF and ABC) with cutout in them (FGH and ADE), which are also scale lines of the initial triangles. The drawn figure is similar to Serpinski triangle fractal [7]. In the center of diagonal intersection at the distance $l_1 = \lambda/2$ from electric contact place between resonance rods with longitudinal rods 6 is located a central longitudinal metal rod 7, having electric contact with side covers. At the free ends of the resonance rods it is made circular holes 8 for electron beams transition that are coaxial with circular holes on side covers. The full length of both resonance rods is equal $l_2 = 3/4\lambda$, where λ is TEM – mode operating wavelength. As a result of these transformations it is formed two double high-frequency gaps. The lowest frequency modes in three-dimensional photonic band gap are quasi-TEM modes, which electric and magnetic fields have opposite directions in each gap (π -mode). However, for operation in millimeter and sub-millimeter wavelength ranges in-phase modes similar to TM_{110} and TM_{210} in ordinary prismatic resonant cavities is of the greatest interest.

Simulation results

We have designed a quasi-fractal double-gap cavity based on PBG structure. 3D-models of studied resonance system are illustrated in table.

Table. Computer models of studied PBG structure

Model 1	Model 2	Model 3	Model 4
			

It had the following dimensions: lattice depth 10 mm, metal rods diameter 2 mm, spacing between the rods, 3.7 mm, drift tube radius 1.0 mm; gap length 1.5 mm; resonance rods thickness in along-track beam direction 3 mm. It was studied the influence of number n additional longitudinal rods that are inserted into 3D defect area, at a frequency of indicated modes. During the simulation, it is also determined characteristic impedance (shunt impedance, fig.2) and unloaded Q-factor cavity (fig.3).

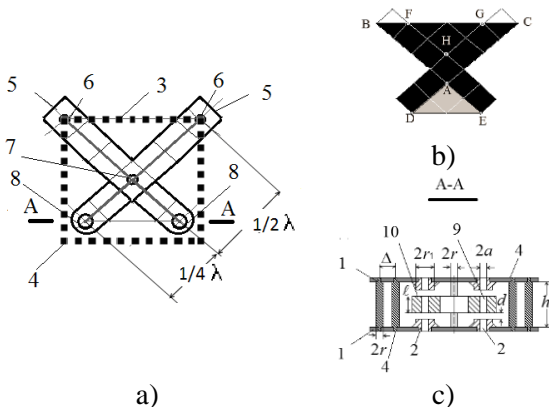


Fig. 1. The structure of the resonator: a) fractal scheme, b) top view, c) transverse section

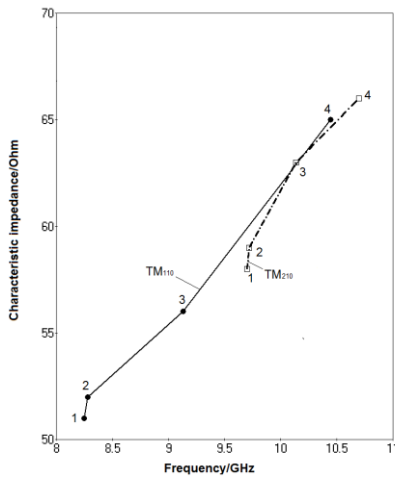


Fig. 2. HOM R/Q_0 as a function of frequency. Numbers indicate the model numbers indicated in table.

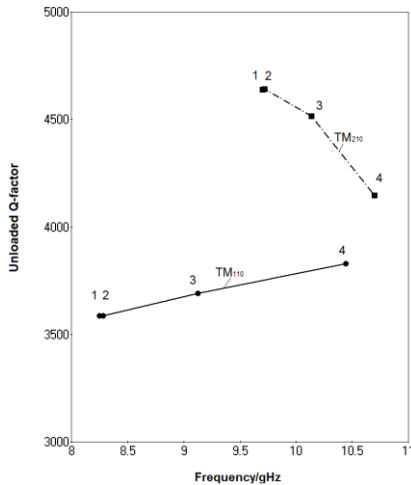


Fig. 3. HOM Q_0 as a function of frequency. Numbers indicate the model numbers indicated in table.

From fig. 2 it is clear that increasing numbers of rods in the cavity volume leads to characteristic impedance increasing of both TM_{110} (1.3 times) and TM_{210} modes (1.2 times). The dependence of unloaded Q-factor on rod numbers (fig. 3) for TM_{110} mode has linear increasing form while for TM_{210} mode Q-factor it falls. Considering both dependence we can conclude: stunt impedance linearly grows with the rods number for TM_{110} and has a maximum at a number of rods $n = 2$ (fig. 4). The dependence of stunt impedance for TM_{210} on frequency has the parabola form, a maximum is at $n = 1$. Having said so this mode has higher stunt impedance values then at TM_{110} mode for any n .

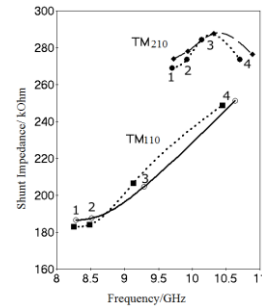


Fig. 4. Shunt impedance for HOM as a function of frequency. Numbers indicate the model numbers indicated in table. Dotted lines represent cavities with the rods, dashed and solid lines represent cavities with solid walls

The presence of the rods in quasi-fractal cavity models leads to frequency decreasing as compared with cavity models with solid walls.

The coupled quasi-fractal double-gap cavity array as a fractal electrodynamic system that capable to slow down electromagnetic wave considerably can be used for TWTs.

Due to increased stunt impedance, quasi-fractal PBG structures for Multi-Beam Devices has potentialities in the areas of high-energy accelerators, multi-beams klystrons, terahertz radiation sources, etc.

References

1. *Ozbay E., Temelkuran B., and Bayindir M.* Microwave applications of photonic crystals // Progress In Electromagnetics Research, 2003. Vol. 41, pp. 185–209.
2. *Ashutosh, Jain P.K.* Design and analysis of metallic photonic band gap cavity for a gyrotron // Journal of Microwaves, Optoelectronics and Electromagnetic Applications. 2012. Vol. 11, № 2. P. 242.
3. *Han S.-T., Jeon S.-G., Shin Y.-M., Jang K.-H., So J.-K., Kim J.-H., Chang S.-S., Park G.-S.* Experimental investigations on miniaturized high-frequency vacuum electron devices // IEEE Trans. Plasma Sci. 2005. Vol. 33, № 2. P. 679.
4. *Jeon S.-G., Shin Y.-M., Jang K.-H., Han S.-T., So J.-K., Joo Y.-D., Park G.-S.* High order mode formation of externally coupled hybrid photonic-band-gap cavity // Appl. Phys. Lett. 2007. Vol. 90, № 2. 021112.
5. *Smirnov A. V. et. al.* PBG Cavities for Single-Beam and Multi-Beam Electron Devices // Proceedings of Particle Accelerator Conference, 2003, pp. 1153-1155.
6. *Xu, Y. and Seviour, Rebecca.* Design of Photonic Crystal Klystrons. In: Proceedings of the 1st International Particle Accelerator Conference IPAC 2010. JACoW, Kyoto, Japan, pp. 4002-4004. ISBN 978-92-9083-352-9.
7. Sierpinski triangle // Wikipedia, the free encyclopedia. – URL: https://en.wikipedia.org/wiki/Sierpinski_triangle. – 06.09.18.

Generation of Ultrashort Microwave Pulses in Passive Mode-Locked Electron Oscillators with Homogeneous and Inhomogeneous Line Broadening

M. N. Vilkov, N. S. Ginzburg, I. V. Zotova, A. S. Sergeev

Institute of Applied Physics RAS, Nizhny Novgorod, Russia, vilkovmn@ipfran.ru

Introduction

In the laser physics the generation of ultrashort pulses (USP) via passive mode-locking [1] is broadly used. Gain media with homogeneous and inhomogeneous line broadening are applied [2]. The analog of homogeneous and inhomogeneous line broadening in microwave electronics is electron-wave interaction with beams having small or large initial energy spread. USP electron oscillators with passive mode locking with homogeneous line broadening were investigated in [3-4]. In this paper we will study peculiarities of the USP microwave oscillators with both homogeneous and inhomogeneous line broadening.

Model and basic equations

The schema of USP generators is presented in Fig. 1. It consists of an electronic amplifier, a nonlinear (saturable) absorber in the feedback circuit, and a partially transparent mirror for output of the signal.

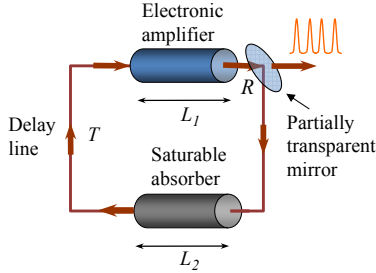


Fig. 1. Principal scheme of a USP oscillator with a saturable absorber in the feedback loop.

We will use a rather general model of the electronic amplifier with prevailing inertial particle bunching [5]. Under conditions of a relatively small energy change of particles $|1 - \varepsilon / \bar{\varepsilon}| \ll 1$ (where $\varepsilon = mc^2\gamma$, γ is the relativistic factor, $\bar{\varepsilon}$ is an average value of electron energy in the initial distribution), the process of amplification can be described by the universal system of equations [5,6]

$$\begin{aligned} \frac{\partial a_n}{\partial Z} + \frac{\partial a_n}{\partial \tau} &= J, \\ \frac{\partial u}{\partial Z} &= \text{Re}(a_n e^{i\theta}), \quad \frac{\partial \theta}{\partial Z} = u. \end{aligned} \quad (1)$$

The boundary condition for electrons is

$$u|_{Z=0} = u_0, \quad \theta|_{Z=0} = \theta_0 \in [0; 2\pi). \quad (2)$$

We will suppose initial energy spread of electrons of the beam is normal

$$f_0(u_0) = \frac{1}{\sqrt{2\pi}\sigma} e^{-\frac{u_0^2}{2\sigma^2}} \quad (3)$$

where $\sigma = \mu C^{-1} \Delta\varepsilon / \bar{\varepsilon}$ is a parameter characterizing the electron energy spread, $J = 1 / \pi \times$

$\int_{-\infty}^{+\infty} \int_0^{2\pi} f_0(u_0) e^{-i\theta} d\theta_0 du_0$ is an amplitude of the

high-frequency electron current, θ is an electron phase relative to a synchronous running wave,

$u = \mu C^{-1} (1 - \varepsilon / \bar{\varepsilon})$ is the normalized electron energy variations, $Z = C\omega z / c$, $\tau = C\omega(t - z / V_{|0}) \times$

$(c / V_{gr} - c / V_{|0})^{-1}$, $a_n = \chi \mu C^{-2} eA / mc$ is the normalized wave amplitude, n is the number of the field passages through the feedback loop, $L = C\omega l / c$ is the length of amplification region,

$C = (eI_0 \chi^2 \mu / mc^3 \bar{\gamma} N)^{1/3}$ is the parameter of amplification (Pierce' parameter), I_0 is the beam current, χ is the electron-wave coupling coefficient (see [6]), N is the operating mode norm, and $V_{gr} = d\omega / dh$ is the wave group velocity.

The signal passage in a feedback circuit with absorber is described by the equation

$$\frac{\partial a_n}{\partial Z} + \frac{\partial a_n}{\partial \tau} + \nu(a_n) a_n = 0. \quad (4)$$

where the coefficient of attenuation ν for a saturable absorber can be specified as

$$\nu(a_n) = \frac{\nu_0}{1 + \nu |a_n|^2}. \quad (5)$$

In accordance with the scheme shown in Fig. 1 boundary conditions can be presented in the form

$$\begin{aligned} a_{n,in}^{(2)}(\tau) &= R a_{n,out}^{(1)}(\tau), \\ a_{n+1,in}^{(1)}(\tau) &= b_{n,out}^{(2)}(\tau - T) \end{aligned} \quad (6)$$

where index "1" and "2" corresponds to section of amplification and absorbing, respectively, $R < 1$ is the reflection coefficient, T is a delay time.

Electron efficiency of the oscillator is determined by the relationships

$$\eta = \frac{C}{\mu(1 - \bar{\gamma}^{-1})} \hat{\eta}, \quad (7)$$

$$\hat{\eta} = \frac{1}{2\pi} \int_0^{2\pi} u(Z = L_1) f_0(u_0) d\theta_0 du_0.$$

Results of simulations

Results of simulations of USP generation via passive mode-locking with homogeneous (the initial electron energy spread is absent) and inhomogeneous line broadening (the initial electron energy spread $\sigma = 2$) are presented in Fig. 2. For both cases one can

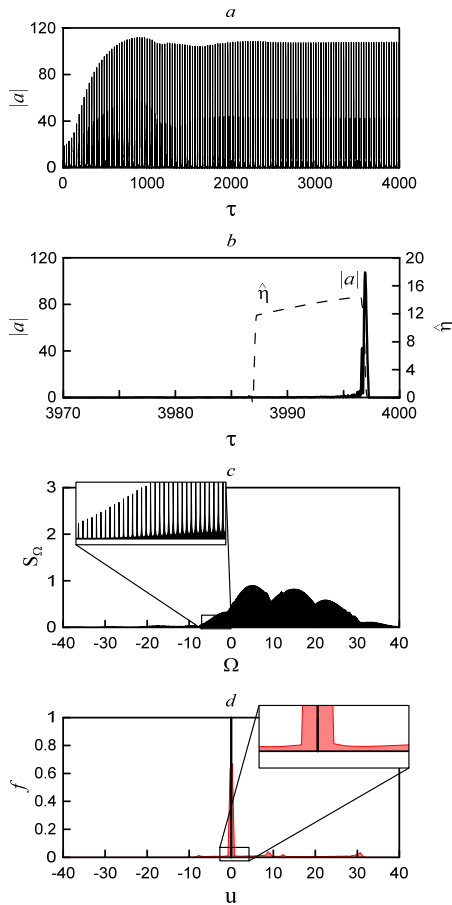


Fig. 2. Setting on a USP regime in the oscillator with homogeneous line broadening ($L_1=10$, $R=0.9$, $L_2=5$, $v_0=1.5$, $v=0.6$, $T=20$, $\sigma \rightarrow 0$): (a) time dependence of the field amplitude, (b) detailed profile of pulses and the instant electron efficiency in the extended time scale, (c) radiation spectrum, and (d) electron energy distribution function at the initial (black line) and final (red line) stages.

see that there is possibility of arrangement of mode locking regime accompanied by USP pulse production. For the same beam current, gain parameter and the length of amplification section the characteristic of generated pulses in regime with homogeneous and inhomogeneous line broadening is very closed. Nevertheless the peak amplitude of USP pulses is larger for the homogeneous line broadening.

Thus based on our analysis we can conclude that passive mode locking is an effective way to exploiting of powerful electron beams possessed by substantial energy spread (like high current relativistic electron beams) for generation of coherent radiation.

This work was supported by Russian Scientific Foundation (RSCF), grant No. 16-42-01078.

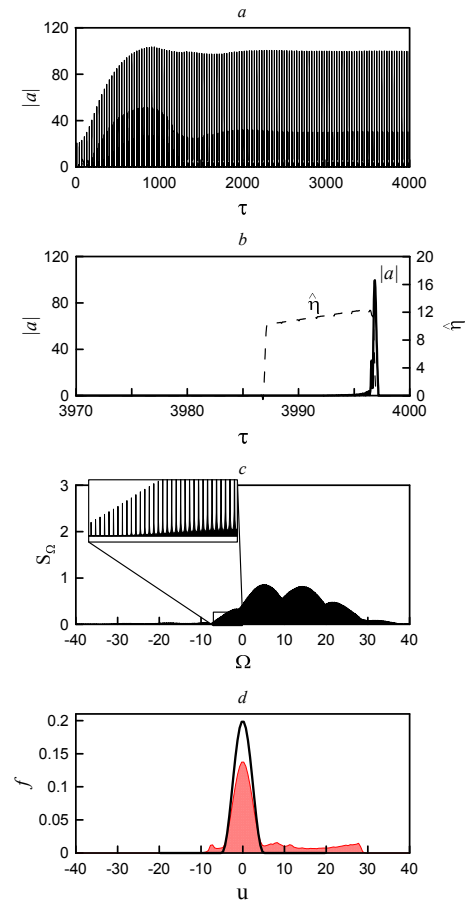


Fig. 3. Setting on a USP regime in the oscillator with inhomogeneous line broadening ($\sigma = 2$, other parameters are same as in Fig. 2): (a) time dependence of the field amplitude, (b) detailed profile of pulses and the instant electron efficiency in the extended time scale, (c) radiation spectrum, and (d) electron energy distribution function at the initial (black line) and final (red line) stages.

References

1. Haus H.A. Mode-Locking of Lasers // IEEE J. of Select. Topics in Quant. Electron. 2000. V. 6, No. 6. P. 1173-1185.
2. Yariv A. Quantum electronics // J. Wiley and Sons. 1975
3. Ginzburg N.S., Denisov G.G., Vilkov M.N., Zotova I.V. Sergeev A.S. Generation of a Periodic Sequence of Powerful Ultrashort Pulses in a Traveling Wave Tube with Bleachable Absorber in the Feedback Loop // Technical Physics Letters, 2015, V. 41, No. 9. P. 836-839
4. Ginzburg N.S., Denisov G.G., Vilkov M.N. et al. Generation of "gigantic" ultra-short microwave pulses based on passive mode-locking effect in electron oscillators with saturable absorber in the feedback loop // Phys. Plasmas. 2016. V. 23. P. 050702-1-4.
5. Bratman V.L., Ginzburg N.S., Kovalev N.F., et al., in Relativistic High Frequency Electronics, Ed. by A. V. Gaponov-Grekhov (IPF RAS, Gorky 1979), p. 249
6. Ginzburg N. S. Sergeev A. S., Sov. Phys. Tech. Phys. 1991. V. 36, P. 665.

Transformation of High-Power Gyrotron Output Radiation Frequency under Conditions of Raman Scattering on Additional Electron Beam

L.A. Yurovskiy, N. S. Ginzburg, A.M. Malkin, A.S. Sergeev, I.V. Zotova

Institute of Applied Physic RAS, Nizhny Novgorod, Russia, ginzburd@appl.sci-nnov.ru

Development of microwave oscillators and of gyrotrons in particular [1] increases the field of potential applications, for which the radiation spectrum control is essential. For example, in gyrotron applications as a source for plasma heating, set frequencies are chosen based on a compromise between the absorption in central and peripheral areas of plasma. Along with this, the investigations show [2] that plasma heating can be much more efficient if the frequency tuning of the generated signal is possible in the gyrotrons involved. In this paper, we propose using the Stimulated Raman Backscattering (SRB) regime on the additional weakly relativistic electron beam. Currently, this regime is under investigations for compression and amplification of optical frequency pulses scattered on the plasma with neglect of frequency transformation [3-5]. However, in microwave frequency range, if the electron beam is used, Doppler shifts values become of the same order as the pump and the scattered signal frequencies. Moreover, the feature of this regime is energy transfer from higher-frequency (HF) pump wave concurrent with the electrons to the lower-frequency (LF) backward propagating scattered wave. Energy transfer, accompanied by the development of the absolute instability, leads to the system self-excitation in the absence of external resonators. This allows for a smooth frequency tuning by varying energy of the electron beam.

The model, where SRB regime take place, is presented in Fig.1. Here the pump wave concurrent with the electrons is scattered on the magnetized cylindrical electron beam in the waveguide, into the backward signal with a frequency downshift. The strong guiding field can increase the transverse oscillations of the electrons in the pump field. However, the magnetic field should be far from the values corresponding to the cyclotron resonance with the pump wave. Otherwise, excitation of parasitic cyclotron oscillations leads to the violation of combination synchronism conditions.

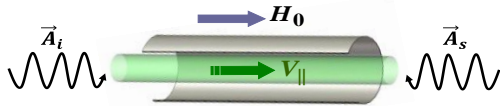


Fig. 1. The model of scattering of the concurrent pump wave into the LF backward wave

In case of sufficiently large density of electron beam, it can be considered as a material medium supporting the space-charge waves. Pump wave leads to the excitation of the Fast Space-Charge Wave (FSCW) possessing positive energy in the absorbing beam. As a result, selecting appropriate combination

synchronism detuning, leads to emerging of SRB on space-charge waves with next synchronism conditions:

$$\omega_i - h_i V_{\parallel} - \omega_s - h_s V_{\parallel} = \omega_{p_i} \quad (1)$$

where ω_{p_i} is the longitudinal plasma frequency, i, s - indexes of pump and scattered waves correspondingly.

This process described by a three-wave interaction equations, which include the equations for a HF pump wave, an LF scattered wave and a FSCW:

$$\frac{dA_b}{dz} = A_i A_s \quad \frac{dA_i}{dz} = -A_b A_s \quad \frac{dA_s}{dz} = -A_b A_i \quad (2)$$

with boundary conditions

$$A_b|_{z=0} = 0 \quad A_s|_{z=L} = 0 \quad A_i|_{z=0} = A_{i0}$$

where A_b, A_i, A_s - normalized amplitudes of space-charge wave, pump wave and scattered wave correspondingly, L - normalized length of scattering region.

Equations (2) possess the following integrals:

$$A_i^2 - A_s^2 = A_{i0}^2 - A_{s0}^2 \quad A_s^2 + A_b^2 = A_{s0}^2 \quad (3)$$

where $A_{s0} = A_s|_{z=0}$ is the signal wave amplitude at the output of the electrodynamic system. Taking into account (3), the equation for the signal wave amplitude reduced to the form:

$$\frac{dA_s}{dz} = -\sqrt{A_{i0}^2 - A_{s0}^2 + A_s^2} \sqrt{A_{s0}^2 - A_s^2} \quad (4)$$

In the steady state oscillations regime, the longitudinal distributions of the wave amplitudes are represented by Jacobi elliptic functions (Fig.2).

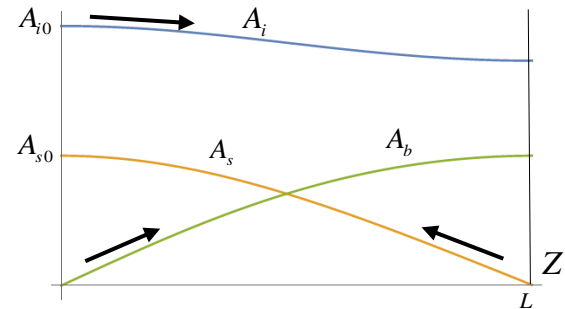


Fig. 2. Longitudinal amplitude distributions in the steady-state oscillations regime

For instance, integrating (4) yields:

$$A_s = A_{s0} \operatorname{cn}[A_{i0} z, \sqrt{\mathfrak{R}}] \quad (5)$$

Here $\mathfrak{R} = A_{s0}^2 / A_{i0}^2$ is the quantum yield (the number of pump quants transformed into the signal quants), to be found from equation:

$$A_{i0} L = K(\sqrt{\mathfrak{R}}) \quad (6)$$

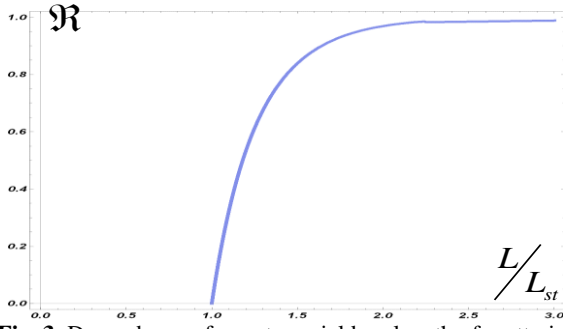


Fig. 3. Dependence of quantum yield on length of scattering region

where $K(x)$ is the complete elliptic integral of the first kind. Fig. 3 shows that quantum yield tends asymptotically to unity as the length of scattering region L increases and when L is two times greater than starting value L_{st} almost all pump power transferred to the scattered signal. Starting value L_{st} can be found from the self-excitation condition, derived from (6) at $\mathfrak{R} \rightarrow 0$:

$$A_{i0}L_{st} = \pi/2 \quad (7)$$

In physical variables, equation (7) can be rewritten for the oscillator starting current:

$$I_{st} = 2\pi^4 \cdot I_0 \frac{P_0^2}{P^2} \cdot \frac{\omega_i^2 h_s^2 h_i^2}{T^4 \omega_c^4 l^4} \cdot \beta_{i0}^7 \cdot \frac{r_w^8 D_1 (N_s^{m_s, p_s})^2 (N_i^{m_i, p_i})^2}{r_b^2}$$

Here l - the length of scattering region, T - coupling coefficient, $I_0 = 17kA$, $P_0 = 8.7GW$, D_1 - space-charge forces depression coefficient, $N_j^{m_j, p_j}$ - waveguide mode norm and P is the input pump power.

Estimations were carried out for the input pump power $P = 1MW$ at wavelength $\lambda_i = 2mm$. Radius and length of the scattering section were chosen to be $r_w = 6mm$ and $l = 30cm$, correspondingly. Magnetic field H_0 was taken 3% off cyclotron resonance value. Both pump and scattered waves were assumed to be $TE_{1,1}$ modes of the cylindrical waveguide. Calculations show (Fig.4) that there exists an optimal radius of the electron beam $r_{b_{min}}$ providing the minimum value of the starting current. For $TE_{1,1}$ mode $r_{b_{min}} = 1.6mm$.

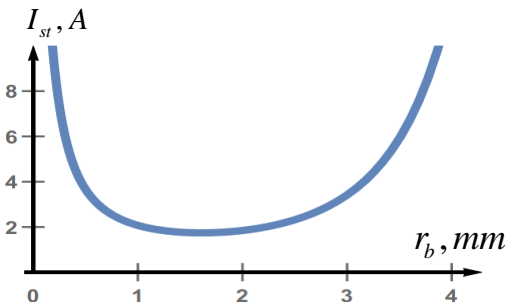


Fig. 4. Dependence of the starting current on the electron beam radius

Further calculations were carried out for $r_b = r_{b_{min}}$. As can be seen from (Fig.5-a), in the case when electron energy is in the range of values $U = 2 - 20keV$ starting current does not exceed $6A$ and remains much less than the limiting current of the cylindrical waveguide I_{max} . The magnitude of frequency tuning (Fig.1.4-b), is found from the synchronism condition (1) and is 20-40% of the pumping frequency, when electron energy is varied in the same interval of electron energies as in (Fig.1.4-a). The change in the frequency of the scattered wave in the range of 5-7% is achieved by varying the electron energy within the limits of $\pm 2.5keV$.

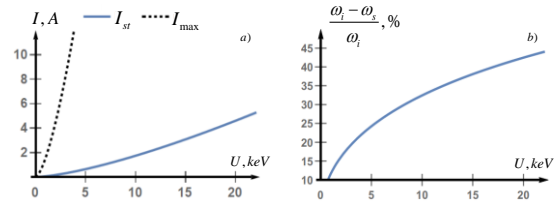


Fig. 5. a) Dependence of limiting (dotted curve) and starting (solid curve) current on electron beam energy, b) Dependence of relative magnitude of frequency tuning on electron beam energy

Magnitude estimations of the electric field on the waveguide surface shows that its values does not exceed $17kV/cm$ and therefore breakdown will not develop. Also an important parameter for estimation is the typical scale of the fields insertion L_{sw} . To obtain radiation on the combination synchronism, without oscillations at cyclotron resonance $\omega_s - h_s V_{||} \approx \omega_H$, an adiabatically smooth insertion of the fields is necessary $(\Omega - \omega_{H_0}) L_{sw} V_{||}^{-1} \sim 2\pi$, when only stimulated oscillations of the electrons are excited. The estimation of the length L_{sw} for the electron energy range $U = 2 - 20keV$ shows that L_{sw} it is within the limits of $2.5 - 3cm$.

This work was supported by the Russian Scientific Foundation (RSCF), Grant No. 16-42-01078.

References

1. A.G. Litvak, G.G. Denisov, et al. Development in Russia of 170 GHz/ 1MW/ CW Gyrotron for ITER // 2011 International Conference on Infrared, Millimeter and Terahertz Waves. 2-7 Oct. 2011. Houston, USA.
2. H. Zohm, M. Thumm. On the use of step-tunable gyrotrons in ITER. // Journal of Physics: Conference Series. Vol. 25. 2005. pp. 274-282.
3. V. M. Malkin, G. Shvets, N.J. Fisch. Fast Compression of Laser Beams to Highly Overcritical Powers. // Physics Review Letters. Vol. 82. No. 22. 1999. pp. 4448-4451.
4. I.Y. Dodin, G.M. Fraiman, V.M. Malkin, N.J. Fisch. Amplification of Short Laser Pulses by Raman Backscattering in Capillary Plasmas. // Journal of Experimental and Theoretical Physics. Vol. 95. No. 4. 2002. pp. 625-638.
5. A.A. Balakin, N.J. Fisch, G.M. Fraiman, V.M. Malkin, Z. Toroker. Numerical modeling of quasitransient backward Raman amplification of laser pulses in moderately undercritical plasmas with multicharged ions. // Physics of Plasmas. Vol. 18. 2011. pp. 102311/1-7.

Various types of echelette resonators for gyrotrons

V.E.Zapevalov, S.N.Vlasov, E.V.Koposova, A.N.Kuftin, A.B.Paveliev, N.A.Zavolsky

Federal Research Center Institute of Applied Physics, RAS, Nizhny Novgorod, Russia, zapev@appl.sci-nnov.ru,

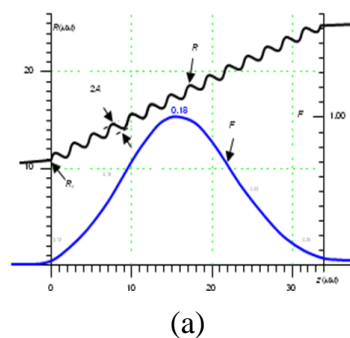
In recent years, significant progress has been made in the development of high-performance gyrotrons and various applications based on them [1, 2]. In the gyrotrons of the millimeter wavelength range the resonators (cavities) in the form of waveguides of variable cross section are used. In the operating regime, they radiate into the output waveguide one rotating operating TE_{mp} mode with azimuthal m and radial p indices. These resonators have the so-called minimum diffraction Q-factor, determined by the ratio of the resonator length to the wavelength of the radiation. The existence of this quantity is due to the operation of the resonator at the quasicritical frequency of the working mode and the presence of a "diffractive" single-mode output from the resonator. The existence of a lower limit of the diffraction Q-factor (at a finite value of the ohmic Q-factor) limits the power that can be obtained from a gyrotron with a given mode. The increase in power is achieved by increasing the surface area of the resonator, for which it is necessary to increase its cross section. However, this is possible up to a certain limit because of the thickening of the spectrum of eigen frequencies of the resonator and the deterioration of the mode selection. Thus, the possibilities of increasing the output power and operating frequency are limited, especially in gyrotrons working on gyrofrequency harmonics. Overcoming this limitation is possible with the use of resonators in which the minimum value of the diffraction Q-factor is not limited so rigidly by their length. In this paper the results of a study of several variants of gyrotrons with echelette-type resonators are presented.

Echelette resonator is one of the possible resonators with the required properties. In comparison with conventional resonators, the power flux density to the wall here can be reduced severalfold. The principles of constructing echelette resonators are described in [3-6]. In such resonators the operating modes are formed by reflection of waves from corrugated surfaces in an autocollimation regime. Three types of echelette resonators are discussed: a) two-mirror resonator, in which the field is represented as waves propagating towards each other, b) three-mirror resonator, in which only one mirror is corrugated, and the field represents a wave traveling along the azimuth, c) an axially symmetric resonator with a corrugated surface. Resonators a) and c) are investigated in this paper in more detail. The electron beam is assumed to be axially symmetric, which has by now been well developed. However, in some cases, in particular for a two-mirror circuit, it is advisable to use ribbon beams to increase the efficiency and additional selection.

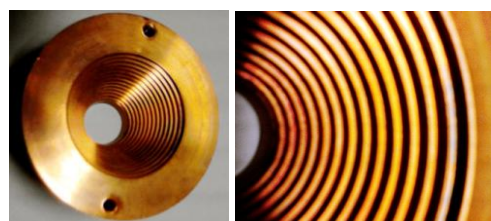
In Fig. 1 the profile of the axially symmetric echelette resonator, RF field distribution (a), and the photo of this resonator (b) are presented. The resonator has sinusoidal corrugation and was designed

to operate at the 1st harmonic of the gyrofrequency and a symmetrical operating mode.

The operating frequency of the gyrotron is 150 GHz and the accelerating voltage - 80 kV. With the chosen parameters of the resonator and the electron magnetron-injector gun described in [7], the theoretical value of $Q \approx 4200$ provides the achievement of the maximum value of electron efficiency.



(a)



(b)

Fig. 1. The profile of the echellette resonator and the distribution of the high-frequency field (a) and the photos of the resonator and its part (b)

An experimental study of the gyrotron was carried out according to the routine scheme using the apparatus described in [8]. The dependences of the pulse output power P (pulse duration $\tau = 50 \mu s$ at repetition frequency $f_0 = 5 Hz$) on the magnetic induction in cryomagnet B_0 (current in the solenoid) were obtained at a voltage $U = 80 kV$ for different values of the electron beam current I_b taken from cathode (see Fig. 2).

The experimental data demonstrates only one oscillation in the magnetic field tuning band. A high value of the output efficiency $\eta \approx 32 \%$ took place at the current of the electron beam $I_b = 35 A$. Thus, the axially symmetric echelette gyrotron has a much more sparse spectrum of eigenfrequencies and a noticeably lower specific thermal load on the resonator walls compared with the canonical gyrotron (1.8 times) with a close efficiency. The decrease in the thermal load is due to both a decrease in the quality factor in comparison with a cylindrical resonator of similar length and a certain increase in the surface.

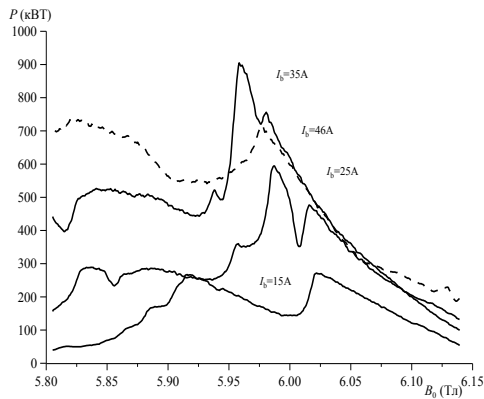


Fig. 2. Dependence of the output power of the gyrotron on the magnetic field in the resonator for different values of the electron beam current

For a number of applications a two-mirror version of the echelette gyrotron is interested. In this variant, there are some possibilities for frequency tuning and the radiation output system is simplified but with the use of a cylindrical beam an efficiency decrease of 1.5-2 times is inevitable. This scheme is the development of gyrotrons with a quasioptical resonator with additional selection due to the echelette mirror. Fig. 3 shows a gyrotron in which a two-mirror echelette resonator is used. Here the RF field can be represented in the form of waves propagating towards each other.

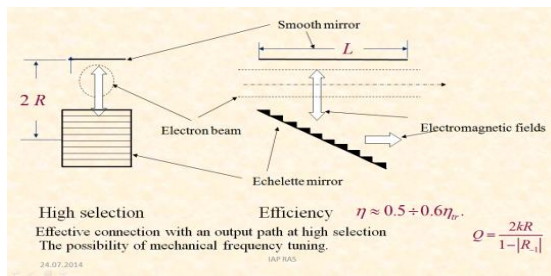


Fig. 3 Scheme of the gyrotron with a two-mirror echelette resonator

Calculations carried out for gyrotrons with two-mirror echelette resonators operating at the third harmonic of the gyrofrequency demonstrate the promises of these systems. Estimations of the Q -factor of resonators and start-up regimes for these gyrotrons were performed. The electron beam was assumed to be axially symmetric and had the same design parameters as indicated above. The possibilities of smooth tuning of the frequency in such systems were investigated. Calculations show that the use of two-mirror echelette resonators in gyrotrons operating at the 1st to 3rd harmonics of the gyrofrequency makes it possible to realize a smooth tuning of their operating frequency in the band of about 1% by varying the distance between the mirrors and corresponding correction of the magnetic field.

To increase the efficiency and additional selection in a two-mirror scheme it is expedient to use ribbon beams. For the same purposes, it is also possible to develop cylindrical beams with axially inhomogeneous emission. The development of electron-optical

systems for the formation of such beams has its own specifics and is in the initial stage.

A three-mirror echelette resonator consisting of one echelette (corrugated) and two smooth mirrors possesses all the advantages of a two-mirror resonator exceeding its efficiency in the use of an electron beam of a cylindrical configuration.

Theoretical and experimental studies have shown that the axially symmetric echelette gyrotron has a significantly more rare spectrum of eigenfrequencies and a lower thermal load (by a factor of 1.8) on the resonator walls compared to the canonical gyrotron with close efficiencies. This allows us to hope for obtaining in the echelette gyrotrons more power at long-pulsed and continuous regimes. The output radiation in the form of a conical wavebeam can be converted, for example, into the TE_{01} wave of a waveguide of circular cross section.

The performed analytical estimations and results of numerical simulation show the possibility to realize the smooth frequency tuning within the band of about 1% in the gyrotrons with two-mirror echelette resonators operating on the 1-3th harmonics of the gyrofrequency.

Echelette gyrotrons have great prospects, but in their calculation and manufacturing technology serious problems are encountered. A complex structure of the output radiation requires the development of new variants of the converter.

Acknowledgements

The work was supported by the Russian Foundation for Basic Research (Grant 18-02-00832 A)..

References

1. Nusinovich G.S., Thumm M., Petelin M.I. The Gyrotron at 50: Historical Overview. // J. Infrared Mm THz Waves. 2014. V. 35, No. 4, P. 325–381.
2. Zapevalov V.E. Evolution of gyrotrons // Radiophysics and Quantum electronics. 2011. V. LIV, No. 8-9, P. 559-572.
3. Kosarev E.L. Resolution of the Spectrum of an Open Resonator with the Aid of an Echelette Grating // JETP Letters. 1966. V. 3, No. 7, P. 190-192.
4. Vlasov S.N., Kuposova E.V., Pavel'ev A.B., Khizhnyak V.I. Gyrotrons with echelette resonators // Radiophysics and Quantum Electronics. 1996. V. 39, No. 6, P. 458–462.
5. Vlasov S.N., Zavolsky N.A., Zapevalov V.E., Kuposova E.V., Moiseev M.A. Axisymmetric multistage cavity resonators // Radiophysics and Quantum electronics. 2009. V. 52, No. 9, P. 642–654.
6. Vlasov S.N., Kuposova E.V. Traveling-wave echelette cavity // Radiophysics and Quantum electronics. 2014. V. 56, No. 10, P. 658-663.
7. Zapevalov V.E., Kuftin A.N., Lygin V.K. Numerical simulation and experimental study of an electron-optical system of a megawatt gyrotron with step frequency tuning in the range 100–170 GHz. 2007. V. 50, No. 9, P. 702–712.
8. Zapevalov V.E., Bogdashov A.A., G.G. Denisov, Kuftin A.N., Lygin V.K., Moiseev M.A., Chirkov A.V. Development of a prototype of a 1-MW 105-156-GHz multi-frequency gyrotrons // Radiophysics and Quantum electronics. 2004. V. 47, No. 5-6, P. 396–404.

Generation of Powerful Subterahertz Superradiance Pulses for High-Gradient Acceleration of Charged Particles

A. Vikharev¹, N. Ginzburg^{1,2}, S. Kuzikov¹, I. Zotova¹, M. Yalandin³

¹Institute of Applied Physics RAS, Nizhny Novgorod, Russia, alvikharev@appl.sci-nnov.ru

²N. I. Lobachevsky State University, Nizhny Novgorod, Russia

³Institute of Electrophysics, UB RAS, Ekaterinburg, Russia

In currently existing conventional linear accelerators fed by klystrons operating in S-band and X-band, acceleration gradients typically not exceeded 100 MV/m [1]. This is the reason why for electrons acceleration up to high energies long and, correspondingly, cost-demanding setups are required. Substantial increase in acceleration gradient would allow for practical implementation of colliders with TeV power level of colliding particles; for substantial improvement of parameters and/or reducing the cost of X-ray free electron lasers currently being designed; for development of compact accelerators for radiography with sub-nanosecond synchronization and definition, for medical, industrial and other applications, etc. Correspondingly, this problem became a subject of rather intense investigation including the development of brand new concepts such as laser-plasma and beam-plasma acceleration, and also acceleration in optical nanostructures. However, investigations on improving the conventional schemes of accelerators based on electrons acceleration in hollow metallic non-superconducting (“warm”) structures fed by RF radiation remain relevant. Increasing the acceleration gradient in so-called “warm” accelerators operating at room temperature is limited by effects of near-wall breakdown and pulsed thermal heating of the walls which limit the accelerating field values and deterioration of the structures surface under cyclic action of powerful microwave radiation. Despite the fact that investigations of breakdown phenomena and of walls heating have been conducted for several decades already, the only efficient method of suppressing these negative effects is considered to be the use of systems operating in the short pulse regimes when those effects have no time for settling. At that, shortening of RF pulse with simultaneous increase of its frequency, which would increase the shunt resistance considerably, would allow for relatively easy way of reaching accelerating fields of about 200 MV/m and more without exceeding threshold heat loads and surface breakdown fields. Whereas at higher frequencies the output power of RF klystrons conventionally used in accelerators decreases, the problem of design and development of high-power high-efficiency pulse sources operating in millimeter wavelength range.

In this paper we propose to use for the purpose of high-gradient particles acceleration the new class of pulsed relativistic RF generators based on the Cherenkov superradiance (SR) of high-current extended electron bunches. Currently, SR generators provide record-breaking power level in mm wavelength range up to 2 GW in ultrashort pulses with a duration of 250-300 ps [2]. Investigations conducted lately show

viability both of further increase of SR pulses peak power at 8-mm wavelength band (due to coherent summation of such pulses [3,4]) and for advancement of SR generators into the short-wavelength part of the millimeter band with a power level of 50-70 MW due to using oversized electrodynamic structures [5].

In experiments on particles acceleration the experimental setup [4] consisting of two synchronized high-voltage RADAN modulator could be used. Based on the electron beam in the first section, pulsed high-frequency radiation would be generated. The accelerating structure would be positioned on the course of the electron beam in the second section. Thus, a nanosecond or subnanosecond RF radiation pulse after transmission through the quasi-optical line and reflection from the special reflector at the cathode side would feed the positioned structure in the regime of wave co-moving with the accelerated beam. Further results of PIC simulations are presented for two experimental configurations.

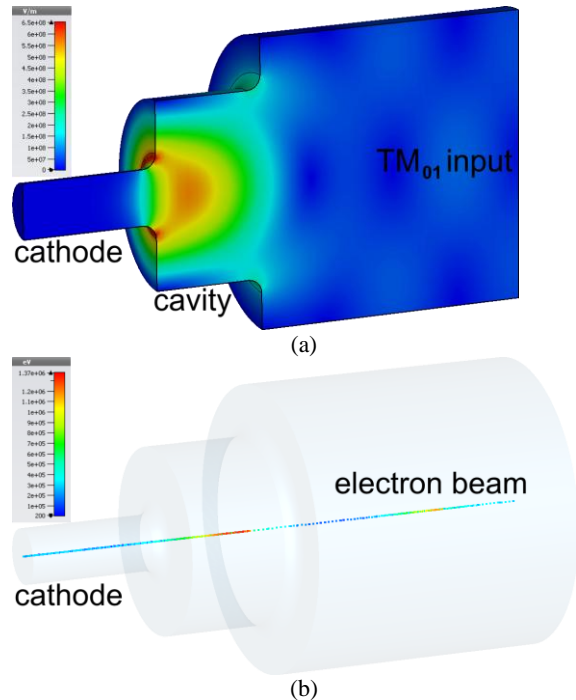


Fig. 1 (a) Geometry of a pillbox-type resonator with distribution of em field of a SR pulse. (b) The energy distribution of an electron beam with an initial energy of 300 keV (the maximum energy of the accelerated fractions is of 1.3 MeV, the acceleration gain is of 550 MV/m).

In the first experiments, SR pulses would be used at 38 GHz frequency with a duration of up to 250 ps and power of ~500 MW. In this combination of parameters, acceleration in short half-wave resonator is

of interest, which allows to obtain rather high acceleration gradient. Pillbox-type resonator at TM010 mode (see Fig. 1) with loaded quality factor of $Q = 30$ at the resonance frequency is capable of providing maximum accelerating field on the axis when fed by a pulse with duration of 250 ps. According to simulations, maximum acceleration gradient reaches 550 MV/m with surface waves of up to 650 MV/m. Maximum energy gain at the parameters stated would be more than 1 MeV.

It should be noted, that implementation of the described scheme at higher frequency, 140 GHz, is of unquestionable interest. At the pulse parameters (200 ps, 50 MW) obtained in experiments on pulse generation [5], acceleration gradient twice as high could be obtained as the parameters of the experiment to be conducted at 38 GHz frequency. Accelerated electrons energy would be less (up to 700 keV), but due to smaller resonator dimensions, accelerating gradient and surface fields appear to be larger.

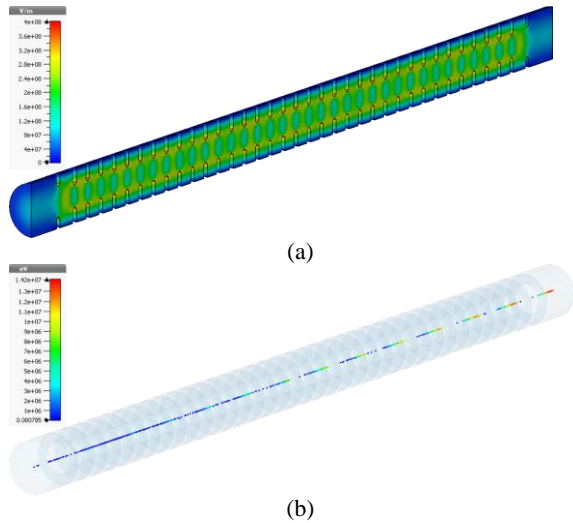


Fig. 2 (a) Geometry of an accelerating structure with distribution of em field. (b) The energy distribution of an electron beam with an initial energy of 300 keV (the maximum energy of the accelerated fractions is of 14 MeV).

In the second experimental configuration, a relatively long (2.5 ns) electromagnetic pulse with a power of up to 100 MW at the 38 GHz frequency generated by a relativistic BWO would be used for feeding of periodic hollow metallic structure with a length of 10 cm (see Fig. 2). Such $2\pi/3$ structure consists of coupled accelerating cells with a length of 3 mm. Group velocity in the structure should be 11% of the velocity of light according to the considerations of its full feeding by a 2.5 cm pulse, shunt resistance of about 90 MOhm/m and the cells Q-factor ~ 3500 . These pa-

rameters are close to those of the CLIC structure at a frequency of 30 GHz ($R_{sh} = 97.5$ Mohm/m, $Q = 3900$, $V_{gr}/c = 7\%$). According to simulations, averaged over the length acceleration gradient would be 220 MV/m with gained accelerated particles energy over 20 MeV. Such an experiment is of considerable interest because it simulates a so-called RF gun, which represents a source of electron beams of accelerators with higher energies (in the presence of synchronized laser providing the photoemission of the electron bunch). Implementation of such gun layout would allow for decrease of the dark current, breakdown frequency and potentially higher brightness of accelerated electron bunches comparing to conventional design.

This research was performed within the framework of the RAS Presidium project No. 10

References

1. A. Degiovanni, S. Doebert, W. Farabolini, A. Grudiev, J. Kovermann, E. Montesinos, G. Riddone, I. Syratchev, R. Wegner, W. Wuensch, A. Solodko, B. Woolley, High-gradient test results from a CLIC prototype accelerating structure: TD26CC, Proceedings of IPAC2014, Dresden, Germany, WEPME015. P. 22885-2287.
2. Rostov, V.V., Romanchenko, I.V., Pedos, M.S., Rukin, S.N., Sharypov, K.A., Shpak, V.G., Shunailov, S.A., Ul'masculov, M.R., Yalandin, M.I. Superradiant Ka-band Cherenkov oscillator with 2-GW peak power // Physics of Plasmas 2016. V. 23, No. 9. P. 093103 (1-4).
3. Ginzburg, N.S., Cross, A.W., Golovanov, A.A., Mesyats, G.A., Pedos, M.S., Phelps, A.D.R., Romanchenko, I.V. Rostov, V. V., Rukin, S.N., Sharypov, K.A., Shpak, V.G., Shunailov, S.A., Ulmaskulov, M.R., Yalandin, M.I., Zotova, I.V. Generation of electromagnetic fields of extremely high intensity by coherent summation of Cherenkov superradiance pulses// Phys. Rev. Lett. 2015. V. 115. P.114802 (1-4).
4. Mesyats, G. A., Ginzburg, N. S., Golovanov, A. A., Denisov, G. G., Romanchenko, I. V., Rostov, V. V., Sharypov, K. A., Shpak, V. G., Shunailov, S. A., Ulmaskulov, M. R., Yalandin, M. I., Zotova, I. V. //Phase-imposing initiation of Cherenkov superradiance emission by an ultrashort-seed microwave pulse // Phys.Rev.Lett. 2017. V.118. P. 264801.
5. Ginzburg, N.S., Malkin, A.M., Sergeev, A.S., Zheleznov, I.V., Zotova, I.V., Zaslavsky, V.Yu., Boltachev, G.Sh., Sharypov, K.A., Shunailov, S.A., Ul'masculov, M.R., Yalandin, M.I. Generation of sub-terahertz superradiance pulses based on excitation of a surface wave by relativistic electron bunches moving in oversized corrugated waveguides // Phys. Rev. Lett. 2016. V. 117. P. 204801.

The project of third harmonic medium power W-band gyrotron

A.S. Zuev¹, A.P. Fokin¹, M.Y. Glyavin¹, R.M. Rozental¹, A.S. Sedov¹, E.S. Semenov¹

¹IAP RAS, Nizhny Novgorod, Russia, alan.zuev@yandex.ru

One of the most interesting ranges is the W-band due to the presence of a transmission line in this range in the atmosphere, which is used for communication, radiolocation, security and for other applications [1-4]. These applications require continuous and pulsed W-band sources. One of the powerful devices in this band is the gyrotron [5]. The gyrotron is a vacuum electronics device based on the interaction between an electron beam and microwave fields, which coupling is achieved by the cyclotron resonance condition. High power subterahertz and terahertz radiation gyrotrons require strong external static magnetic field typically provided by a superconducting magnet. Such magnets are quite expensive; moreover they require special operating conditions.

One way to reduce the cost of this device is to develop gyrotrons operating at higher harmonics on the cyclotron frequency, in which the required external magnetic field in the interaction space is significantly less and allows the use of low-cost versions of magnetic systems. At present, there are projects of "warm" (i. e., with liquid or oil cooling) magnets with a cavity diameter sufficient for the gyrotron and the magnetic field level of more than 1 T [6]. The operation at high harmonics on the cyclotron frequency in gyrotrons encounters the problem of competition of modes, synchronous with lower harmonics of the electron beam. In addition, in order to reach the effective electron-wave interaction for operation at high harmonics, one needs to use resonators with higher quality factor. It leads to an increase in ohmic losses and, consequently, a drop in the output power for the same parameters of the electron beam. In this report, we consider the project of a gyrotron at frequency 95 GHz of medium power operating at the third harmonic. To solve the problem of mode competition, it is planned to use a relatively unusual method - the addition of an annular diaphragm in the output part of the resonator (fig 1). By introducing the annular diaphragm, it is possible to reduce the diffraction quality factor and, respectively, to increase the starting current of the competing mode.

For the operation of the gyrotron at the third harmonic, mode $TE_{1,3}$ was chosen. This mode is isolated from modes operating at the fundamental harmonic, and is almost isolated from modes synchronous with the second harmonic. The nearest competitor for it is the counterrunning wave $TE_{1,2}$ on the second harmonic. The gyrotron was designed for operation at an accelerating voltage 30 kV. We used a model with a non-fixed structure of the RF field taking into account the velocity spread of the electron beam. The dependences of the starting currents on the magnetic field for the working and competing modes were calculated and shown in figure 2. The presence of a parasitic mode in the excitation region of the operating mode

limits the operating current to 3 A and ultimately determines the maximum possible output power of the gyrotron. In this case, at the operating current 3 A the optimum length of resonator is 62 mm with the output efficiency 5.8%, while the share of ohmic losses is 64%. On the other hand, if one can effectively suppress the parasitic mode, it would be possible to increase the operating current, at which the optimum length of the resonator becomes less. In particular, at operating current 10 A the maximum efficiency 11.4% is achieved with the optimum resonator length 49 mm. Figure 3 shows the dependence of the share of ohmic losses and the output efficiency on the resonator length at operating currents 3 A and 10 A. In addition, the length of the resonator is limited by the characteristic size of the magnetic systems. For further calculations, the resonator length 50 mm with the output efficiency 4.7% at current 3 A and the output efficiency 11.3% at current 10 A was chosen. For a longer resonator length it becomes difficult to realize a homogeneous section of the magnetic field in the interaction space.

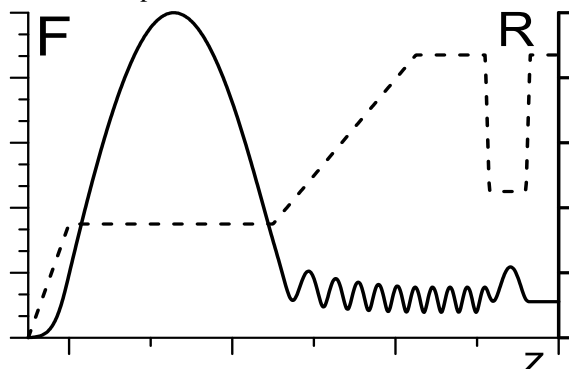


Fig. 1. General view of the cavity profile with an annular diaphragm (dashed line) and longitudinal structure of RF field (solid line).

One of the electrodynamic methods of suppressing the parasitic mode in the gyrotron is the addition of an annular diaphragm in the output part of the resonator. This method of solving the problems of mode competition was proposed earlier, for example, in [7], where the influence of the "external reflector" on the quality factors of the neighboring longitudinal modes was considered. By solution of the cold problem of the longitudinal field structure in the entire volume of the gyrotron electrodynamic system, the parameters of the annular diaphragm for optimal mode selection were chosen. The system with the annular diaphragm drops the diffractive quality factor of the competing $TE_{1,2}$ mode by more than four times, while the diffraction quality factor of the operating mode remains at the same level. Figure 2 shows that the addition of the annular diaphragm results in a significant increase of the starting current of the parasitic mode $TE_{1,2}$ in the

field of excitation of the operating mode. Also the starting current of the $TE_{1,3}$ mode nearly unchanged. The new electrodynamic structure allows to increase the operating current up to 10A and thus to increase the output power by 7 times.

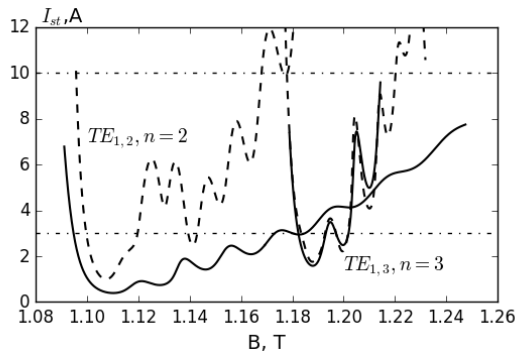


Fig. 2. Dependence of the starting currents on the magnetic field for the operating mode and the main competing mode in a gyrotron at a frequency of 95 GHz with a traditional electrodynamic structure (solid lines) and with diaphragm (dashed lines).

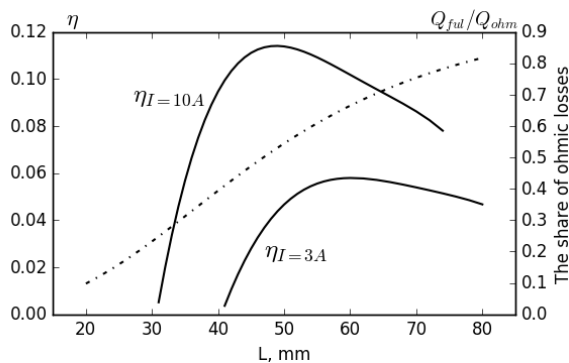


Fig. 3. Dependence of the share of ohmic losses and the output efficiency in the gyrotron on the resonator length at operating currents of 3 A and 10 A.

The estimation of the stability of this method of mode selection for errors in the manufacture of a gyrotron allows us to hope for scaling this method to the region of higher frequencies. Further development of the system consists of optimization of the resonator profile, which will reduce the share of ohmic losses while maintaining high efficiency, and also exclude the possibility of transforming the operating mode into modes with other azimuthal variations. In addition, an experimental verification of this selection method is planned.

The paper is based on the research results, which was conducted in the framework of projects of the Russian Science Foundation No17-79-10422.

References

1. Bratman, V. L., Litvak, A. G., Suvorov, E. V. Mastering the terahertz domain: sources and applications // *Physics-Uspekh*. 2011. V. 54, No. 8, P. 837-870.
2. Kumar, N., Singh, U., Singh, T. P., Sinha, A. K. A Review on the Applications of High Power, High Frequency Microwave Source: Gyrotron // *Journal of Fusion Energy*. 2011. V. 30, No. 4. P. 257-276.

3. Manheimer, W. M. On the possibility of high power gyrotrons for super range resolution radar and atmospheric sensing // *International Journal of Electronics*. 1992. V. 72, No. 5-6. P. 1165-1189.
4. Pilosof, M., Einat, M. A 95 GHz mid-power gyrotron for medical applications measurements // *Review of Scientific Instruments*. 2015. V. 86, No. 1. P. 016113.
5. Nusinovich, G. S., Thumm, M. K. A., Petelin, M. I. The Gyrotron at 50: Historical Overview // *Journal of Infrared, Millimeter, and Terahertz Waves*. 2014. V. 35, No. 4. P. 325-381.
6. Proyavin, M. D., Glyavin, M. Yu., Manuilov, V. N. Development of high-efficient gyrotron based complex for industrial applications. // *EPJ Web Conf*. 2017. No. 149, P. 04034.
7. Rozental, P. M., Ginzburg, H. C., Zaitsev, N. I., Ilyakov E.V., Kulagin I.S. Controllable spectrum of an axial-mode gyrotron with external reflections // *Tecnical Physics. the Russian Journal of Appl. Phys*. 2006. V. 76, No. 1. P. 78-81.

Terahertz-Range Gyrodevices of Planar Geometry

V.Yu. Zaslavsky, N.S. Ginzburg, I.V. Zotova, M.Yu. Glyavin,
A.S. Sergeev, R.M. Rozental, A.M. Malkin, I.V. Zheleznov

Institute of Applied Physics of the Russian Academy of Sciences, Nizhny Novgorod, Russia, zas-vladislav@ipfran.ru

For drastic increase in the output power of short-wavelength gyrotrons, we suggest to use the planar scheme with a sheet electron beam and transverse (with respect to the electrons translation velocity) electromagnetic energy extraction. The main advantage of this scheme comparing to the conventional cylindrical geometry is the possibility of effective mode selection over the open transverse coordinate in combination with radiation out-coupling, which leads to substantial reduction of Ohmic losses [1, 2]. The formation of ribbon helical electron beam (HEB) in planar magnetron-injection gun (MIG) was demonstrated in [3]. In this paper we consider gyrotrons and gyrokystrons of planar geometry driven by sheet electron beams. Possibility of power increasing and selectivity improvement in the terahertz band is shown.

High-Order Cyclotron Harmonic Excitation in a THz-Range Planar Gyrotron

An additional advantage of the planar scheme is the peculiarity associated with excitation of odd ($s = 1, 3, \dots$) and even ($s = 2, 4, \dots$) cyclotron harmonics. Under assumption that the sheet electron beam is injected in the middle of the cavity between the plates, the interaction at odd cyclotron harmonics occurs only for resonator modes with odd transverse indexes $n = 1, 3, \dots$, while interaction at even harmonics occurs only for modes with even transverse indexes $n = 2, 4, \dots$. Moreover, for example, for operation at the second harmonic it is beneficial to use an even resonator mode with indexes n equal to doubled even number. In this case interaction at second harmonic will be not accompanied by simultaneous excitation of a lower order mode at the first cyclotron harmonic due to the coupling factor for the 1st harmonic with an even mode is equal to zero. From the other hand, for excitation at the odd cyclotron harmonic the number of the resonator mode should not be dividable by s . For example, for $s = 3$, the resonator mode number may be $n = 5, 7, 11, \dots$. In this case the parasitic mode at the 2nd cyclotron harmonic is not excited. At the same time, excitation at the 1st cyclotron harmonic can be suppressed due to sensitivity to the spread of electrons velocity and due to additional diffraction losses caused by some penetration of low-frequency running wave through collector narrowing.

Further results of simulations of 1.2 THz planar gyrotron operating at the 3^d cyclotron harmonic are presented. Simulations were carried out in the frame of averaged multi-modes approaches:

$$s_n \frac{\partial a_n}{\partial \tau} + i \frac{\partial^2 a_n}{\partial X^2} + i \frac{\partial^2 a_n}{\partial Z^2} + (i\Delta_n + \sigma_n) a_n = \frac{I_n}{2\pi} \int_0^{2\pi} p^s d\vartheta_0,$$

$$\frac{\partial p}{\partial \tau} + \frac{g^2}{4} \frac{\partial p}{\partial Z} + ip(|p|^2 - 1) = -\sum_n a_n (p^*)^{s-1}.$$

Here a_n is the amplitude of the TE_n mode excited at the s_n harmonic of cyclotron gyrofrequency, p is the transverse electron momentum, Δ_n is the cyclotron resonance detuning, I_n is the parameter proportional to electron current and the coupling factor $G_n(y)$, σ_n is the parameter of Ohmic losses proportional to the skin depth. Due to the diffraction extraction of radiation is realized in transverse x direction (Fig.1a), at the edges of interaction space the nonreflecting boundary conditions may be applied. In the direction of translational motion of electrons the waveguide is considered to be closed by cut-off necks. Thus we can apply zero boundary condition along z coordinate.

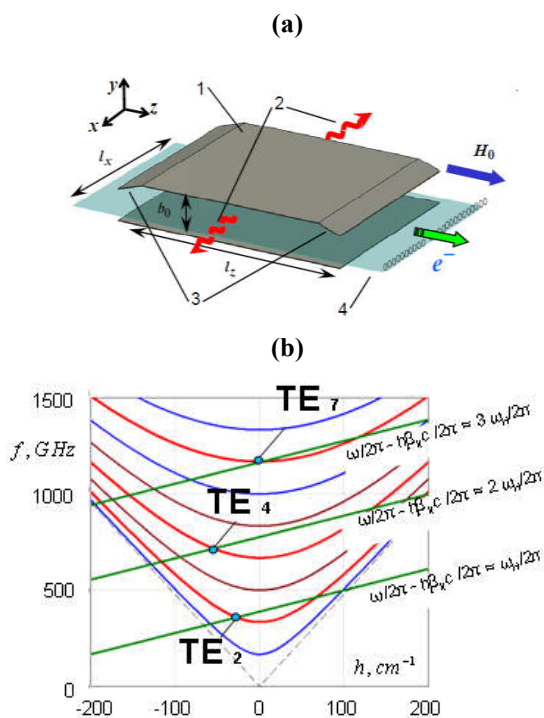


Fig. 1. (a) Scheme of a planar gyrotron with transverse energy extraction: (1) - planar waveguide, (2) - energy output channels, (3) - cutoff narrowing, (4) - sheet helical electron beam. (b) Dispersion diagram of competing modes in the case of exciting the 3^d cyclotron harmonic.

Simulations were carried out for following parameters: energy of electrons of 30 keV, electron current of 6 A, pitch-factor of 1, the distance between plates of 0.9 mm, resonator length and width of

20 mm both. Three modes exciting at the 1st, 2nd and 3^d cyclotron harmonics were included in consideration. Results of simulations (see Fig.2) confirm the possibility of selective excitation of the operating TE_7 mode at the frequency of 1.2 THz.

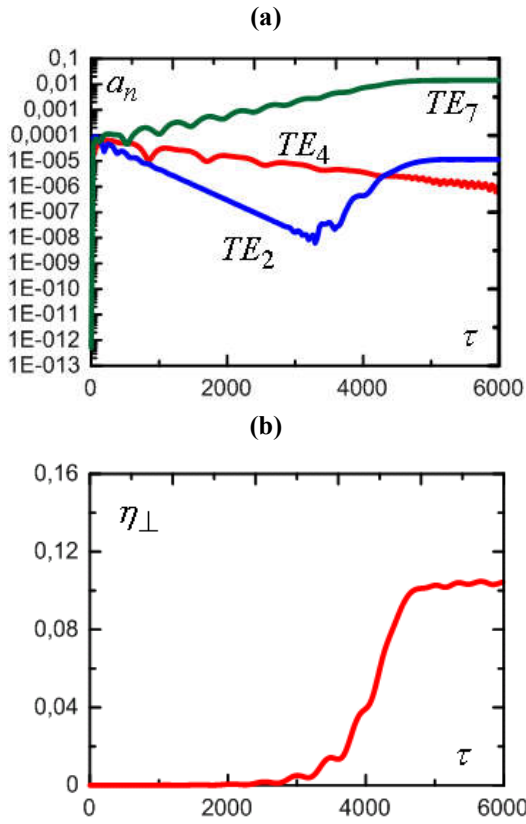


Fig. 2. Temporal dependencies of amplitudes of competing modes (a) and the transverse electron efficiency (b).

Planar Gyro-Klystrons

Using of planar configuration in gyro-klystrons is of interest as a method of increasing the power of output radiation. The considered scheme is presented in Fig. 3a. Analysis was carried out based on 3D PIC (Particle-in-cell) simulations using the code KARAT. Parameters of electron beam were following: energy of 20 kV, total current of 2 A, pitch-factor of 1.3. For distance between plates of 2.2 mm and excitation of the TE_3 mode the operating frequency was of 200 GHz. According to simulations for input power of 10 W output power achieves 4.5 kW. It corresponds to the amplification depth of 26 dB and efficiency of about 10%.

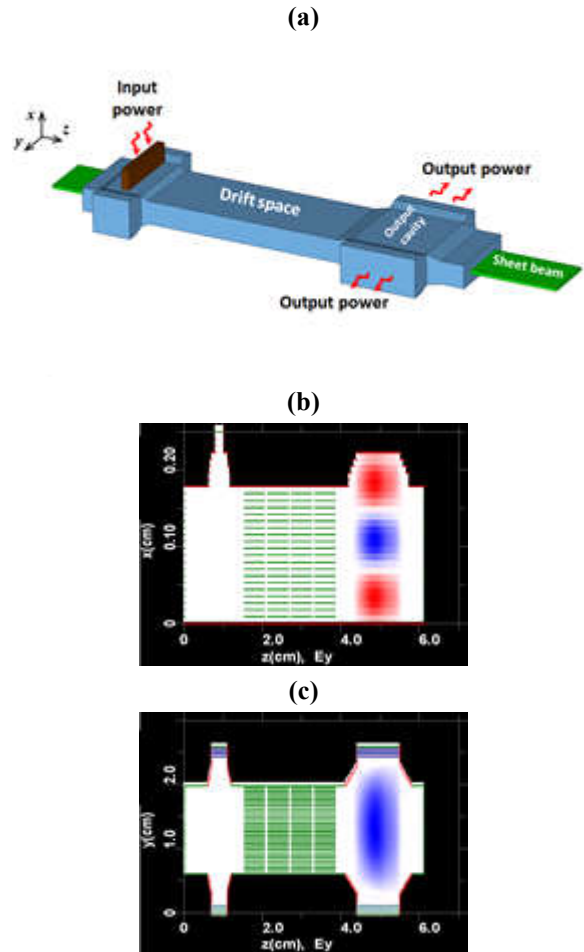


Fig. 3. (a) Scheme of gyroklystron of planar geometry. (b), (c) Field distributions in the input and output resonator over x and y coordinates.

The work was supported by the Russian Science Foundation under grant No. 18-19-00704.

References

1. Ginzburg N.S., Zotova I.V., Sergeev A.S., Zaslavsky V.Yu., Zheleznov I.V., High-power terahertz-range planar gyrotrons with transverse energy extraction// Phys. Rev. Lett. 2012. V. 108. Art.no. 105101.
2. Zaslavsky V.Yu., Ginzburg N.S., Glyavin M.Yu., et al. Three-dimensional particle-in-cell modeling of terahertz gyrotrons with cylindrical and planar configurations of the interaction space. // Physics of Plasmas. 2013. V. 20. P. 043103.
3. Manuilov V.N., Zaslavsky V.Yu., Ginzburg N.S., et al. Electron-optical systems for planar gyrotrons. // Physics of Plasmas. 2014. V. 21. P. 023106.

Design of mm-wave slow-wave devices with sheet and hollow electron beams

A. E. Fedotov¹, V. L. Bratman^{1,2}, P. B. Makhalov¹, and V. N. Manuilov^{1,3}

¹ Institute of Applied Physics, Nizhny Novgorod, Russia, fedotov@appl.sci-nnov.ru

² Ariel University, Ariel, Israel

³ Nizhny Novgorod State University, Nizhny Novgorod, Russia

Abstract

The frequency increase of the slow-wave electron devices is accompanied by inevitable increase of the electron current density and ohmic losses which strongly restricts the attainable power. In recent years, the use of the spatially-developed sheet electron beams is considered as the major way to develop the medium-power slow-wave devices at mm and sub-THz waves. Hollow electron beams is another configuration which could be used for this purpose. The designs of the oscillators and amplifiers in Ka-band and W-band with both sheet and hollow electron beams are considered and compared.

Introduction

The development of the powerful amplifiers in the millimeter and sub-terahertz wavelength ranges is one of the most topical problem in vacuum microwave electronics. In particular, millimeter-wave amplifiers with an output power of several hundred watts are of interest for spectroscopy, telecommunications, remote sensing, and also as preamplifiers for even more powerful gyro-amplifiers. The difficulty of development of traveling wave tubes (TWT) and extended-interaction klystrons (EIK) with the required parameters is caused largely by a very high required beam current density (up to 1 kA / cm²) if conventional electron beam with pencil-like configuration is used. Due to evanescent nature of the synchronous space harmonic of the operating mode, this beam with high energy density should be guided in close proximity to the surface of the slow-wave structure in order to provide efficient electron-wave interaction. The non-perfection of the beam guiding system and high microwave fields inevitably results in some current deposition and, hence, a high heat load on the small elements of the slow-wave structure, in addition to ohmic losses. In order to alleviate the thermal regime of the devices, a use of planar sheet electron beams for millimeter-wave TWTs and EIKs are extensively studied in recent years [1-3]. The large width of the planar beam allows decrease of the required current density but increase of the total electron current. Therefore, the CW or average output power for the planar-beam slow-wave amplifier can be significantly higher than for the pencil-beam device. An alternative configuration of the spatially-developed electron beam is a cylindrical hollow thin-wall beam [4,5]. In this paper we consider both these options for development of the slow-wave device with medium power at the millimeter wavelengths.

Design of sheet-beam slow-wave TWT and BWO

Two key points in the development of the sheet-beam slow-wave devices are slow-wave structure and electron optical system. Presented design is based on a slow-wave structure consisting of two gratings shifted by half period relative to each other (Fig. 1). This structure is widely explored in recent years since it is simple, wideband, easy to manufacture and compatible with a planar electron beam [6]. The sheet beam can be provided by quasi-Pierce electron gun and then solenoidally focused and guided. The beam guiding in the solenoidal magnetic field seems to be simpler than periodic-permanent-magnet focusing system which is traditional for pencil-beam devices at longer waves. To reduce the magnetic compression ratio, a thermionic cathode with high current density of 30 A/cm² can be used, similar to cathodes of low-power submillimeter backward-wave oscillators, clinotrons and orotrons. Simulations predict that the beam which is 0.2 mm thick and 1.8 mm wide with a current of 300 mA (current density 80 A/cm²) can be compressed and guided between gratings in 0.65 T magnetic field with less than 5 % of the total current being lost. Simulation made for W-beam TWT shows the possibility of obtaining an output power of 250 W at a voltage of 20 kV. The calculated gain is 26 dB in the linear regime and about of 21 dB in the saturation. For initial experimental verification of the electron-optical system, a BWO with similar periodic structure was designed with the power of 200-300 W and 7 % tuning band (Fig. 2). The same cathode makes it possible to design the Ka-band BWO and TWT with 500-W output power using beam guiding in the uniform magnetic field, without beam compression.

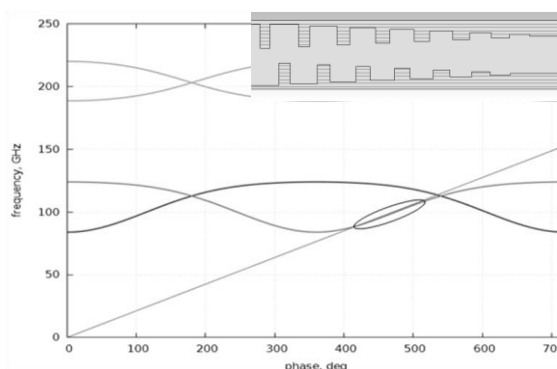


Fig. 1. Calculated dispersion of the operating mode for designed W-band TWT and line of synchronism with 20-kV electron beam. Inset: the staggered-gratings slow-wave structure with the smooth taper of the gratings near the collector end of the interaction region.

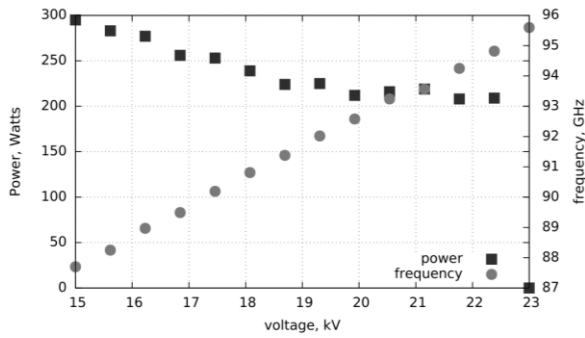


Fig. 2. Calculated output power and frequency vs. voltage for sheet-beam W-band BWO with the staggered-gratings slow-wave structure.

Design of hollow-beam BWOs

The use of hollow electron beams permits a significant increase in the diameter of the beam tunnel in comparison with the conventional pencil-beam slow-wave electron devices. Hollow beam can efficiently interact with a lowest azimuthally-symmetric TM mode of the azimuthally-symmetric slow-wave structure. This configuration is similar to the relativistic high-current electron devices. However, the slow-wave structures with deep corrugation should be used in non-relativistic devices due to weak electron-wave coupling in the millimeter wavelength range. W-band and Q-band axisymmetric BWOs has been designed on the base of 30 kV/1 A hollow thin-wall electron beam with an outer diameters of 1.6 mm and 3.4 mm, respectively. This beam is produced in a Pierce-like electron gun with the hundredfold magnetic compression (Fig. 3). Simulations based on the averaged equations and 3D PIC-code predict an output power of 300-500 W (depending on the beam wall thickness) for W-band BWO and about of 800 W for Q-band BWO. 5% frequency tuning is simulated for the W-band device. To reduce ohmic losses, the wave reflections at the collector end of slow-wave structures are minimized by using specially designed last matching tooth (Fig. 4).

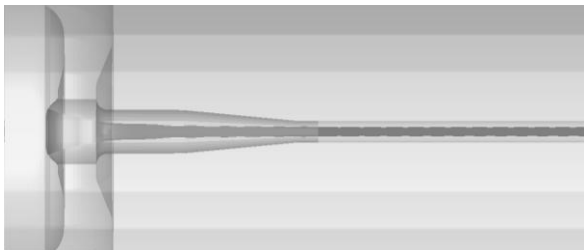


Fig. 3. Designed electron gun producing 30-kV, 1 A hollow electron beam with simulated electron trajectories.

In conclusion, let us compare both configurations of the spatially-developed electron beams. The slow-wave structures for sheet beam devices are easier for manufacturing, and they could provide wider frequency band. The electron-wave coupling for sheet-beam devices could be stronger since electrons travel between two gratings, while for hollow beam there is

single grating at the outer side of the beam. On the other hand, the formation of the sheet electron beam is difficult due to diocotron instability, but this difficulty can be avoided if cathodes with high emission density are used.

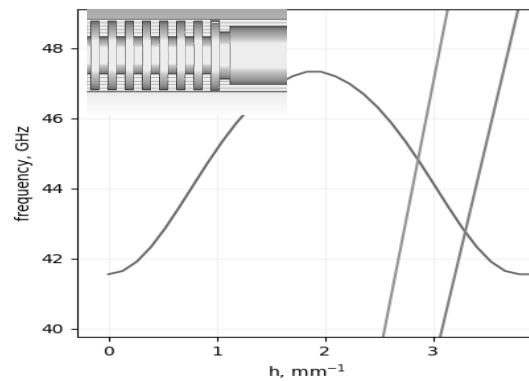


Fig. 4. Calculated dispersion of the operating mode for designed Q-band BWO and line of synchronism with 20- and 30-kV hollow beams. Inset: the axisymmetric slow-wave structure with the matching tooth at the collector end.

The development of the planar-beam devices is supported by Russian Science Foundation under grant No. 18-79-10252. The development of the hollow-beam devices is supported by RFBR under grant No. 16-08-01174.

References

1. Pershing, D. E., Nguyen, K. T., Abe, D. K., Wright, E., Larsen, P. B., Pasour, J., Cooke, S. J., Balkcum, A., Wood, F. N., Myers, R. E., and Levush, B. Demonstration of a wideband 10-kW Ka-band sheet beam TWT amplifier. // IEEE Transactions on Electron Devices. 2014. V. 61, No. 6. P. 1637-1642.
2. Pasour, J., Wright, E., Nguyen, K. T., Balkcum, A., Wood, F. N., Myers, R. E., and Levush, B. Demonstration of a multikilowatt, solenoidally focused sheet beam amplifier at 94 GHz. // IEEE Transactions on Electron Devices. 2014. V. 61, No. 6. P. 1630-1636.
3. Karetnikova, T. A., Rozhnev, A. G., Ryskin, N. M., Fedotov, A. E., Mishakin, S. V., and Ginzburg, N. S. Gain analysis of a 0.2-THz traveling-wave tube with sheet electron beam and staggered grating slow wave structure. // IEEE Transactions on Electron Devices. 2018. V. 65, No. 6. P. 2129-2134.
4. Bratman, V. L., Fedotov, A.E., and Makhalov, P. B. High-frequency devices with weakly-relativistic hollow thin-wall electron beams. // Physics of Plasmas. 2012. V. 19, No. 2. Art. 020704.
5. Bratman, V. L., Fedotov, A. E., Makhalov, P. B., and Manuilov, V. N. Design and numerical analysis of W-band oscillators with hollow electron beam. // IEEE Transactions on Electron Devices. 2014. Vol. 61, No. 6. P. 1795-1799.
6. Shin, Y. M., Barnett, L. R., and Luhmann, N. C. Phase-shifted traveling-wave-tube circuit for ultrawideband high-power submillimeter-wave generation. // IEEE Transactions on Electron Devices. 2009. V. 56, No. 5. P. 706-712.

Generation of Sub-Terahertz Surface Waves by Relativistic Electron Beams: Quasioptical Theory, Simulations and Experiments

Naum S. Ginzburg¹, A.M. Malkin¹, I.V. Zheleznov¹, V.Yu. Zaslavsky¹, A.S. Sergeev¹,
I.V. Zotova¹, and M.I. Yalandin²

¹Institute of Applied Physics RAS, Nizhny Novgorod, Russia, ginzburg@appl.sci-nnov.ru

²Institute of Electrophysics RAS, Ekaterinburg, Russia

Advancement of vacuum electronic devices into sub-THz and THz frequency ranges calls for oversized beam-wave interaction space due to the fact that the dimensions of the beam guiding systems can not be reduced lower than the millimeter scale. Thus, in order to provide coherent THz radiation from the spatially extended beams, excitation of surface modes existing in 1D and 2D corrugated systems appears to be attractive [1,2,5,6].

In this paper, we present recent results of theoretical and experimental studies of sub-terahertz generation based on excitation of surface waves by electron beams and extended bunches. Using oversized slow-wave structures allows for a significant increase of total current and, correspondingly, radiation power. Based on superradiance of electron bunches, 150 ps superradiant pulses with a central frequency of 0.14 THz, and an extremely high peak power of 50-70 MW were obtained in the joint effort by the Institute of Electrophysics RAS and IAP RAS. We also report of the first successful experiments on the cylindrical 0.03 THz Cherenkov oscillator with a 2D corrugation conducted at IAP RAS with an output power of 1.5 - 2 MW.

Generation of Sub-THz SR Pulses Based on Excitation of Surface Waves in Oversized Waveguides

Cherenkov SR of electron bunch exciting the surface wave in an oversized 1D corrugated cylindrical waveguide (Fig. 1a) can be considered within quasioptical approach [1]. In this case the radiation field near a shallow corrugation is presented as a sum of two counter-propagating *TM* polarized wave-beams:

$$H_\varphi = \text{Re}(A_+(z, r, t)e^{i\omega t - ikz} + A_-(z, r, t)e^{i\omega t + ikz}), \quad (1)$$

propagation and mutual coupling of which is described by two non-uniform parabolic equations. The synchronous interaction of electrons with a forward partial wave leads to development a self-bunching and formation of powerful SR pulse.

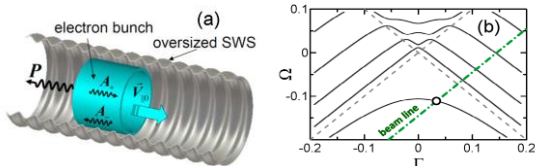


Fig. 1. (a) Scheme of SR pulse generation with excitation of a surface wave in an oversized periodically corrugated waveguide. (b) Dispersion characteristics of a corrugated waveguide and an electron beam.

Simulations show that the most optimal conditions for SR emission correspond to excitation of the backward surface wave near the Bragg frequency (π -regime, Fig.1b). For parameters of an electron bunch formed by an accelerator RADAN (electron energy of 300 keV, a total current of 2 kA, a bunch duration of 500 ps) and a corrugated waveguide with the mean radius of 3.75 mm, corrugation period of 0.825 mm, and corrugation depth of 0.36 mm the operating frequency in the resonant point is of 0.14 THz ($2r_0/\lambda \approx 3.5$). In this case the power of generated SR pulse emitted in $-z$ direction achieves ~ 200 MW for pulse duration of ~ 200 ps (Fig. 2a). As it is seen in Fig. 2b the instant spatial structure of the partial wave corresponds to formation of the evanescent surface wave with the field amplitude exponentially decaying from the corrugation.

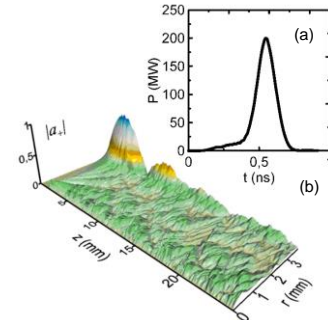


Fig. 2. SR emission with excitation of the backward surface wave: (a) generated SR pulse, (b) the structure of the forward partial wave.

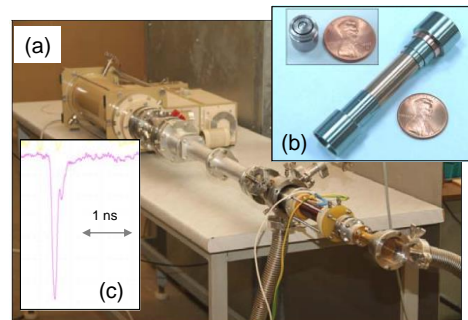


Fig. 3. Photo of the experimental set-up (a), corrugated waveguide and coaxial reflector (b) used for observation of superradiance with excitation of a surface wave. (c) Oscilloscope trace of the 0.14 THz SR pulse with duration of 150 ps and peak power up to 70 MW.

Based on a theoretical analysis, experiments on observation of the sub-terahertz SR pulse generation were carried out in IEP RAS (Ekaterinburg). Photo of the experimental set-up is shown in Fig. 3. A typical

oscilloscope trace of generated SR pulses with a duration of about 150 ps and a rise time of 100 ps reconstructed in the “power-time” coordinates is presented in Fig. 3c. Frequency measurements using a set of cut-off waveguide filters show that the pulse spectrum has a central frequency in the interval 0.13-0.15 THz. The peak power of generated SR pulses was estimated by integrating the detector signal over the directional pattern and achieved of 50-70 MW, that strongly exceeds the value obtained in the previous sub-terahertz experiments [2] with single-mode waveguides.

Ka-band surface-wave oscillator based on 2D periodical corrugated structure

For spatially extended relativistic electron beams, the use of two-dimensional (2D) distributed feedback is beneficial for providing spatial coherence of radiation and can be exploited in order to increase the total radiation power in the microwave generators [3]. Such 2D feedback can be realized in planar or coaxial 2D Bragg structures (resonators) having double-periodic corrugation (Fig.4a)

$$r = \frac{\tilde{r}}{4} \left[\cos(\bar{M}\varphi - \bar{h}_z z) + \cos(\bar{M}\varphi + \bar{h}_z z) \right], \quad (2)$$

which provides coupling and mutual scattering of the four wavebeams (Fig.4b),

$$\vec{H} = \text{Re} \left[\vec{x}_0 (C_z^+ e^{-ihz} + C_z^- e^{ihz}) + \vec{z}_0 (C_x^+ e^{-ihx} + C_x^- e^{ihx}) \right] e^{i\omega t}$$

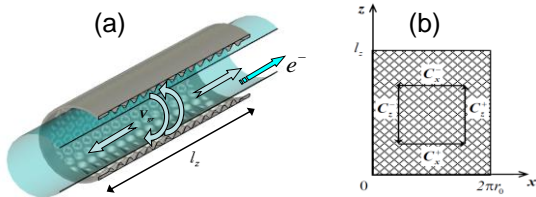


Fig. 4. (a) Scheme of an oversized SWO with 2D corrugated structure. Directions of propagation of the partial wave fluxes and tubular electron beam are shown. (b) Diagram illustrating coupling of partial waves at the 2D corrugation.

Experimental studies of free electron masers (FEMs) based on the novel feedback mechanism have been performed in Ka-band and in W-band in collaboration with the Institute of Applied Physics RAS [4]. As a result, narrow-band generation with an output power of 50 - 100 MW, which is a record for millimeter wavelength FEMs, was obtained.

At present, theoretical and experimental studies of Cherenkov masers with 2D distributed feedback are in progress [5,6]. Among relativistic masers of such type, surface wave oscillators (SWO) appear to be preferable due to the larger values of the electron-wave coupling impedance. Besides, formation of a surface mode ensures the regular field distribution along the coordinate directed perpendicularly to the corrugated surface and, thus, can solve the problem of mode selection over this coordinate. In SWOs, a 2D periodic structure can be exploited both as a slow-wave system and as a highly selective Bragg resonator simultaneously. It provides effective mode control over azimuthal coordinate.

Numerical simulations within the quasi-optical model and using 3D numerical codes show that the resulting mode to be excited in such system depends on the accelerating voltage rise time. In order to excite an azimuthally symmetric mode, this value should be small in the scale of the field excitation increment.

Experimental investigations of the SWO with 2D slow-wave structure based on the 300 keV / 100 A / 4 μs SATURN thermionic accelerator were conducted at IAP RAS [6]. The results are presented in Fig.5. Narrow-spectrum excitation of the 3rd azimuthal mode was observed.

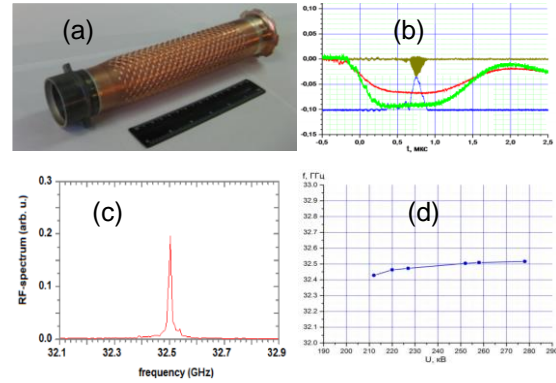


Fig. 5. Results of experimental studies of oversized Ka-band SWO based on the SATURN accelerator: (a) photograph of double periodic slow-wave structure; (b) typical oscilloscope traces of the accelerating voltage (green curve), beam current (red curve), signal from a heterodyne mixer (brown curve) and output RF-pulse (blue curve); (c) spectrum of the output radiation and (d) dependence of the radiation frequency on the accelerating voltage.

This research was performed within the framework of the state task (projects No. 0035-2014-012), and, in part, by RFBR Grant No. 17-08-01072

References

1. Ginzburg, N.S., Malkin, A.M., Sergeev, A.S. et al. Generation of Sub-Terahertz Superradiance Pulses Based on Excitation of a Surface Wave by Relativistic Electron Bunches Moving in Oversized Corrugated Waveguides // Phys. Rev. Lett. 2016. V.117 P.204801
2. Yalandin, M.I., Shpak, V.G., Shunailov, S.A., et al. Generation of powerful subnanosecond microwave pulses in the range of 38–150 GHz// IEEE Trans. on Plasma Sci. 2000. V.28, Iss.5 P.1615
3. N.S.Ginzburg, N.Yu.Peskov, A.S.Sergeev, Dynamics of free-electron lasers with two-dimensional distributed feedback // Optics Commun., **112**, 151 (1994).
4. A.V.Arzhannikov, N.S.Ginzburg, P.V.Kalinin, et al., Using Two-Dimensional Distributed Feedback for Synchronization of Radiation from Two Parallel-Sheet Electron Beams in a Free-Electron Maser // Phys. Rev. Lett. V. **117**, 114801 (2016).
5. N.S.Ginzburg, A.M.Malkin, A.S.Sergeev, and V.Yu.Zaslavsky, Powerful surface-wave oscillators with two-dimensional periodic structures // Appl. Phys. Lett. 100, 143510 (2012)
6. N.S.Ginzburg, E.V.Ilyakov, I.S.Kulagin, et al., Theoretical and experimental studies of relativistic oversized Ka-band surface-wave oscillator based on 2D periodical corrugated structure // Phys. Rev. AB. V. **21**, 080701 (2018).

Powerful surface-wave oscillators with one-dimensional and two-dimensional periodic planar structures

V.Yu. Zaslavsky, N.S. Ginzburg, A.M. Malkin, A.S. Sergeev

Institute of Applied Physics of the Russian Academy of Sciences, Nizhny Novgorod, Russia, zas-vladislav@ipfran.ru

Within the framework of a quasi-optical approach, we develop self-consistent theory of relativistic surface-wave oscillators [1]. Presenting the radiation field as a sum of two counter-propagating wave-beams coupled on a shallow corrugated surface, we describe formation of an evanescent slow wave. Dispersion characteristics of the evanescent wave following from this method are in good compliance with those found from the direct CST simulations. Considering excitation of the slow wave by a sheet electron beam, we simulate linear and nonlinear stages of interaction, which allows us to determine oscillation threshold conditions, electron efficiency and output coupling. The transition from the model of surface-wave oscillator operating in the π -mode regime to the canonical model of relativistic BWO is considered. We also described a modified scheme of planar relativistic surface-wave oscillators exploiting two-dimensional periodic gratings [2]. Additional transverse propagating waves emerging on these gratings synchronize the emission from a wide sheet rectilinear electron beam allowing realization of a Cherenkov millimeter-wave oscillators with subgigawatt output power level.

Simulations of surface-wave oscillators with conventional single periodic slow-wave structures in the framework of a 3D model

We start with consideration of a surface-wave oscillator driven by a sheet electron beam with a finite width of l_x^e over the x axis (Fig. 1a). We should assume that the field structure is non-fixed over all three spatial coordinates. Thus, 3D quasi-optical model was used in simulations [3].

Results of simulations are depicted in Fig. 1 for the electron beam width of $l_x^e = 10$ cm. At a relatively small width of the beam $l_x^e = 5$ cm the transverse (over x) field structure possesses a regular symmetric distribution (an exponential decay in the y -direction perpendicularly to the corrugated structure takes place in all variants). For wider beams, for example, for the electron beam width of $l_x^e = 10$ cm, multistability regimes take place. For various initial conditions, we observed the excitation of both symmetrical and anti-symmetrical modes, as shown in Fig. 1. For explanation we analyzed the dependence of temporal gain on beam width for symmetrical and anti-symmetrical modes. For rather small widths, gain for the symmetrical mode strongly exceeds gain for anti-symmetrical one. Under such conditions, a regular symmetric distribution sets on in the steady-state regime. With increasing beam width, gains for symmetrical and anti-

symmetrical modes (and other modes) become very close, which leads to multistability.

Thus, diffraction of radiation in the x -direction is sufficient for formation of regular field structure over this coordinate while the beam size is restricted by Fresnel condition, $N_F = l_x^e / 4l_z \lambda \leq 1$. For practical estimations of the conventional scheme of a surface-wave oscillator we can take the beam width of 4-5 wavelengths, which corresponds to the regular field distribution. For a relatively high electron efficiency of about 10 %, the total output power amounts about 40 MW. For a metallic (brass) surface, Ohmic losses did not exceed several per cent of radiated power.

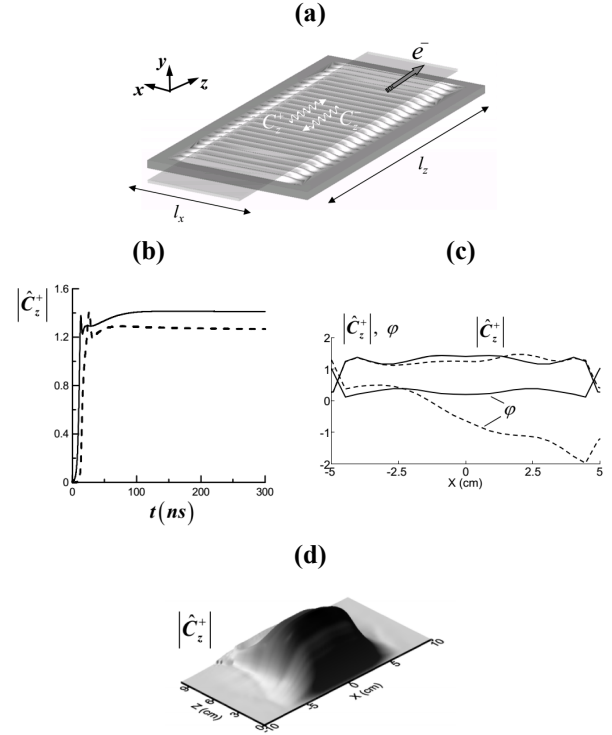


Fig. 1. (a) Scheme of surface-wave oscillator with 1D periodic gratings driven by a rectilinear sheet electron beam. Simulations of surface-wave oscillator based on 3D quasi-optical model for electron beam width $l_x^e = 10$ cm : (b) Temporal dependence of amplitude $|\hat{C}_z^+|$, (c) distributions of amplitude $|\hat{C}_z^+|$ and phase $\varphi = \arg(\hat{C}_z^+)$ at the output cross-section $z = l_z$ ($I_0 = 0.3$ kA/cm, $\gamma_0 = 3$, $l_z = 10$ cm), (d) spatial distribution of this amplitude in the steady-state regime in the cross-section $y = \text{const}$. Solid line corresponds to excitation of symmetrical mode, dashed line - to anti-symmetrical one.

It should be noted that in 3D quasi-optical analysis we considered an idealized model of grating infinite in the transverse x direction. On the basis of *CST STUDIO SUITE* software, we simulated a more realis-

tic model of the grating with the same transverse width as the electron beam. In this case we found more severe restrictions on stability of single-frequency oscillation regime. In fact, for electron beam and corrugation parameters indicated above, we observed single-frequency oscillation at the system width of up to 4-5 wavelengths. For larger width values, multifrequency generation regimes with simultaneous excitation of several modes with different numbers of variations over the x coordinate are more typical.

Surface-Wave Oscillators with Two-Dimensional Periodic Structures

In the case when the beam width substantially exceeds the wavelength, we suggest a more effective mechanism for provision of transverse radiation coherence based on the improved version of the slow-wave structure, namely a double periodic grating [2, 3]. Similarly to free electron masers (FEMs) with 2D distributed feedback, these gratings allow organizing additional transverse (with respect to the translational velocity of the electrons) electromagnetic energy fluxes that synchronize the radiation from wide sheet electron beams (Fig. 2).

Based on quasi-optical approach [2, 3], we simulated the operation of a powerful W-band relativistic surface-wave oscillator driven by a sheet beam with parameters close to those of the beam realized at a high-current ELMI accelerator (Budker Institute, Novosibirsk). We took the electron energy of 1 MeV, the beam width of $l_x=27$ cm, and the linear current density of $I_0=0.3$ kA/cm.

Onset of steady-state oscillations is shown in Fig. 2b. Temporal dependencies of energy fluxes radiated from different edges of the interaction space demonstrate that in the variant under consideration the most part of the power is radiated in the backward and forward directions (Fig. 2c). The power associated with transverse fluxes is relatively small. In accordance with the negative frequency, the shift from the Bragg frequency in the steady-state regime the partial wave fields are evanescent. In the (z, x) plane the partial wave amplitudes possess bell-shaped profiles which are also similar to those found for the "cold" mode. Electron efficiency of about 10% at the chosen parameters corresponds to the integral radiation power of ~ 0.9 GW.

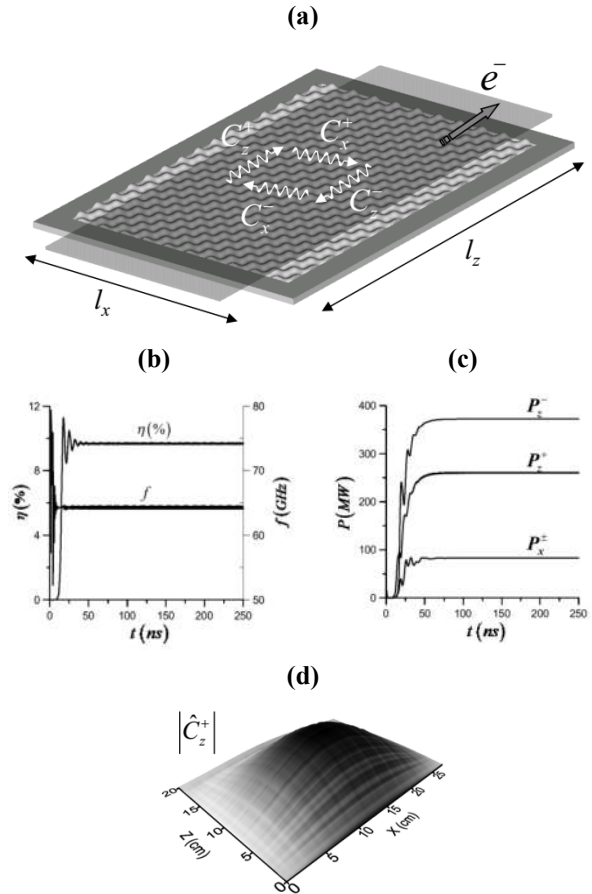


Fig. 2. (a) Scheme of surface-wave oscillator with 2D periodic grating. Temporal dependencies of (b) the efficiency and (c) the radiation power emitted in the different directions during the onset of a steady-state regime. (d) Spatial distribution of partial wave-beam $|\hat{C}_z^+|$ in the steady-state regime ($I_0 \approx 0.3$ kA/cm, $\gamma_0 = 3$, $l_z = 19.6$ cm, $l_x = 27$ cm).

The work was supported by the Russian Science Foundation under grant No. 18-79-10252.

References

1. N.S. Ginzburg, A.M. Malkin, A.S. Sergeev, V.Yu. Zaslavsky. Quasi-optical theory of relativistic submillimeter surface-wave oscillators. *Applied Physics Letters*. 2011. V. 99. P. 121505.
2. Ginzburg N.S., Malkin A.M., Sergeev A.S., and Zaslavsky V.Yu. Powerful surface-wave oscillators with two-dimensional periodic structures. // *Applied Physics Letters*. 2012. V.100. P. 143510.
3. N.S. Ginzburg, A.M. Malkin, A.S. Sergeev, V.Yu. Zaslavsky. Quasi-Optical Theory of Relativistic Surface-Wave Oscillators with 1D and 2D Periodic Planar Structures. // *Physics of Plasmas*. 2013. V. 20, P. 113104.

YBaCuO Josephson generators fabricated by preliminary topology masks

L.S. Revin^{1,2}, A.L. Pankratov^{1,2,3}, D.V. Masterov¹, A.E. Parafin¹, S.A. Pavlov¹, A.V. Chiginov^{1,2}, I.V. Rakut^{2,3}, A.V. Gordeeva^{1,2}, V.O. Zbrozhek², A.V. Blagodatkin^{1,2}, L.S. Kuzmin^{2,4}

¹Institute for Physics of Microstructures of Russian Academy of Sciences, Nizhny Novgorod, Russia, rls@ipmras.ru

²Nizhny Novgorod State Technical University n.a. R.E. Alexeev, Nizhny Novgorod, Russia

³Lobachevsky Nizhny Novgorod State University, Nizhny Novgorod, Russia

⁴Chalmers University of Technology, Gothenburg, Sweden

The investigation of flux-flow regimes in the Josephson junction is of practical interest. In a long junction the mode of fluxon motion may occur under the action of external magnetic field in which solitons are created at one edge of the junction, move along the junction, and are radiated at the other edge. Such regimes can be useful in creation of THz band oscillators [1], heterodyne and Hilbert spectrometers.

It is well known that the properties of thin YBCO films are very sensitive to the processes of formation of planar structures. New technology of preliminary mask (PM) with CeO₂ buffer layer, which determines the necessary topology of the structure directly during the growth of the YBCO film has been developed [2-4]. The exclusion of the etching operation of the YBCO film from the technological process is important for structures with weak links, where the film is most sensitive to possible destructive factors. The PM method has been successfully used to create Josephson junctions on a bicrystal YSZ substrate with a sublayer of epitaxial cerium dioxide CeO₂ [2,4].

As the results of preliminary study, the samples of Josephson junctions with 6-350 μm length and 0.3 μm thickness have been fabricated on symmetric 24° [001]-tilt bicrystal YSZ substrate.

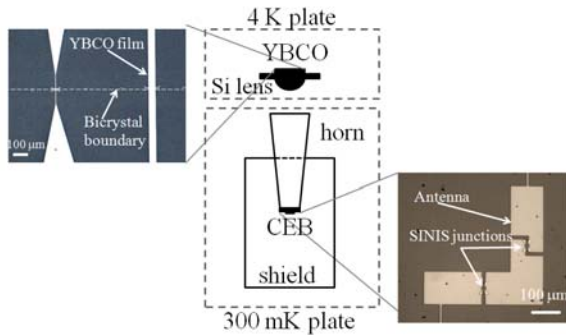


Fig. 1. Schematic of the experiment and samples design.

To register the radiation from long bicrystal junction the sample of Cold Electron Bolometer (CEB) [5-8] was used. CEBs represent SINIS junctions with nanoabsorber made of aluminum with suppressed superconductivity. One CEB can receive up to 0.5 pW without going into saturation. Based on the requirements of the power load the 2D array of CEB realized as meander-type structure. CEBs are connected in series and parallel at DC for optimal matching with the amplifier. A pair of half lambda dipoles with wide electrodes is connected to another pair by high-inductive 1 μm wide lines. The design is optimized for the frequency band of 240-280 GHz.

In figure 1 the scheme of experimental setup as well as samples design are presented. The Josephson oscillator chip consists of several junctions integrated with planar dipole antennas. The substrate with the sample was attached to Si hyperhemisphere lens at the 4 K plate. The bolometer with horn on the back side of silicon substrate was placed at the 300 mK plate. The absorbing shield was used to avoid reflections. The magnetic field perpendicular to the grain boundary of HTSC sample was produced by a current through the copper wire coil, having the inner diameter more than order of magnitude larger than the junction length.

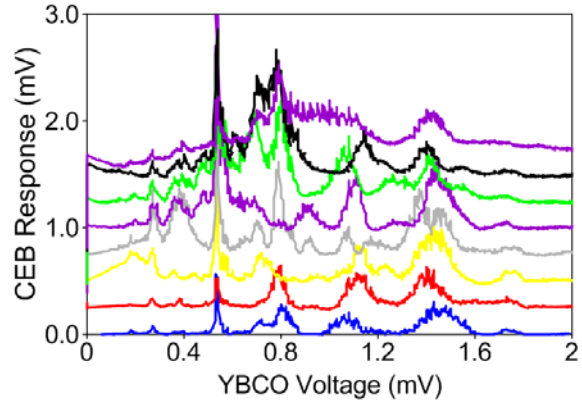


Fig. 2. CEB response for a different magnetic field through the YBCO generator. For clarity, each curve from the second is shifted relative to the other by 0.25 mV.

Changing the current through the Josephson junction the bolometer response was measured as well as the voltage on YBCO oscillator (Josephson frequency $f = 2eV_{\text{YBCO}}/\hbar$). Figure 2 shows the bolometer response (received power) for different values of the external magnetic field. For clarity each curve from the second one is shifted relative to the other by 0.25 mV. It can be seen that the response represents several distinct peaks and a pedestal. The maximum of this pedestal shifts towards higher voltage with increasing of magnetic field.

Finding the maximum response for each frequency for all values of the magnetic field, we obtain the frequency response of the radiating system together with the receiving system, figure 3. Comparing the result with the CEB amplitude-frequency characteristic based on the calibrated backward-wave source (enlarged part of Fig. 3), it can be concluded that the signal peaks are determined by the characteristic of the receiving system rather than the oscillating one.

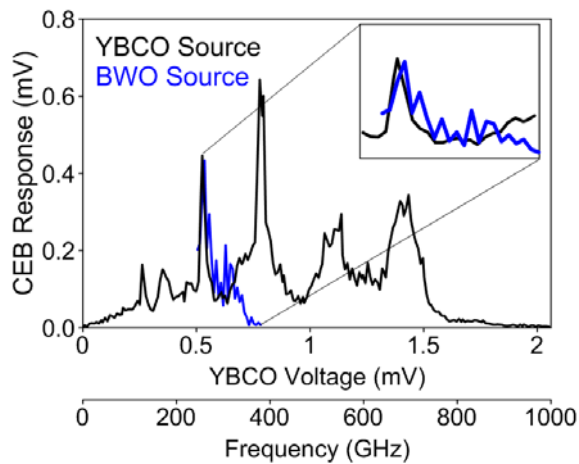


Fig. 3. Maximum registered response of the bolometer depending on the frequency of radiation. Comparison with experiments using BWO.

In conclusion, the samples of YBCO long Josephson junctions on YSZ bicrystal substrate have been fabricated using original technology of preliminary topology mask and good characteristics of the samples have been achieved. The observation of flux-flow regime in long grain-boundary junctions is evidenced. Using the cold-electron bolometer, the subTHz emission up to 900 GHz was registered. Magnetic field controlled regime make long junctions promising candidates for THz applications. It can also be used as a THz band cryogenic network analyzer in combination with a cryogenic bolometer.

The work is supported by RSF (projects 16-19-10478 and 16-19-10468).

References

1. *Stepantsov, E., Tarasov, M., Kalabukhov, A., Kuzmin, L., Claeson T.*, THz Josephson properties of grain boundary YBaCuO junctions on symmetric, tilted bicrystal sapphire substrates // *Journal of Appl. Phys.* 2004. V. 96, No. 6. P. 3357.
2. *Masterov, D.V., Parafin, A.E., Revin, L.S., Chiginev, A.V., Skorokhodov, E.V., Yunin, P.A., Pankratov, A.L.*, YBCO long Josephson junctions on bicrystal $Zr_{1-x}Y_xO_2$ substrates fabricated by preliminary topology masks // *Supercon. Sci. Technol.*, vol. 30, no. 2, pp. 025007, 2017.
3. *Masterov, D.V., Pavlov, S.A., Parafin, A.E.*, A new approach to formation of the topology of planar structures on the basis of a YBCO high-temperature superconductor // *Physics of the Solid State*. 2017. vol. 59, pp. 2133-2136.
4. *Revin, L.S., Pankratov, A.L., Masterov, D.V., Parafin, A.E., Pavlov, S.A., Chiginev, A.V., Skorokhodov, E.V.*, Features of Long YBCO Josephson Junctions Fabricated by Preliminary Topology Mask // *IEEE Trans. on Appl. Supercon.* vol. 28, no. 7, pp. 1100505, 2018.
5. *Kuzmin, L., Hoste, S., Ausloos, M.*, An Array of Cold-Electron Bolometers with SIN Tunnel Junctions and JFET readout for Cosmology Instruments // *8th European Conference on Applied Superconductivity*. 2008. vol. 97, pp. 17.
6. *Kuzmin, L.S., Devyatov, I.A., Golubev, D., et al.* "Cold-electron" bolometer with electronic microrefrigeration and the general noise analysis // *Millimeter and Submillimeter Waves Iv*. 1998. vol. 34 pp. 193-199.
7. *A.V. Gordeeva, V.O. Zbrozhek, A.L. Pankratov, L.S. Revin, V.A. Shamporov, A.A. Gunbina, L.S. Kuzmin*, *Appl. Phys. Lett.*, 110, 162603 (2017).
8. *L.S. Kuzmin, A.L. Pankratov, A.V. Gordeeva, V.O. Zbrozhek, L.S. Revin, V.A. Shamporov, A.A. Gunbina, S. Masi, P. de Bernardis*, "Realization of Cold-Electron Bolometers with Ultimate Sensitivity due to Strong Electron Self-Cooling", *Proceedings of 16th International Superconductive Electronics Conference (ISEC'2017)*, DOI: 10.1109/ISEC.2017.8314194